**Title**
Hybrid Thermal and Compressed Air Energy Storage System (HT-CAES): Thermodynamic Analysis and Thermoeconomic Optimization



**Author**
Houssainy, Sammy

**Publication Date**
2017

Peer reviewed|Thesis/dissertation

UNIVERSITY OF CALIFORNIA

Los Angeles

# Hybrid Thermal and Compressed Air Energy Storage System (HT-CAES): Thermodynamic Analysis and Thermoeconomic Optimization

A dissertation submitted in partial satisfaction

of the requirements for the degree

Doctor of Philosophy in Mechanical Engineering

by

Sammy Houssainy

2017

ABSTRACT OF THE DISSERTATION

Hybrid Thermal and Compressed Air Energy Storage System (HT-CAES): Thermodynamic Analysis and Thermoeconomic Optimization

by

Sammy Houssainy

Doctor of Philosophy in Mechanical Engineering

University of California, Los Angeles, 2017

Professor Hossein Pirouz Kavehpour, Chair

Global warming concerns, volatile oil costs, and government incentives are leading to increased interest in the adoption of renewable energy sources. However, the integration of renewable sources in our existing infrastructure is challenging, as renewable generation is unpredictable and intermittent by nature. Energy storage compensates for the inherent intermittency of renewable energy sources, by storing energy during surplus power production periods and discharging the stored energy during low production periods. Compressed Air Energy Storage has received much attention as a viable solution due to its economic feasibility, low environmental impact, and large-scale capability. However, conventional CAES systems rely on the combustion of natural gas, require large storage volumes, and operate at high pressures, which possess inherent problems such as high costs, strict geological locations, and the production of greenhouse gas emissions. Through this research, a novel and patented hybrid thermal-compressed air energy storage (HT-CAES) design is investigated as a possible solution. The HT-CAES system allows a portion of the available energy, from the grid or renewable

sources, to operate a compressor and the remainder to be converted and stored in the form of heat, through joule heating in a solid-state sensible thermal energy storage medium. The hybrid design has the beneficial effect of mitigating the shortcomings of conventional CAES systems and its derivatives by eliminating combustion emissions and reducing storage volumes, operating pressures, and costs. Therefore, the hybrid system provides flexibility of adjusting to a myriad of storage volumes based on available geological restrictions. Additionally, The hybrid system possesses a wide range of possible operations, without a compromise in its storage capacity, which may prove useful as we move towards a sustainable future.

An ideal HT-CAES system is investigated and the thermodynamic efficiency limits within which it operates have been drawn. The efficiency of the HT-CAES system is compared with its Brayton cycle counterpart, in the case of pure thermal energy storage (TES). It is shown that the efficiency of the HT-CAES plant is not theoretically bound by the Carnot efficiency and always higher than that of the Brayton cycle, except for when the heat losses following compression rise above a critical level. The results of this work demonstrate that the HT-CAES system has the potential of increasing the efficiency of a pure TES system, executed through a Brayton cycle, at the expense of an air storage medium.

Subsequently, a realistic and irreversible hybrid configuration is presented that incorporates two stages of heating through separate low-temperature and high-temperature thermal energy storage units. A thermodynamic analysis of the HT-CAES system is presented along with parametric studies, which illustrate the importance of the operating pressure and thermal storage temperature on the performance of the storage system. Realistic isentropic component efficiencies and throttling losses were considered. Additionally, two extreme cavern conditions were analyzed and the cyclic behavior of an adiabatic cavern was investigated. An

optimum operating pressure resulting in maximum roundtrip storage efficiency of the hybrid storage system is reported. Additionally, a modified hybrid design is investigated that includes a turbocharger in the discharge process, which provides supplementary mass flow rate alongside the air storage. This addition has the potential of drastically reducing the necessary storage volume and pressures, thus further increasing the operational flexibility of the system. The results of this work provide an efficiency and cost map of the HT-CAES system versus both the operating pressure and the distribution of energy, between thermal and compressed air storage. The results of this work illustrate and properly quantify a tradeoff that exists between the HT-CAES system cost and performance. Both roundtrip energy and exergy efficiencies are quantified, presented, and compared. Lastly, a local optimum-line of operation, which results in a local maximum in efficiency and a local minimum in cost, is presented.

The HT-CAES system is also investigated and optimized based on a minimum entropy generation criteria. Regenerative and non-regenerative configurations are examined. It is illustrated that an HT-CAES system designed based on a minimum entropy generation objective may be at a lower energy and exergy efficiency, and lower output power, than otherwise achievable. Therefore, in the case of a hybrid energy storage system, minimization of entropy generation does not always coincide with minimization of energy losses. Only under certain conditions does the point of minimum entropy generation coincide with maximum energy efficiency. Specifically, this occurs only when the input energy, thermal energy storage mass, specific heat, and temperature swing, are a constant. Similarly, only in the specific case where the total input exergy is a constant, does minimum entropy generation coincide with maximum exergy efficiency. Lastly, an exergy analysis of the hybrid system is presented. The calculated and normalized exergy destruction maps provide a means of comparing the component exergy

destruction magnitudes for assessing and pinpointing the sources of largest irreversibilities. In addition to the exergy destruction, the exergetic component efficiencies are also presented and compared. Both component exergy destruction and their exergetic efficiencies demonstrate that the largest source of avoidable exergy destruction results from the irreversibilities associated with throttling and the irreversibilities associated with mixing losses within the air storage medium.

This dissertation of Sammy Houssainy is approved.

Jeffrey D. Eldredge

Adrienne G. Lavine

Stephanie S. Pincetl

Hossein Pirouz Kavehpour, Committee Chair

University of California, Los Angeles

2017

*In loving memory of my father*

*Waleed Houssainy*

*For sparking the engineer in me*

# Table of Contents

# List of Figures

# List of Tables

# Acknowledgements

I would like to express the deepest appreciation to my advisor and committee chair Professor Kavehpour for his support, guidance, patience, and encouragement throughout my graduate pursuit. He was always an inspirational, dedicated, and passionate instructor and advisor, it has been an honor working with him. I am indebted by his ability to foster professional confidence and encourage critical thinking, skepticism, and creativity.

I would like to thank my committee members, Professor Eldredge, Professor Lavine, and Professor Pincetl for their encouragement, help, and insightful comments. I am particularly thankful for Professor Eldredge and Professor Lavine for their uncompromising support and willingness to provide their many letters of reference on my behalf.

I wish to acknowledge and thank the California Energy Commission for supporting this research, Award No, EPC-14-027.

I would like to express my sincerest gratitude to Dr. Janbozorgi for his willingness to engage in many technical discussions, and for his altruistic help with my research. I am greatful for his insightful comments, review, and skepticism. Dr. Janbozorgi was co-authored in much of my published work and submitted publications, as indicated in my VITA, all of which are relevant to this dissertation. His enthusiasm and passion for thermodynamics had lasting effects.

I am grateful for the endless help, love, support, and encouragement of my parents (Nadia Mouassess and Waleed Houssainy) and all my siblings (Suzanne, Omar, Hend, Samar, and Mariam Houssainy), which they offered throughout my graduate study. In addition, I would like to thank my lab mates (Mohammad Janbozorgi, Aysan Rangchian, Elaheh Alizadehbirjandi, Kelly Connelly, Peggy Ip, Walid Ismail, Ariana Thacker, Alireza Mohammad Karim, and Sahar

Andalid) for creating a family environment within the lab. My lab mates allowed for fruitful discussions and much needed mental support throughout my research endeavor.

Last but not least, I would to thank the love of my life, Dana Pickett, for her relentless support these past years. I am indebted by Dana's patience with me. Her boundless love was the anchor of my emotional wellbeing and motivation.

# VIT

**Education**

Master of Science in Mechanical Engineering
University of California, Los Angeles (June, 2015)

Bachelor of Science in Mechanical Engineering, summa cum laude
University of California, Los Angeles (December, 2013)

Associates of Science in Engineering
Saddleback College (June 2011)

**Professional Experience**

National Renewable Energy Laboratory (November 2017 - Present)
Research Engineer

UCLA Fluid Mechanics and Aerodynamics Lab (March 2015 – June 2015)
Teaching Assistant

L3 Communications Electron Technologies Inc. (June 2013 – December 2013)
Mechanical Engineering Internship

**Publications**

1. Sammy Houssainy, Mohammad Janbozorgi, Peggy Ip, Pirouz Kavehpour, Thermodynamic Analysis of a High Temperature Hybrid Compressed Air Energy Storage (HTH-CAES) System, Renewable Energy, Available online 12 September 2017, ISSN 0960-1481, https://doi.org/10.1016/j.renene.2017.09.038.

2. Ip PP, Houssainy S, Kavehpour. Modeling of a Low Cost Thermal Energy Storage System to Enhance Generation From Small Hydropower Systems. 2017, ASME Power Conference, doi:10.1115/POWER-ICOPE2017-3684

3. Houssainy, S Baghaei Lakeh R., Kavehpour, H.P., 2016, A Thermodynamic Model of High Temperature Hybrid Compressed Air Energy Storage System for Grid Storage, Paper No. PowerEnergy2016-59431, Proc. of 2016 ASME Int. Conference on Energy Sustainability Charlotte, NC

4. Baghaei Lakeh R., Villanava, I., Houssainy, S., Anderson, K., Kavehpour, H.P., 2016, Design of a Modular Solid-Based Thermal Energy Storage for a Hybrid Compressed Air Energy Storage System, Paper No. PowerEnergy2016-59160, Proc. of 2016 ASME Int. Conference on Energy Sustainability Charlotte, NC

5. Houssainy, S, Kavehpour, H.P., (2015), "Free Surface Profiles of Evaporative Liquids at the Vicinity of the Contact Line", Journal of Coating Technology and Research. VOL 12, Issue 5, Pages: 863-867

**Submitted Publications**

6. Houssainy, S, Janbozorgi, M, Kavehpour, H.P., (2017), "Thermodynamic Performance and Cost Optimization of a Novel Hybrid Thermal-Compressed Air Energy Storage System Design", 2017, *Journal of Energy Storage*

7. Houssainy, S, Janbozorgi, M, Kavehpour, H.P., (2017), "Performance of an Isobaric Hybrid Compressed Air Energy Storage System at Minimum Entropy Generation", *International Journal of Energy Research*

8. Houssainy, S, Janbozorgi, M, Kavehpour, H.P., (2017), "Theoretical Performanice Limits of an Isobaric Hybrid Compressed Air Energy Storage System", *Journal of Energy Resources Technology*

**Patents**

"*LOW COST HYBRID ENERGY STORAGE SYSTEM* ", Application Number: PCT/US2016/050819, Publication number: WO2017044658, Publication Date: 3/16/2017

**Presentations**

1. Houssainy, S, Janbozorgi, M, Kavehpour, H.P., (2017), "Thermodynamic Performance and Cost Optimization of a Hybrid Thermal Compressed Air Energy Storage System", *Off Shore Energy Storage Conference, Cape Cod, MA*

2. Houssainy, S, Lakeh, R. B., Kavehpour, H.P. (2016). "A Thermodynamic Model of a High Temperature Hybrid Compressed Air Energy Storage System for Grid Storage", *Proceedings of the ASME international conference on Power and Energy, Charlotte, North Carolina,* 2016

3. Lakeh, R. B., Villazana, I., Houssainy S., Anderson, K., Kavehpour, H.P. (2016). "Design of a Modular Solid-Based Thermal Energy Storage for a Hybrid Compressed Air Energy Storage System", *Proceedings of the ASME international conference on Power and Energy, Charlotte, North Carolina,* 2016

4. Houssainy, S, Kavehpour, H.P "Free surface profile of evaporative liquids at the vicinity of the contact line" *67th Annual meeting of the APS Division of Fluid Dynamics, San Francisco, CA,* 2014

5. Houssainy, S, Kavehpour, H.P "Free surface profile of evaporative liquids at the vicinity of the contact line" 17th *International Coating Science and Technology Symposium, San Diego, CA,* 2014

**Awards & Scholarships**

1. UCLA Dissertation Year Fellowship, for Exceptional Doctoral Accomplishments (2017)
2. UCLA Mechanical and Aerospace Engineering Departmental Fellowship (2014-2015)
3. The Boeing Company Scholarship, for Outstanding Achievements in Mechanical Engineering (2012)
4. Saddleback College Mathematics Scholarship Award (2011)

# Chapter 1: Introduction

Increased awareness of the threatening environmental effects of fossil fuel emissions, and the rising concern over global warming is accelerating incentives to harness and integrate sustainable sources of energy in our existing infrastructure. The price of photovoltaics and wind turbines are drastically reducing with time, with a convincing projection in the same direction. Conversely, the continued depletion of our limited supply of fossil fuels, a commodity, inevitably and persistently increases their price. Therefore, in addition to environmental protection incentives, eventually fossil fuels will become economically illogical and the effort to advance our sustainable energy supply is imperative for a prosperous future. However, renewable power is inherently chaotic by nature, and our efforts of increasing their integration is hindered by the challenges associated with their intermittency [1-6]. To solve this problem, the general consensus is to incorporate large-scale energy storage systems, which would serve to store the low quality (fluctuating) power, and provide high quality (smooth) and dispatchable power based on consumption needs. [7-11]

As compared with chemical energy storage (batteries), mechanical energy storage systems, such as compressed air energy storage (CAES), pumped hydro storage (PHS), and flywheels are generally capable of more cycles, their efficiencies remain persevered, and they are more suitable of large-scale applications, with the exception of flywheels. However, among the mechanical system, PHS requires stricter geological locations and requires higher maintenance and capital costs as compared with CAES systems, therefore rendering CAES most suitable for renewable integration [12-15]. Three types of CAES systems have been extensively investigated in the literature: diabatic (D-CAES), isothermal (I-CAES), and advanced adiabatic (AA-CAES)

[16-21]. In conventional, or diabatic, CAES the exergy portion associated with compression heat is not utilized and destroyed, which is detrimental to its performance. The only two existing CAES systems in the world are based on the diabatic method. Furthermore, natural gas is used as an external heat source, providing up to 60% of the total output energy, contingent upon the fuel conversion efficiency. Therefore, diabatic CAES is more properly classified as a mutual power generation and energy storage system [22-23]. For these reasons, significant efforts have been devoted towards I-CAES and AA-CAES, which address the drawbacks of conventional CAES systems by avoiding the use of fossil fuels, and enhancing their performance.

Through high heat transfer rates, Isothermal CAES intends to isothermally compress and expand the air. I-CAES is advantageous, as it minimizes compression work and eliminates the need for combustion emissions. However, its major drawback results from the exceedingly high storage pressures necessary for adequate energy densities [24-27]. Several methods have been proposed that aim to achieve isothermal compression conditions. Hydro-pneumatic energy storage (HyPES) is one common type, where a liquid performs the air compression process. Hydraulic oils are most commonly investigated in HyPES, due to their high heat capacity and stability at high pressures [28-29]. Recent works investigate the spraying of water, in a reciprocating piston, as a means of collecting the generated heat of compression while minimizing the rise in air temperature. The warm water is then used similarly to minimize the drop in air temperature during expansion. Research and development efforts of such machinery must be undertaken, which would need to tolerate moisture [30]. In addition to water, foam has also been investigated for enhanced heat transfer [31].

Another CAES derivative, which also eliminates combustion emissions, is the advanced adiabatic type. Unlike D-CAES, where the compression heat is wasted and natural gas combustion is used as a heat source, in AA-CAES the compression heat is stored and reused as a heat source during expansion. The simplest AA-CAES architecture, which reuses the compression heat, is achieved by storing the hot compressed air itself in a temperature resilient air storage medium [32]. Alternatively, a common method is to store the heat separately, in a thermal energy storage medium, which would require less thermally resistant air storage methods. The performance of AA-CAES with a separate thermal storage unit increases with storage temperature, as demonstrated by several investigations in the literature [33-39]. However, the low exhaust temperatures of available compressors in the market limit the performance and energy density of AA-CAES systems [40-47].

The hybrid thermal and compressed air energy storage (HT-CAES) system, presented in this research, addresses the drawbacks of conventional and AA-CAES systems. Contrary to D-CAES and similar to AA-CAES, in HT-CAES the combustion emissions are mitigated through the utilization of compression heat. However, Unlike AA-CAES, the need for high temperature compressors is eliminated in HT-CAES, by storing electrical power directly in the form of heat through joule heating, therefore reaching high temperatures prior to expansion. Therefore, HT-CAES allows for both high energy densities and efficiencies. The separation of energy between thermal and compressed air energy storage allows for lower storage pressures and volume, as the additional heat increases the capacity of the system. Consequently, increased flexibility associated with the HT-CAES allows for a reduction in geological restrictions. In addition, compressors typically require a constant input power, corresponding to their design point, for optimal performance. Therefore, low quality, fluctuating, and highly intermittent renewable

power signals that are inapplicable for compressors can be utilized through direct conversion to heat, which further increases the capacity of the HT-CAES system. In HT-CAES, part of the available energy is spent on compressing the air, and the rest is directly converted to heat and stored in a High temperature Thermal Energy Storage (HTES) medium. An HT-CAES configuration is presented that includes a turbocharger on the discharge side, which provides supplementary mass flow rate alongside the air storage. Through this analysis it is illustrated that the addition of a turbocharger has the potential of drastically reducing the storage volume and pressure, which reduces the system complexity and cost, in addition to eliminating the need for multistage compression and expansion.

It will be demonstrated that the hybrid design has the following major advantages over an advanced adiabatic design: 1) Assuming identical machinery and air storage sizes, the hybrid design can provide additional output power through the extra stored heat, which would be neglected otherwise in an advanced adiabatic design, 2) The necessary air storage volume/pressure can be reduced due to the increased thermal storage capability, which alleviates the geological constraints of the plant, 3) the complexity is reduced by mitigating the need for high temperature compressors, 4) it is shown that with increased dependence on thermal storage the system cost is reduced.

An overview of the current energy storage technologies and a motivation behind compressed air energy storage systems is provided in chapter 2. In chapter 3, an HT-CAES system is investigated and the thermodynamic efficiency limits within which it operates are investigated. The efficiency of the HT-CAES system is compared with its Brayton cycle counterpart, in the case of pure thermal energy storage (TES). It is shown that the efficiency of the HT-CAES plant is not bound by the Carnot efficiency and always higher than that of the

Brayton cycle, except for when the heat losses following compression rise above a critical level. The results of chapter 3 demonstrate that the HT-CAES system has the potential of increasing the efficiency of a pure TES system, executed through a Brayton cycle, at the expense of an air storage medium.

Chapter 4 is based on my published work [38], which presents a realistic and simple hybrid configuration that incorporates two stages of heating through separate low-temperature and high temperature thermal energy storage units. A thermodynamic analysis of the HT-CAES system is presented along with parametric studies, which illustrate the importance of the operating pressure and thermal storage temperature on the performance of the storage system. Realistic isentropic component efficiencies and throttling losses were considered. Additionally, two extreme cavern conditions were analyzed and the cyclic behavior of an adiabatic cavern was investigated. An optimum operating pressure resulting in maximum roundtrip storage efficiency of the hybrid storage system is reported.

In chapter 5, a modified hybrid design is investigated which includes a turbocharger in the discharge process. This addition has the potential of drastically decreasing the necessary storage volume and pressures, with a compromise in storage capacity. The cost of thermal storage is substantially lower than the cost of air storage, per kilowatt-hour [48]. However, a heat engine is theoretically lower in efficiency than a CAES plant. Therefore, with increased reliance on thermal storage, through the turbocharger, the HT-CAES system cost and efficiency are anticipated to decrease. The results of this work provide an efficiency and cost map of the HT-CAES system versus both the operating pressure and the distribution of energy, between thermal and compressed air storage. This research illustrates and properly quantifies a tradeoff that exists between the HT-CAES system cost and performance. Both roundtrip energy and exergy

efficiencies are quantified, presented, and compared. Lastly, a local optimum-line of operation, which results in a local maximum in efficiency and a local minimum in cost, is presented.

In chapter 6, an internally reversible and irreversible HT-CAES system is investigated and optimized according to a minimum entropy generation criteria. Regenerative and non-regenerative configurations are investigated. It is shown that an HT-CAES system designed to achieve minimum entropy generation may operate at a lower energy and exergy efficiency, and lower output power, than otherwise achievable. Chapter 6 illustrates that minimization of entropy generation does not always coincide with minimization of energy losses in a hybrid compressed air energy storage system. Only under certain conditions does the point of minimum entropy generation coincide with maximum energy efficiency. Specifically, this occurs only when the input energy, thermal energy storage mass, specific heat, and temperature swing, are a constant. Similarly, only in the specific case where the total input exergy is a constant, does the minimum entropy generation coincide with maximum exergy efficiency. In chapter 7, an exergy analysis of the hybrid system is presented. The calculated and normalized exergy destruction maps provide a means of comparing the component exergy destruction magnitudes for assessing and pinpointing the sources of largest irreversibilities. In addition to the exergy destruction, the exergetic component efficiencies are also presented and compared. Both component exergy destruction and their exergetic efficiencies demonstrate that the largest source of avoidable exergy destruction result from the irreversibilities associated with throttling and the irreversibilities associated with mixing losses within the air storage medium.

# Chapter 2: Energy Storage Overview

## 2.1 Introduction

The integration of energy storage into our electrical grid has numerous advantages. First and foremost, energy storage is an enabling technology, which would allow for increased penetration and utilization of renewable sources. In addition, large-scale, efficient, and reliable energy storage can be used during low demand/price periods to store cheap electricity from conventional power generation systems and provide the electricity during high/expensive periods, which allows for participation in energy arbitrage. Furthermore, energy storage creates a safer and more resilient electrical grid, which is capable of withstanding sudden and unexpected failures and blackouts.

Current energy storage systems can be generally categorized into 1) mechanical (which includes CAES, PH, and flywheels, 2) thermal (which includes latent heat, sensible heat, and thermochemical), 3) electromagnetic (which includes capacitors and super-conducting magnetic), and 4) chemical (such as batteries, and hydrogen) [48]. The energy storage systems that are most suitable for large-scale applications are compressed air and pumped hydro energy storage. Compressed air energy storage however has fewer geological restrictions and lower costs, rendering it more attractive as compared with pumped hydro. [49-54]

Various CAES concepts are being investigated and under research and development, which are intended to solve the environmental issues associated with their conventional design. Advanced adiabatic, is one such example, which includes a thermal storage unit that is intended to store the generated heat of compression for subsequent use during the discharge process. [55-57]. Alternatively, isothermal types aim to minimize the heat generated during compression, which is typically achieved by spraying water during compression to allow for high heat transfer

rates, thus maintaining nearly constant temperatures during both charge and discharge processes [53]. Underwater CAES, as the name entails, represents the idea of storing the compressed air underwater, typically through the use of bags, which maintains isobaric conditions using hydrostatic pressure [58-63].

The existing CAES technologies and those investigated in literature, rely on high storage pressures for adequate energy densities. This introduces inherent component complexities, strict geological locations, as well as increased production and maintenance costs. Moreover, conventional CAES system rely on the combustion of natural gas as a heat source, therefore produce global warming emissions. The novel hybrid thermal and compressed air energy storage, the subject of this dissertation, solves both conventional CAES problems regarding high-pressure operations and global warming emissions, by storing energy in the form of compression and directly in the form of heat. This has the advantage of eliminating the need for an external heat source, mitigating the geological restrictions, in addition to increasing the storage capacity of the system. The various available energy storage technologies are discussed in detail in this chapter, in addition to numerous CAES derivatives. Comparing the system with various CAES derivatives naturally motivates the hybrid thermal and compressed air energy storage system. Moreover, different types of air storage mediums are discussed.

## 2.2 Current Energy Storage Technologies

Increased integration of renewable sources of energy, particularly photovoltaics, has a clear effect and consequence on the electrical grid, and undoubtedly demonstrates the necessity and motivation behind the utilization of energy storage. The so-called “Duck Curve” is a plot of the net load on the electrical grid as a function of time, in the span of a full day. A typical plot of the duck curve is shown in Figure 1, as provided by the California Independent System Operator

[64]. During the morning hours, a relatively steady supply of power is necessary to meet the demand. However, as time progress, leading to increased solar irradiation, and with increased integration of renewable sources into the electrical grid to utilize the irradiation, the demand for electricity is substantially reduced. This reduction in electricity demand during the day is projected to drastically decrease as more photovoltaics are integrated and utilized. However, eventually a sharp increase in demand results during the evening hours, as solar irradiation subsides, and the electrical demand is increased as most return to their homes and require energy needs.

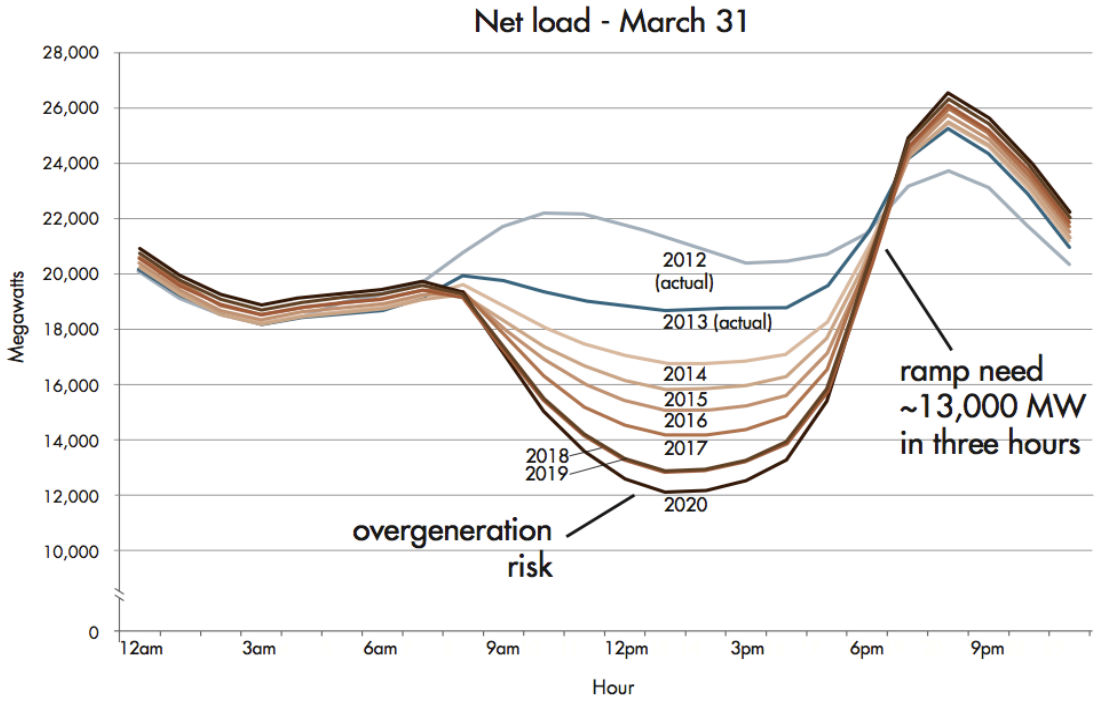


**Figure 2.1: The duck curve: Net Load profile in a typical day provided by the California independent system operator[64]**

The duck curve, illustrated in Figure 1, illustrates a need for various energy storage applications, as we increase our dependence on renewable sources and reduce our depletion of fossil fuels. First, a large-scale bulk energy storage system is required to store excess power generated during the peak day hours, and provide the stored energy during the evening hours

when supply is low and demand is high. Second, an energy storage system with short/quick start-up times is necessary, which is capable of following the ramp-up in demand leading to the evening hours. The Table below summarizes important technical parameters of some current and common energy storage technologies.

**Table 2.1: Energy Storage Technology Specifications [65]**

| | **Lead-acid batteries** | **Li-Ion batteries** | **NaS batteries** | **Flow batteries** | **Flywheel** | **Pumped hydro** | **Conv. CAES** |
|---|---|---|---|---|---|---|---|
| System Power Output (kW/MW) | ≤10 MW | ≤10 MW | ≥100 MW | 25 kW–10 MW | 100 kW–200 MW | ≥200 MW | ≥200 MW |
| Discharge time | 4 hr | 6 hr | 4 hr | 4 hr | 15 min | >10 hr | >10 hr |
| Lifetime (years) | 3-10 | 10-15 | 15 | 5-15 | 20 | 30+ | 30+ |
| Lifetime (cycles) | 500-800 | 2000-3000 | 4000-40,000 | 1500-15,000 | ≥100,000 | ≥50,000 | ≥10,000 |
| Round-trip efficiency | 70%-90% | 85%-95% | 80%-90% | 70%-85% | 85%-95% | 75%-85% | 45%-60% |
| Capital cost per discharge power ($/kW) | $300-$800 | $400-$1000 | $1000-$2000 | $1200-$2000 | $2000-$4000 | $1000-$4000 | $800-$1000 |
| Capital cost per capacity ($/kWh) | $150-$500 | $250-$1500 | $125-$250 | $350-$800 | $1500-$3000 | $100-$250 | $50-$150 |
| Levelized cost of electricity ($/kWh) | $0.25-$0.35 | $0.10-$0.45 | $0.05-$0.15 | $0.15-$0.25 | $0.2-$0.9 | $0.05-$0.15 | $0.10-$0.20 |

It is important to note that other technologies, such as batteries, have substantially lower discharge times, which limits their applications. The discharge time and energy capacity, or power output, predominantly dictates the type of applications suitable for each energy storage

system. Figure 2 below is more of a visual demonstration of where energy storage technologies stand. Compressed air energy storage and pumped hydro are the highest in terms of discharge time and power capacity, this makes them very suitable for large-scale, utility, applications [66]-[69]. Pumped hydro requires specific geological applications, which can be hard to come by. Compressed air energy storage has the potential to utilize promising geological sites in the form of underground salt deposits, which can be leached to form salt caverns, or underground rock formations. However, compressed air energy storage can also use large tanks above grounds. As compared with pumped hydro storage, CAES has fewer geological restrictions, therefore rendering CAES as the most promising for large scale energy storage applications.

### 2.3 Types of Compressed Air Energy Storage

When air is compressed adiabatically from ambient conditions, both pressure and temperature are increased. Therefore a substantial portion of the input energy, used to operate a compressor, is converted to heat, as significantly high temperatures can be reached particular at high compression ratios. Multi-stage compression, coupled with intercooling, is often utilized to control the drastic increase in temperature during compression. However, the lost heat can be quite detrimental on the performance of the storage system, unless the generated compression heat is scavenged for later use during the discharge process. The manner in which the heat of compression is managed precisely dictates the three types of compressed air energy system, diabatic, isothermal, and advanced adiabatic compressed air energy storage. [67-69]

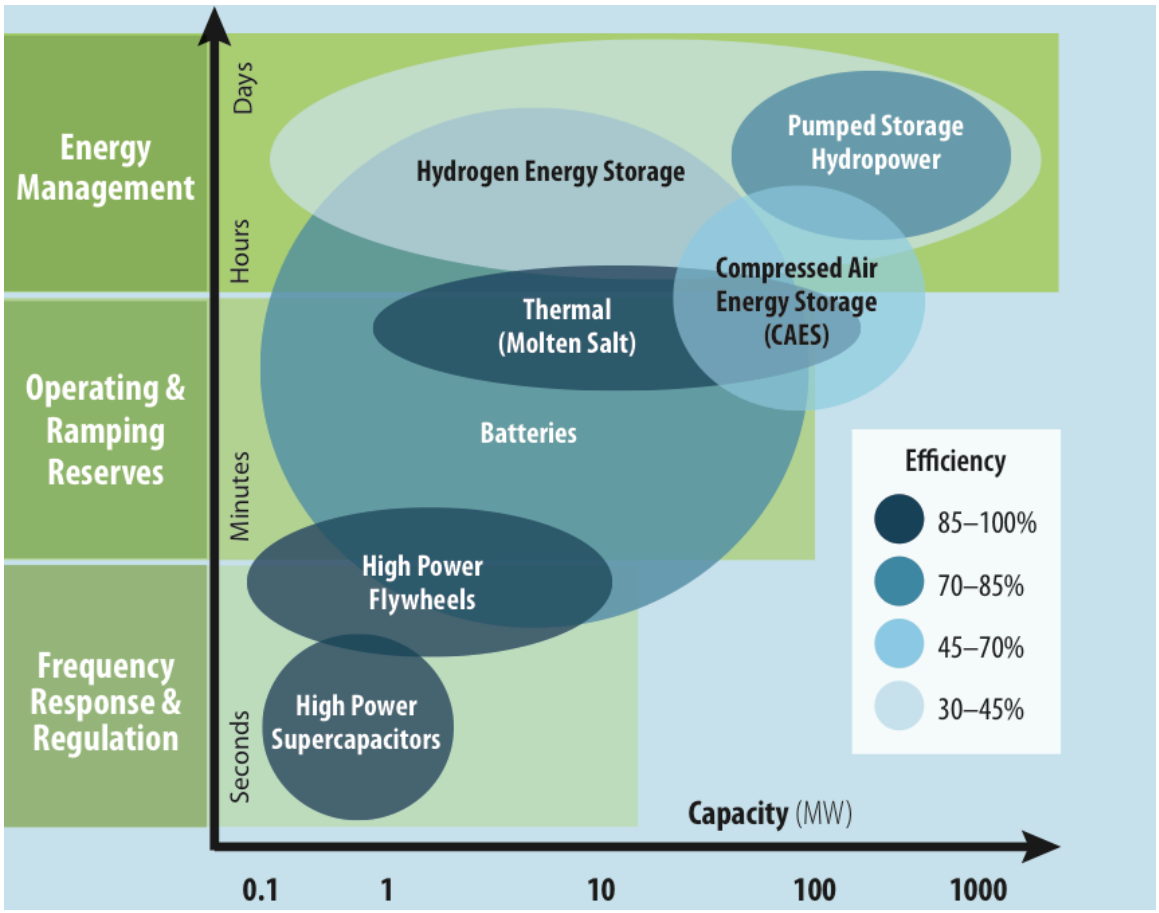


**Figure 2.2: Discharge Versus Capacity of Current Energy Storage Technologies [70]**

### 2.3.1 Isothermal

In isothermal compressed air energy storage, the objective is to minimize any increase in temperature during the compression process. Fundamentally, this is achieved by very high heat transfer rate, as a significant portion of the compression energy is converted directly to heat. Therefore, specific compressor designs are necessary to achieve such conditions. Theoretically, isothermal compression can be achieved through a high number of compression stages and respective intercooling heat exchangers. However such architecture is impractical and results in significant pressure losses and costs. Several other means of achieving near isothermal compression have been suggested. Of the more attractive proposals, one seeks to spray water in

the compression chamber, which allows for high heat transfer rates, considering the high specific heat of water and the high surface area of a droplet [71], [72].

### 2.3.2 Advanced Adiabatic

The major premise in an adiabatic design is to utilize the generated heat of compression, during the charge process, for later use during the discharge process. Theoretically this results in higher roundtrip efficiencies, as this configuration would not intentionally waste the invested compression power associated with heat. An advanced adiabatic design typically requires the use of an external thermal energy storage system, which captures the generated heat during the compression process, and supplies the heat to the air stream during the expansion process. The thermal energy storage medium could be a fluid, such as oil. In which case the oil is circulated as a heat carrier fluid for intercooling during compression, and reheating during expansion.

### 2.3.3 Diabatic

The only two existing compressed air energy storage plants in the world, located in Huntorf, Germany, and in McIntosh, Alabama, are both based on the diabatic method. In diabatic compressed air energy storage, multi-stage compression coupled with intercooling heat exchangers are utilized to control the significant rise in temperature of the compressor exhaust. The collected heat of compression is however not utilized and dissipated into the environment. This dissipation of compression heat significantly hinders the performance diabatic designs. Important specification of the two existing CAES plants is provided in Table 2.

**Table 2.2: Specifications of The Two Existing CAES Plants [73], [74], [75]**

| Data of Operational CAES plants | | |
|---|---|---|
| | Huntorf | Mcintosh |
| Power In | 60MW | 51MW |
| Charge Time | 8hrs | 51hrs |
| Power Out | 350MW | 110MW |
| Discharge Time | 2hrs | 26hrs |
| Cavern Volume | 310,000$m^3$ | 540,000$m^3$ |
| Max Pressure | 72bar | 75bar |

## 2.4 Compressed Air Energy Storage Thermodynamic Cycles

Conventional compressed air energy storage systems are cost effective, however their wasted heat of compression hinders their performance. In advanced adiabatic systems, the generated heat of compression during the charge process is stored in thermal energy storage (TES) unit for later use during the discharge process. These TES units consist of a thermal transport fluid, a heat exchanger, a heat reservoir, and an auxiliary circulation pump, as shown in Figure 3.

The higher theoretical performance limits associated with an advanced adiabatic design have made it an attractive alternative to conventional compressed air energy storage systems. However, advanced adiabatic systems suffer from increased capital cost and implementation complexity. This is the main reason why advanced adiabatic designs are not commercially available. Neither one of the only two existing compressed air energy storage plants are based on an advanced adiabatic design.

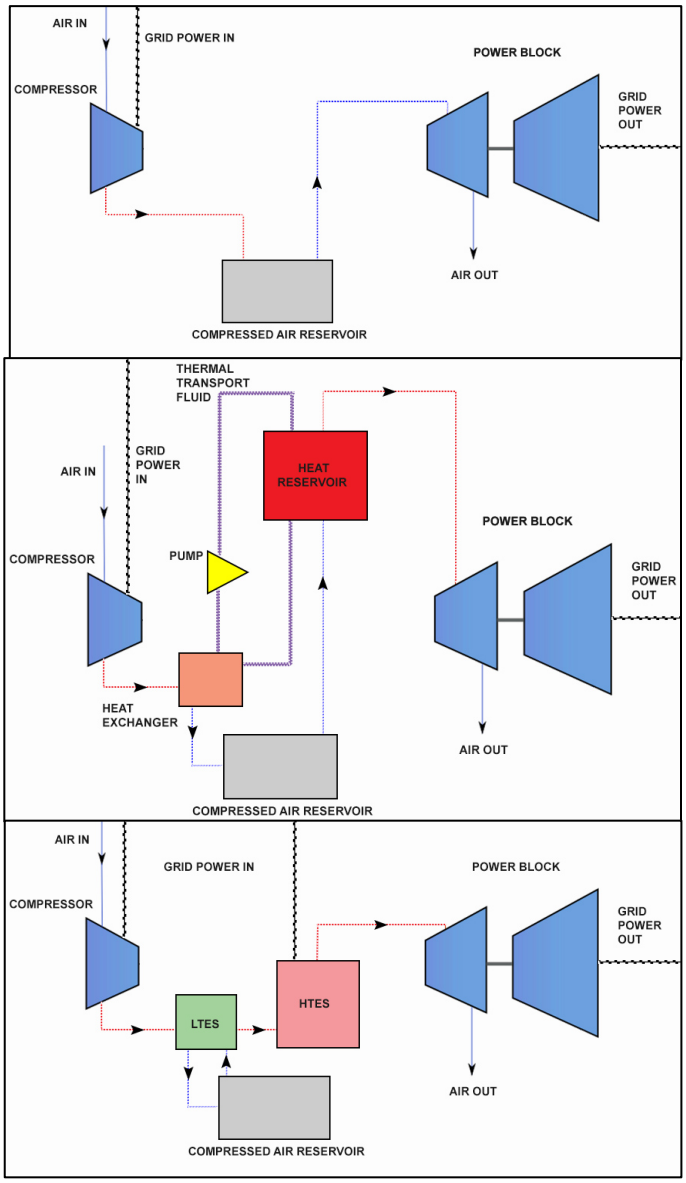


**Figure 2.3: Top) Conventional CAES. Middle) AA CAES system. the TES unit consists of the thermal transport fluids, heat exchanger, heat reservoir and pump. Bottom) HTH-CAES system with LTES and HTES units used to reheat compressed air**

The compromise between CAES and AA-CAES is the hybrid thermal and CAES (HT-CAES). In the hybrid system, the TES is replaced with low and high temperature thermal energy storage units, as shown in Figure 3. As in the thermal storage unit of an advanced adiabatic deign, the

low temperature thermal energy storage (LTES) unit stores the heat generated during air compression. But unlike TES, the high temperature thermal energy storage (HTES) unit acts as a scalable energy reservoir without the complexity of a thermal transport fluid or recirculation pumps. The HTES unit takes advantage of the high thermal capacity of an inexpensive thermal medium to store heat that will later be used to superheat the compressed air. HT-CAES allows for the addition of grid energy directly to the HTES through thermoelectric heaters to achieve temperatures much higher than traditional CAES and AA-CAES, paving the way for a new class of energy storage systems.

With the addition of a HTES unit, the workload is shifted from pure compression to thermal storage. This separation of energy storage between compressed air and thermal storage has the effect of expanding the energy capacity of the compressed air system without the need to increase the air pressure or air storage capacity. HTES allows the system to be dynamically scaled up or down as the load leveling demand changes without any structural change in system configuration. More importantly, since the energy storage reservoir is now split between air compression and thermoelectric heaters, the working fluid does not need to be compressed to the same pressures as in an AA-CAES system to achieve the same energy output. Using a smaller compression ratio, far less energy is lost due to non-adiabatic conditions. That has the added benefit of allowing the LTES unit to be much less expensive than a traditional adiabatic system since the requirements are much lower. This advancement in compressed air technology will allow HT-CAES systems to perform as well as a much larger and more complex AA-CAES system, while costing approximately the same as a small conventional CAES system.

The P-v and T-s diagrams, for the three different CAES systems, are provided in Figure 4, where (a) and (c) correspond to the charge process, and (b) and (d) correspond to the discharge

process. For the same output power, the HT-CAES system needs the least amount of energy charged into compression while the conventional CAES system requires the most. As shown in 4(b) and (d), the HT-CAES delivers the most amount of energy during the discharge cycle due to the HTES unit being an abundant source of energy, while the AA-CAES system has the least, being limited by the amount of energy stored purely during compression.

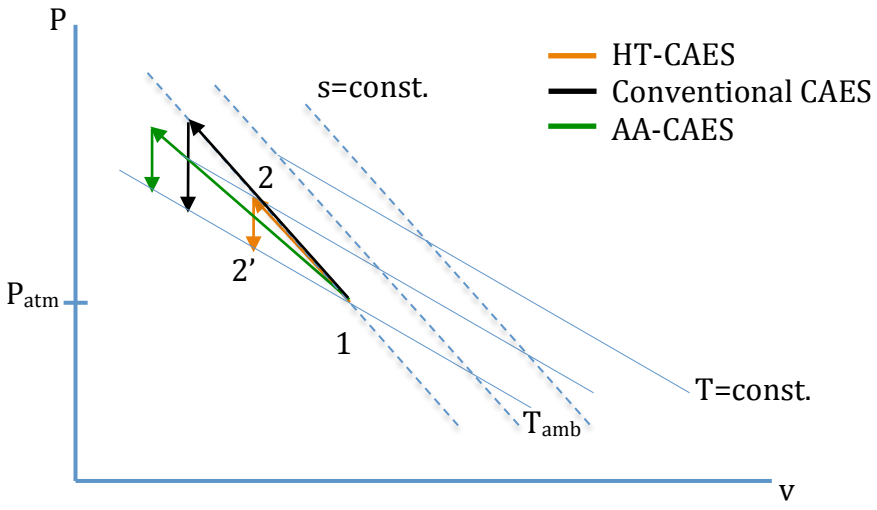


(a)

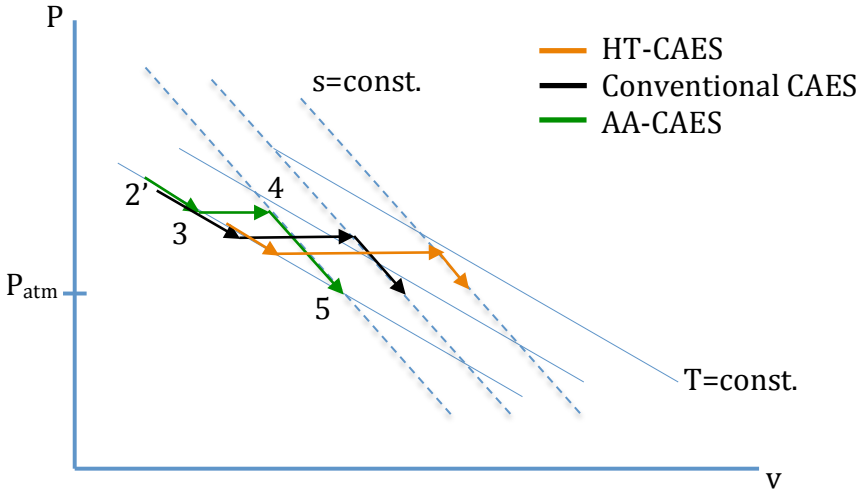


(b)

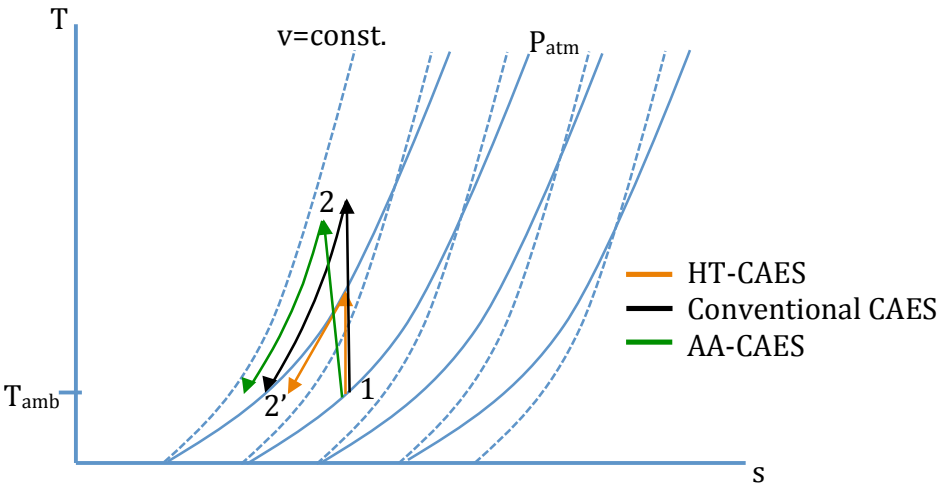


(c)

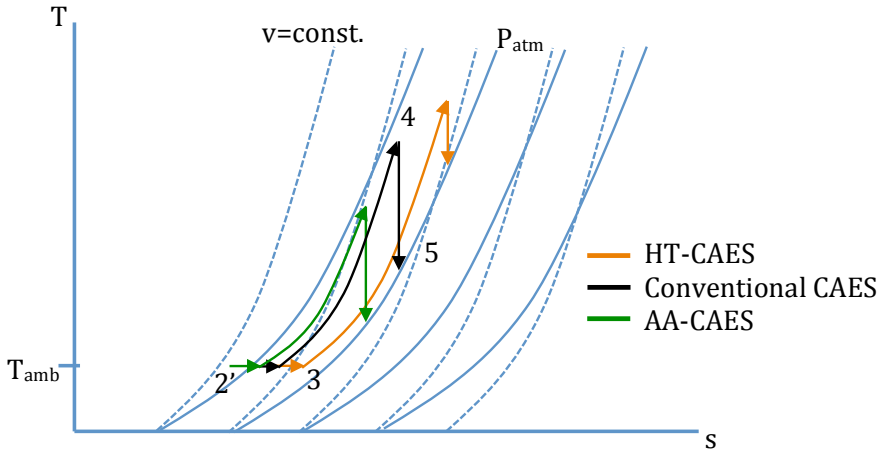


(d)

**Figure 2.4: a) The P-v diagram of the charge cycle (comparison of HT-CAES, AA-CAES and Conventional CAES) b) The P-v diagram of the discharge cycle c) T-s diagram of the charge cycle d) T-s diagram of the discharge cycle**

A detailed quantitative analysis and comparison of the hybrid storage system with an advanced adiabatic design is provided in chapter 4.

## 2.5 Air Storage Types

There are two different types of underground air storage, or caverns, 1) isobaric storage (constant pressure), and 2) isochoric storage (constant volume), or sliding pressure. For both

types of underground storage, both naturally occurring and man-made underground caverns can be used. The details of both are described next and illustrated in Figure 5.

### 2.5.1 Sliding Pressure Storage

In a sliding pressure storage, the volume of the cavern or air storage remains constant and the air pressure increases during the charge process, and decreases during the discharge process. In order to maintain a constant pressure during the discharge process of the storage cycle, the pressure is throttled to the operating pressure dictated by the optimal performance of the turbine. Through throttling, the output power provided by the plant remains constant and independent of the state of charge. This architecture suffers from throttling losses. Isochoric, sliding pressure, underground caverns are typically constructed in underground salt deposits through a leaching process. a drilling process allows water to dissolve the salt in the underground deposit, which is then pumped back up, eventually resulting in a cavern. Both existing plants in Huntorf, Germany and Alabama use a sliding pressure, isochoric underground salt cavern. An illustration of a sliding pressure underground cavern is provided in Figure 5. [75]

### 2.5.2 Constant Pressure Storage

In constant pressure storage, or isobaric storage. The cavern volume is typically increased or reduced in size during the charge and discharge process such that isobaric conditions are attained. Constant pressure storage is not used at the Huntorf or Alabama compressed air energy storage plants. Constant pressure storage cavern are typically constructed in under ground rock formations, where underground salt deposits are unavailable. To maintain isobaric conditions within the cavern, a water-equalizing pit is used and the depth of storage dictates the storage pressure, as specified by the hydrostatic pressure [75].

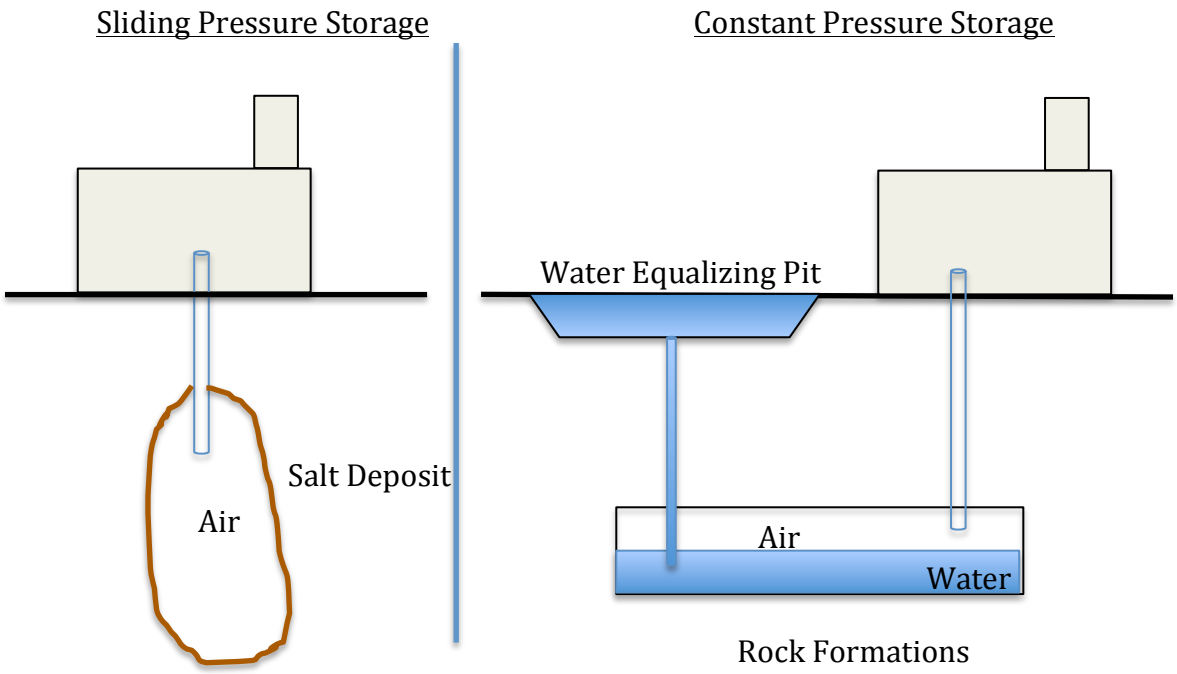


**Figure 2.5: Schematic of the two underground air storage types**

# Chapter 3: Theoretical Efficiency Limits of a Hybrid Thermal-Compressed Air Energy Storage System

## 3.1 Introduction

The thermal efficiency of reversible power cycles is given by the Carnot efficiency [76-80]. Moreover, the thermal efficiency of an irreversible power cycle is always less than the thermal efficiency of a reversible power cycle (the Carnot efficiency) when each operate between the same two thermal reservoirs [81-82]. Therefore, the Carnot efficiency provides an upper performance limit on power cycles. Additionally, the Carnot efficiency illustrates that power cycle efficiencies are always below 100%, assuming finite/non-zero reservoir temperatures. With such a theoretical constraint, the performance of power cycles can be meaningfully compared with the Carnot efficiency in contrast to a naive comparison with 100%. This way, no effort is wasted in attempting to achieve efficiencies very near or over the Carnot limit. Analysis techniques have been developed in various studies to consider the internal and/or external irreversibilities in heat engines [83-90].

A fraction of the stored energy in the hybrid thermal and compressed air energy storage system exploits heat-to-work energy conversion and utilization. Therefore, it is reasonable to assume that high thermal energy storage temperatures correlate with higher efficiencies, as is the case in heat engines. In addition, it is equally reasonable to assume that the roundtrip energy efficiency of the hybrid thermal and compressed air energy storage system is in someway influenced by the theoretical performance limit of heat engines; the Carnot efficiency. However, the Carnot efficiency provides a performance limit on power cycles or heat engines, where the input energy

is low quality heat and the product is high quality useful energy, or electricity. In the case of a hybrid thermal and compressed air energy storage plant, the system is defined as an energy storage machine where high quality electrical energy is stored, in another form, and later converted back to electricity. Therefore, the direct application of the Carnot efficiency on the hybrid energy storage system is inappropriate; nevertheless its influence is undoubtedly present as a portion of the stored energy in the hybrid system is retrieved from the stored heat by the thermal energy storage unit.

This chapter is an attempt to draw the fundamental thermodynamic efficiency limits within which a hybrid thermal CAES system operates, which has not been formerly reported. The thermodynamic models assume a constant pressure cavern, typically constructed in underground rock formation with a water equalizing pit to maintain isobaric conditions [91]. It is shown that the cavern under this assumption reduces to just a delay time in the operation of the plant. A constant volume cavern, on the contrary, changes the state of air through the cavern and has to be accounted for proper modeling of the plant. The novel premise of this work is to demonstrate and compare the fundamental differences and relationships between the efficiencies of a Hybrid CAES cycle with that of an analogous Brayton power cycle, in the case of pure thermal energy storage. Specifically, The efficiency of the hybrid CAES system is compared with a regenerative and non-regenerative Brayton cycle. This unique comparison illustrates the general and fundamental differences in the roundtrip cycle efficiency definitions associated with a heat engine, in the case of pure thermal energy storage utilizing a Brayton cycle, versus a hybrid CAES and their theoretical limiting values.

## 3.2 Model and Assumptions

The models considered in this chapter represent variations of a Hybrid Thermal Compressed Air Energy Storage (HT-CAES), in which part of the available input energy is spent on compressing the air into a storage medium, herein assumed to be a cavern, and the rest is directly converted to heat and stored in a Thermal Energy Storage (TES) medium. Through resistive heating, high temperatures can be achieved in the TES unit, therefore drastically increasing the capacity of the system. The maximum achievable temperature in the TES is dictated by material properties. An alumina based refractory can accommodate storage temperatures in excess of 1700C, and Nichrome wires can provide a continuous operating temperature of ~1680C. The nature of the TES is fundamentally different from the absorbed compression heat, which is either discarded in conventional CAES or stored and then utilized during expansion in advanced adiabatic CAES. The inclusion of the TES intentionally takes the state of the system off the compression isentrope and fundamentally introduces an upper Carnot-like limit on the efficiency of the plant. This is so that the advanced adiabatic CAES ideally aims for the best round-trip efficiency by trying to coincide the compression and expansion isentropes.

It is the aim of this chapter to quantify the performance of HT-CAES vs. the classical Brayton cycle, in the case of pure thermal energy storage, and discover its theoretical efficiency limits. Additionally, the influence of the Carnot limit on the performance of the Hybrid system is investigated. Therefore, to examine the upper performance limits, all components are assumed to be internally reversible and have perfect component performance indices, i.e. isentropic efficiency or heat exchanger effectiveness. Also, it is assumed that 1) the cavern is fully insulated and thus no heat losses are present, and 2) the cavern is isobaric during charge and

discharge processes. Therefore, the thermodynamic conditions of the air into and out of the cavern are the same and all the energy invested in charging the cavern is retrieved during the discharge process. Under these assumptions, the cavern is solely a buffer zone that introduces a delay time in the plant's operation. An analysis of the cavern under constant volume and constant pressure is also presented in this chapter.

### 3.3 HT-CAES vs. Brayton Cycle With Regeneration

To investigate the effect of temperature of the TES on the storage efficiency, a regenerative HT-CAES model is analyzed. Fig. 1(a) shows the HT-CAES configuration in which the compressor is not powered by the turbine, as opposed to the classical Brayton cycle shown in Fig. 1(b).

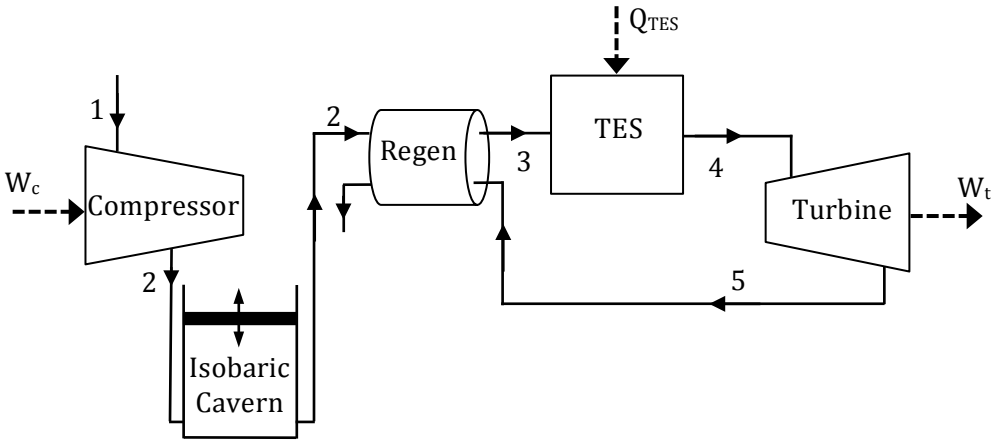


(a)

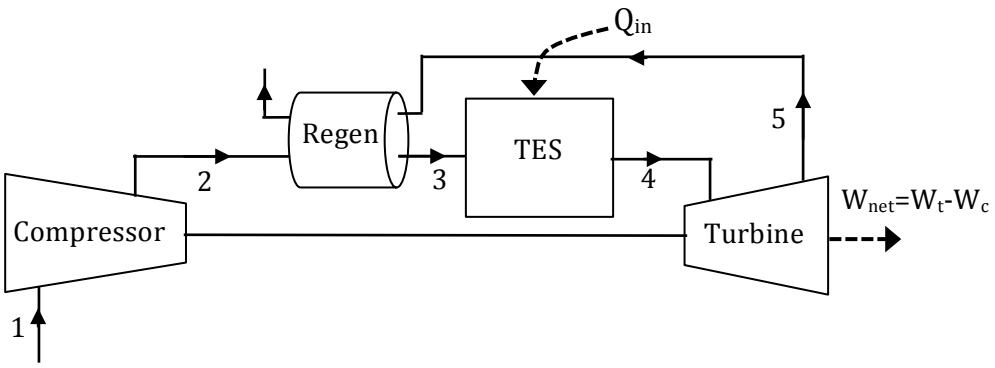


(b)

**Figure 3.1: (a) Hybrid Thermal & Compressed Air Energy Storage Configuration (With Regeneration), the compressor and turbine are decoupled (b) Brayton Cycle with regeneration (turbine and compressor are along the same shaft; the compressor is powered by the turbine)**

The round trip storage efficiency of the HT-CAES is given by

$$\eta_{HT-CAES,R} = \frac{\dot{W}_t}{\dot{W}_c + \dot{Q}_{TES}} \tag{3.1}$$

When the compressor has a compression ratio of $r$, and assuming a constant specific heat, equation (1) can be written

$$\eta_{HT-CAES,R} = \frac{T_4(1 - 1/r^{(k-1)/k})}{T_1(r^{(k-1)/k} - 1) + T_4(1 - 1/r^{(k-1)/k})} \tag{3.2}$$

Where $k$ is the ratio of the specific heats. Equation (2) can be further simplified as follows

$$\eta_{HT-CAES,R} = \frac{1}{1 + \frac{T_1}{T_4} r^{(k-1)/k}} \tag{3.3}$$

It can be shown that the efficiency of an ideal regenerative Brayton cycle, in the case of pure thermal energy storage, with the same compression ratio, $r$, and turbine inlet temperature $T_4$ is given by

$$\eta_{Bryaton,R} = 1 - \frac{T_1}{T_4} r^{\frac{k-1}{k}} \tag{3.4}$$

Eliminating $\frac{T_1}{T_4} r^{(k-1)/k}$ between equations (3) and (4) results in the following relationship between the round-trip efficiency of HT-CAES and the Brayton cycle efficiency:

$$\eta_{HT-CAES,R} = \frac{1}{2 - \eta_{Bryaton,R}} \tag{3.5}$$

One can see that equation (5) can be rewritten as follows:

$$\eta_{HT-CAES,R} - \eta_{Brayton,R} = \frac{\left(1 - \eta_{Bryaton,R}\right)^2}{2 - \eta_{Bryaton,R}} \geq 0 \tag{3.6}$$

Equation (5) illustrated that the efficiency of a regenerative HT-CAES system is always higher than that of a brayton cycle, in the case of pure thermal energy storage. Fig. 2 involves plots of both efficiencies, equations (3) and (4), versus the turbine inlet temperature for a compression ratio of 5, and Fig. 3 shows the plot of equation (5).

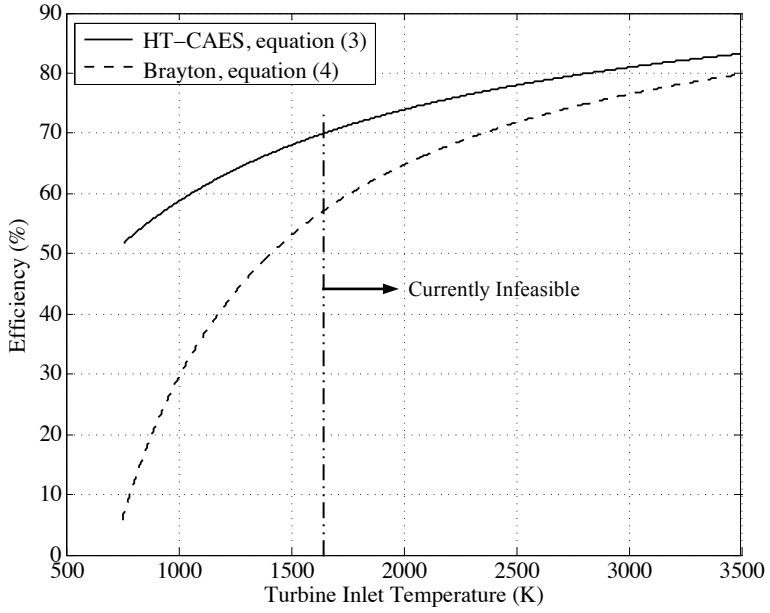


**Figure 3.2: Efficiency of a Hybrid Thermal and Compressed Air Energy Storage System and a Brayton Cycle with Regeneration Versus Thermal Storage Temperatures (compression ratio of 20 in both cycles)**

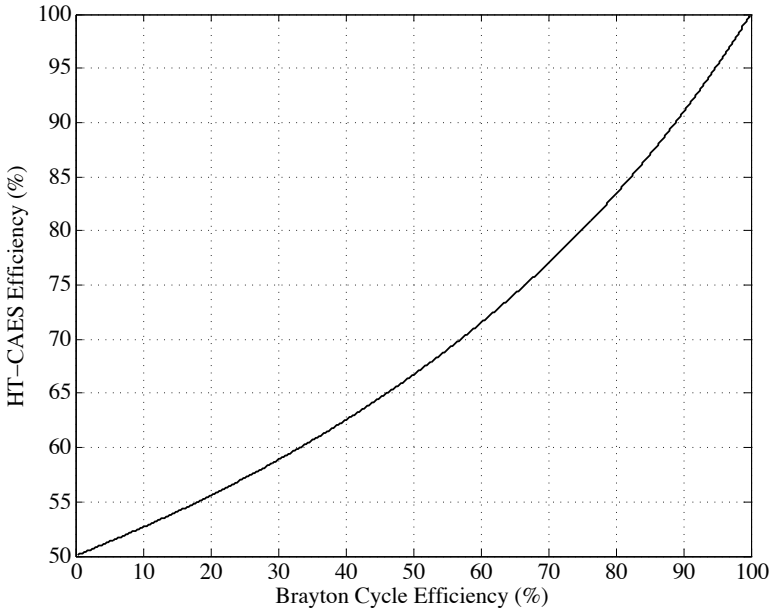


**Figure 3.3: Efficiency of an HT-CAES system versus the corresponding Brayton Cycle with Regeneration, equation (5)**

## 3.4 CAES vs. Brayton Cycle, Without Regeneration

### 3.4.1 No heat losses

A similar analysis is performed in the case of no regeneration. A similarly simplified and ideal configuration of the energy storage cycle with no regeneration given by Fig. 4a is analyzed and compared with a Brayton cycle, Fig. 4b. The configuration given by Fig. 4a assumes isentropic compression and expansion, for simplicity. As explained in section 2, the cavern is neglected under the assumption that no storage losses are present; therefore all energy invested in compression is retrieved during the discharge process. In the storage cycle in Fig. 4a, the turbine does not provide the compressor power, meaning all of the turbine power is available for useful work. In Fig. 4a the compressor and thermal storage power is provided by either the electrical grid, renewable sources or whatever power is available for storage. In contrast, the turbine is coupled with the compressor in the Brayton cycle in Fig. 4b.

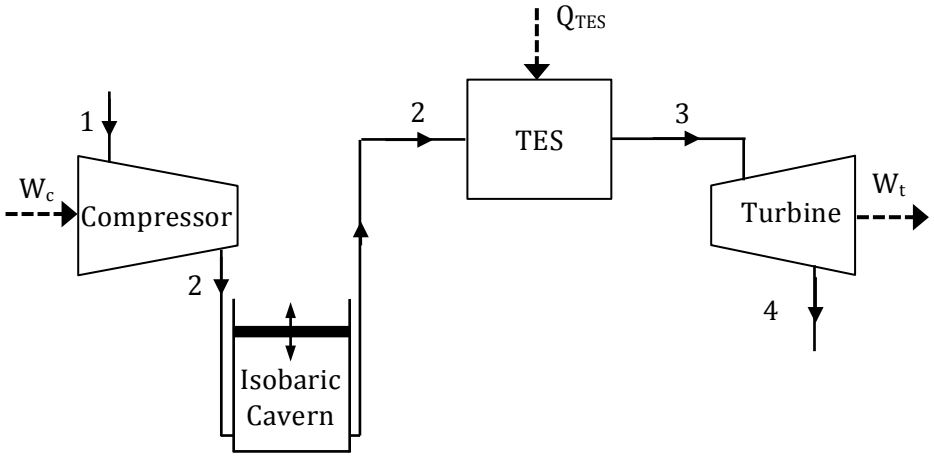


(a)

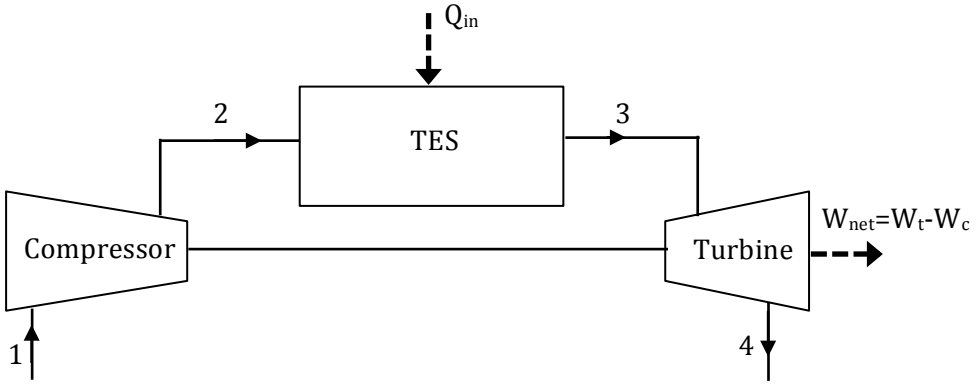


(b)

**Figure 3.4: (a) Hybrid Thermal and Compressed Air Energy Storage Configuration Without Regeneration (b) Brayton Cycle without regeneration**

The round trip efficiency of the simplified and ideal hybrid system given by Fig. 4a is given as

$$\eta_{HT-CAES} = \frac{\dot{W}_t}{\dot{W}_c + \dot{Q}_{HTES}} \tag{3.7}$$

which, assuming constant specific heat, can be simplified to get

$$\eta_{HT-CAES} = \frac{1 - T_4/T_3}{1 - T_1/T_3} \tag{3.8}$$

Keeping in mind that $\frac{T_4}{T_3} = \frac{T_1}{T_2}$ across the turbine and the compressor for isentropic processes, a little scrutiny reveals that the numerator of equation (8) is the Brayton cycle efficiency in Fig. 4b, while the denominator is the Carnot efficiency of the associated Brayton cycle. Equation (8) can therefore be rewritten as follows,

$$\eta_{HT-CAES} = \frac{1 - T_1/T_2}{1 - (T_1/T_2)\times(T_2/T_3)} = \frac{\eta_{Brayton}}{\eta_{Carnot}} \tag{3.9}$$

A sketch of the result given by equation (9) is illustrated in Fig. 5, which demonstrates that the process is 100% efficient when $T_3 = T_2$, meaning there is no heat addition provided by the thermal storage and the compression and expansion processes are along the same isentropic line. The addition of heat through the thermal storage takes the process off the compression isentrope and introduces the Carnot limit into the cycle. In the extreme of very high temperatures of thermal storage, i.e. when the balance between heat and isentropic work of compression shifts predominantly toward heat, the cycle is dominated by the Brayton cycle as the Carnot efficiency approaches unity. In another extreme where the energy put into thermal energy storage approaches zero and $T_3 = T_2$, HT-CAES reduces to an advanced adiabatic system with a theoretical round-trip efficiency of unity, as evident from equation (9). In this limit, where advanced adiabatic CAES aims to operate, the expansion isentrope coincides with the compression isentrope. When there is economic and technological justification, this limit is theoretically the most desirable zone of operation for energy storage/retrieval. One can therefore conclude that the efficiency of a non-regenerative HT-CAES cycle is 1) always greater than the efficiency of the corresponding Brayton cycle, and 2) is not bound by the Carnot efficiency.

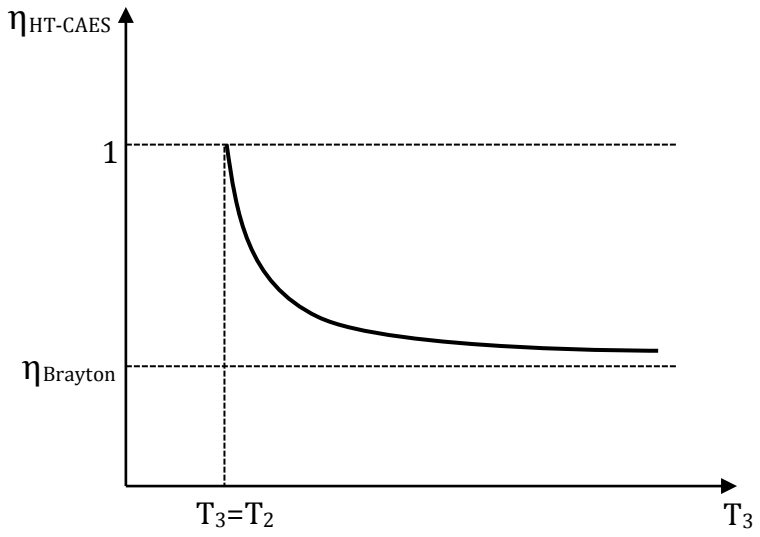


**Figure 3.5: Efficiency Versus Thermal Storage Temperatures of the Simplified Hybrid Compressed Air Energy Storage Cycle given by equation (9), Exclusive of Regeneration**

### 3.4.2 Accounting for heat losses following compression

As noted earlier, there is an advanced adiabatic system built into the HT-CAES. In the analyses done so far it has been assumed that the heat of compression, which is traditionally absorbed in advanced adiabatic CAES, is fully utilized in the system with 100% round trip efficiency prior to heating the air through the TES. This section extends the analysis to take into account the heat losses following compression. The corresponding ideal and simplified model is given by Fig. 6

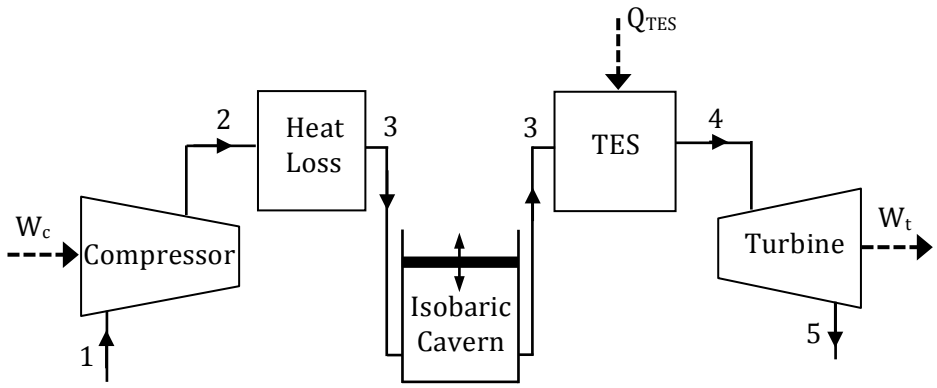


**Figure 3.6 Simplified and Ideal Hybrid Thermal and Compressed Air Energy Storage with a heat loss component following compression**

The round trip storage efficiency is calculated similar to (7), that is:

$$\eta_{HT-CAES} = \frac{\dot{W}_t}{\dot{W}_c + \dot{Q}_{HTES}} \tag{3.10}$$

Assuming constant specific heat, equation (10) reduces to

$$\eta_{HT-CAES} = \frac{T_4 - T_5}{T_2 - T_1 + T_4 - T_3} \tag{3.11}$$

Utilizing isentropic relations and incorporating the compression ratio, $r$, equation (11) reduces to

$$\eta_{HT-CAES} = \frac{T_4\left(1 - 1/r^{(k-1)/k}\right)}{T_4(1 - T_3/T_4) - T_1(1 - r^{(k-1)/k})} \tag{3.12}$$

Further simplification of (12) leads to

$$\eta_{HT-CAES} = \frac{1}{\frac{(1 - T_3/T_4)}{(1 - 1/r^{(k-1)/k})} + \frac{T_1}{T_4} r^{(k-1)/k}} \tag{3.13}$$

Recognizing the Brayton cycle efficiency, equation (13) can be rewritten as follows

$$\eta_{HT-CAES} = \frac{1}{\frac{(1 - T_3/T_4)}{\eta_{Brayton}} + \frac{T_1}{T_4} r^{(k-1)/k}} \tag{3.14}$$

An immediate observation in equation (14) is that as $T_4$ increases the efficiency of the system approaches the Brayton cycle efficiency, i.e.

$$\lim_{T_4 \to \infty} \eta_{HT-CAES} = \eta_{Brayton} \tag{3.15}$$

A plot of the round trip efficiency, given by equation (14), versus the expander inlet temperature ($T_4$) for various $T_3$ temperatures is given in Fig. 7. The uppermost curve in Fig. 7 represents the case where $T_3 = T_2$, which corresponds to no heat loss following compression. That is consistent with equation (9) and its sketch in Fig. 5. As $T_3$ decreases the associated curves in Fig. 7 eventually change in curvature, although all leading to the same limiting case of the Brayton cycle efficiency. The result in Fig. 7 was obtained for a compression ratio of 20, a heat capacity ratio of 1.4, and an ambient temperature of 300K, which leads to a Brayton cycle efficiency of 57.51%. The decrease in the temperature, $T_3$, corresponds to an increase in heat loss following compression. As heat losses increase the necessary amount of heat, supplied by the TES, to reach a specified turbine inlet temperature increases. A significant increase in the necessary heat, provided by the thermal storage, overwhelmingly influences the efficiency of the system, as demonstrated by equation (10), and eventually leads to the change in efficiency curvature.

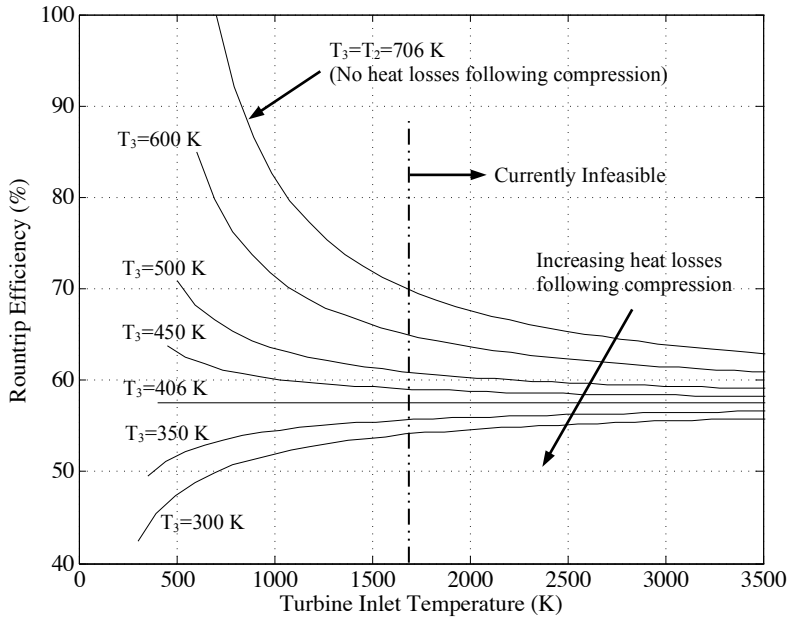


**Figure 3.7: A plot of the roundtrip efficiency (corresponding to the Hybrid CAES cycle of Fig. 6, exclusive of regeneration) versus the turbine inlet temperature (or equivalently TES temperature) given by equation (14) for various $T_3$ temperatures (corresponding to various heat loss curves following compression) for a compression ratio of 20, a heat capacity ratio of 1.4 and an ambient temperature of 300K**

## 3.5 Discussion

Although the Carnot efficiency is more commonly utilized as a performance comparison with power cycles, pure thermal energy storage cycles are also bound by its limit as these systems can be classified as heat engines i.e. TES systems convert low quality energy (heat) to useful work as in the case of power cycles/heat engines. In order to demonstrate the influence of the Carnot limit on the performance of the Hybrid storage system, a plot of the Carnot efficiency, Brayton cycle efficiency, and Hybrid CAES system efficiency as a function of the thermal energy storage temperature, or the turbine inlet temperature, is provided in Figure 8. Both regenerative and non-regenerative Brayton cycle and Hybrid CAES efficiencies are plotted in Figure 8. At lower thermal energy storage temperatures, there is no potential for regeneration, however this

potential increases with temperature. The architecture (with or without regeneration) that leads to the higher efficiency is utilized and plotted in Figure 7 with a solid line.

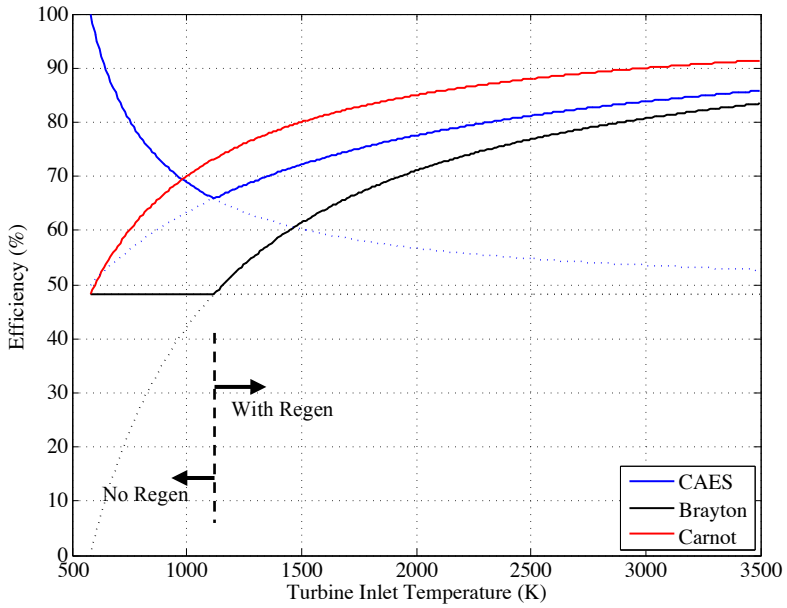


**Figure 3.8: A plot of the Carnot efficiency, Brayton cycle efficiency, and Hybrid CAES system efficiency as a function of the thermal energy storage temperature, or the turbine inlet temperature (assuming a compression ratio of 10 in both Brayton and Hybrid CAES cycles)**

The efficiency of an ideal non-regenerative Brayton cycle is independent of thermal energy storage temperatures. However, with increasing thermal energy storage temperatures, eventually, regeneration becomes effective and the cycle efficiency increases with temperature in such architecture. Conversely, the efficiency of an ideal non-regenerative Hybrid CAES system decreases with thermal energy storage temperatures. However, just as in the Brayton cycle case, with increasing thermal energy storage temperature eventually regeneration becomes effective and the cycle efficiency begins to increase with temperature. As demonstrated by Figure 8 at low thermal energy storage temperatures, the efficiency of a Hybrid CAES system is generally not bound by the Carnot limit. In addition, the efficiency of the Hybrid system is always higher than

that of a pure thermal energy storage system, executed by a Brayton cycle. The Hybrid CAES efficiency approaches the Brayton cycle efficiency at exceedingly high temperatures. Therefore, as thermal energy storage temperatures increase the Carnot limit begins to influence the performance of the Hybrid storage system. The reason being that at high thermal storage temperatures the majority of energy is supplied by the TES unit, which is inherently bound by the Carnot limit.

### 3.6 Cyclic Cavern Analysis

This section illustrates a brief thermodynamic analysis of an isobaric and isochoric cavern. In both cases the cavern is also assumed to be adiabatic. The results below demonstrate that under the isobaric cavern assumption the thermodynamic state of the cavern, inlet, and outlet conditions remain equal and constant. The thermodynamic state of air is assumed fixed by the air pressure and temperature properties. An isochoric cavern, on the contrary, changes the state of air through the cavern.

#### 3.6.1 Governing Equations

The general mass, energy and entropy balance equations together with the calorically perfect gas equations of state are given below:

$$\frac{dM}{dt} = \dot{m}_{in} - \dot{m}_{out} \tag{3.16}$$

$$\frac{dE}{dt} = -P\frac{dV}{dt} + \dot{m}_{in}h_{in} - \dot{m}_{out}h_{out} + \dot{Q} \tag{3.17}$$

$$\frac{dH}{dt} = V\frac{dP}{dt} + \dot{m}_{in}h_{in} - \dot{m}_{out}h_{out} + \dot{Q} \tag{3.18}$$

$$\frac{dS}{dt} = \dot{m}_{in}s_{in} - \dot{m}_{out}s_{out} + \sum_{j}\frac{\dot{Q}_j}{T_j} + \dot{\sigma} \tag{3.19}$$

$$PV = MRT \tag{3.20}$$

Where

$$E = Me \tag{3.21}$$

$$S = Ms \tag{3.22}$$

$$H = Mh \tag{3.23}$$

$$e = C_v T \tag{3.24}$$

$$h = C_p T \tag{3.25}$$

And *e*, *s* and *h*, are the specific energy, entropy, enthalpy and *M* is the mass of air in the cavern at any instant of time.

### 3.6.2 Isobaric Cavern: (P = constant)

*Charge Process: ($\dot{m}_{out} = 0$)*

In order to analyze the conditions of the isobaric and adiabatic cavern during the charge process, equation (18) is expanded while utilizing equation (26), resulting in the following equation:

$$M\frac{dT}{dt} = \dot{m}_{in}(T_o - T) \tag{3.26}$$

with the initial condition of

$$T(t = 0) = T_o \tag{3.27}$$

where $T_o$ is the temperature of the inlet air stream. Solving equation (26) coupled with (27) results in

$$T(t) = T_o \tag{3.28}$$

Meaning the isobaric cavern temperature at any instant of time, during the charge process, is equal to the constant inlet air temperature. With the cavern pressure assumed constant in this

situation, the state of the cavern, which is determined by the air temperature and pressure, remains constant during the charge process.

*Discharge Process: ($\dot{m}_{in} = 0$)*

Similarly, expanding equation (18) and using equation (16) results in the following equation

$$M\frac{dT}{dt} - \dot{m}_{out}T = -\dot{m}_{out}T \tag{3.29}$$

with the initial condition of

$$T(t=0) = T_o \tag{3.30}$$

It is immediately clear that (29) and (30) result in the following solution

$$T(t) = T_o \tag{3.31}$$

The results (28) and (31) together with the isobaric constraint, *P=constant*, indicate that the transients of an isobaric cavern are irrelevant. Specifically, the inlet and exit temperatures are one and the same. Therefore, the inlet state of the cavern air, defined by the inlet air pressure and temperature, is equal to the outlet state of the cavern air and the cavern becomes redundant in the analysis.

### 3.6.3 Isochoric Cavern: (V=constant)

Coupled integration of the mass and energy balance, equations (16) and (17), under calorically perfect gas equations of state and adiabatic boundary conditions enable determination of temperature and pressure during charge and discharge and the cycle-to-cycle variations, as shown in Figure 9. Constants provided in Table 1 were have been used.

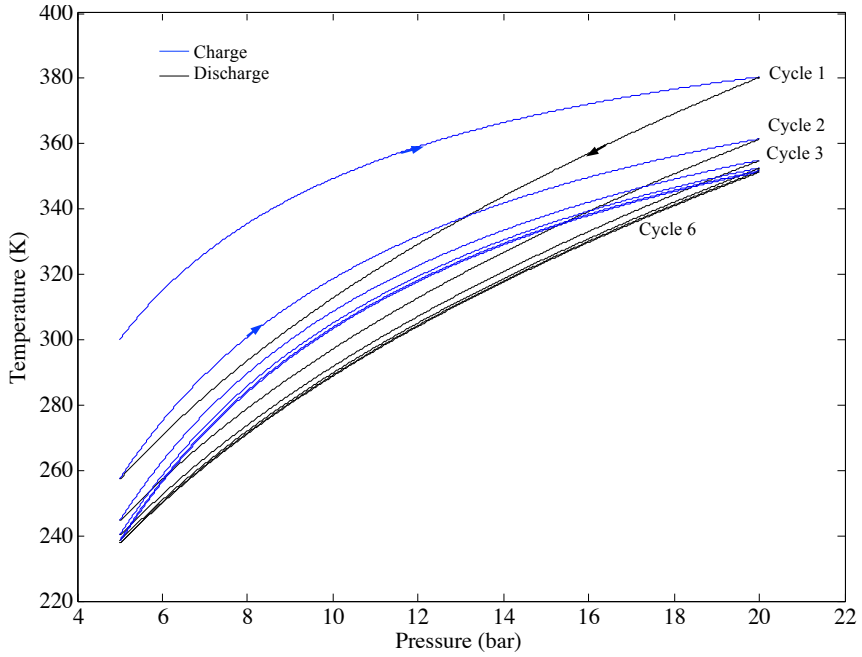


**Figure 3.9: The temperature and pressure of an adiabatic cavern cyclic process. The first 6 cycles of the charge and discharge process are shown.**

**Table 3.1 Assumed constants for the cyclic isochoric and adiabatic cavern example**

| **Constant** | **Value** |
|---|---|
| Cavern Volume, $V_{cavern}$ | 300,000 $m^3$ |
| Specific Heat of Air at Constant Pressure, $C_p$ | 1 kJ/kg.K |
| Specific Heat of Air at Constant Volume, $C_v$ | 0.718 kJ/kg.K |
| Air Gas Constant, $R$ | 0.287 kJ/kg.K |
| Minimum Pressure, $P_{min}$ | 5 bar |
| Maximum Pressure, $P_{max}$ | 20 bar |
| Initial Cavern Temperature, $T_o$ | 300 K |
| Inlet Cavern Temperature, $T_{in}$ | 300 K |
| Mass Flow Rate, $\dot{m}$ | 200 kg/s |

As the pressure varies between the specified maximum and minimum during the charge and discharge processes, the temperature of the cavern reaches an equilibrium profile after

approximately 6 cycles. However, the temperature and pressure remain transient and the conditions of the air through the cavern change drastically. Consequently, the state of the air into and out of the cavern is different. As a result, for a proper modeling of the plant's performance the cavern internal transients must be taken into account.

### 3.7 Concluding Remarks

An ideal thermodynamic model was developed for a hybrid thermal and compressed air energy storage system. The analysis considered perfect performance indices for the components (isentropic efficiency and effectiveness) and explored the integral built-in boundaries of operation of the storage cycle with respect to the corresponding Brayton and Carnot cycles. The models included cycles with and without regeneration. The following conclusions can be drawn:

1. Consistent with the advanced adiabatic compressed air energy storage concept, in the limit of no heat addition to the system the ideal cycle has 100% theoretical roundtrip efficiency. In this limit the compression and expansion occur along the same isentrope.
2. The addition of heat through thermal storage takes the expansion process off the compression isentrope and results in a non-unity round trip efficiency even in the case of perfect components.
3. The efficiency of the storage cycle approaches that of a classical Brayton cycle as the temperature of the thermal storage increases.
4. The energy storage cycle, namely compressed air energy storage, is not bound by the Carnot efficiency, as the Carnot efficiency is limited to heat engines, not energy storage cycles.

# Chapter 4: Thermodynamic Analysis of a Simple Hybrid Thermal-Compressed Air Energy Storage System

## 4.1 Introduction

Numerous CAES configurations have been investigated, such as advanced adiabatic (AA-CAES), diabatic, isothermal, and various hybrid CAES arrangements [92]-[97]. The only two existing CAES plants are based on the diabatic method, in which the heat of compression is not utilized in the system and wasted into the environment. Both plants use natural gas for combustion to heat the discharging air prior to expansion, which produce greenhouse gas emissions [98]. Additionally, both existing CAES plants were designed as peaker plants based on economic motives. They generally run only when there is high demand for electricity. Depending on the fuel conversion efficiency, approximately 40% to 66% of the output energy is provided by fuel. Conventional CAES plants are, therefore, a combination of energy storage and generation plants [99]. In AA-CAES the heat of compression is captured and stored during the charge process and is employed during the discharge phase to heat up the air prior to adiabatic expansion, which is more appealing as it theoretically results in a higher roundtrip efficiency compared with diabatic CAES. As a result, several state-of-the-art make CAES projects have been initiated. RWE Power, which is the largest German power company, launched the ADELE CAES plant based on an advanced adiabatic design in 2010 [100]. However, the project was terminated due to economic issues. Dresser-Rand, the company that supplied the turbo-expander for the McIntosh CAES plant, working in partnership with Apex, is aiming to provide a 317MW conventional CAES system in Texas, with an anticipated operation date in 2020 [101]. An old, yet attractive idea for near isothermal compression – attempted by LightSail, a start-up company

in Berkeley, California – involves spraying a calculated amount of water during the compression phase of a dual-purpose reciprocating compressor/expander to absorb the heat of compression. The so-captured energy is then utilized during expansion when the machine is used as an expander [102]. SustainX and General Compression were also pioneering isothermal CAES. However these companies ceased operation for economic reasons. A Canadian startup, Hydrostor, is initiating underwater CAES, where an underground cavern along with a water-equalizing pit are used to maintain isobaric storage conditions [103].

Although AA-CAES is a very attractive idea, its major drawback results from putting all the available energy into compression, which inevitably results in large storage and operating pressures for adequate energy storage densities. Therefore, multistage compression and expansion have to be employed, which ultimately drive the cost up [104]. Furthermore, air can get very cold over large expansion ratios, which among other technical issues could turn the warm humidity in the air into ice bullets that damage the valves and the expander. In addition to high pressures, isothermal CAES is difficult to achieve as it necessitates high heat transfer rates during compression and expansion to maintain isothermal conditions.

A simple high temperature hybrid compressed air energy storage (HT-CAES) system configuration is presented which eliminates the necessary combustion emissions in conventional CAES and mitigates some of the issues in the otherwise attractive AA-CAES. The HT-CAES allows a portion of the available energy, from the grid or renewable sources, to operate a compressor and the remainder to be converted and stored in the form of heat, through joule heating in a sensible storage medium. As a result, HT-CAES operates on smaller volumes and

lower pressures, which reduce the cost and solve some of the technical issues during expansion. Surprisingly, very few groups have investigated a hybrid thermal and compressed air energy storage design [105]-[108]. This unique HT-CAES design incorporates two stages of heating through separate low-temperature and high-temperature thermal energy storage units, which provide simplicity and practicality for future implementation. In contrast to the only previous hybrid investigation [108], the following thermodynamic analysis incorporates realistic isentropic component efficiencies and throttling losses responsible for maintaining constant pressure conditions following the cavern. While a positive-displacement machine with proper valve-timing control can adjust to the time-varying pressure in the cavern and maintain optimal performance, a variable expander assumption over-estimates the power output with turbo-expanders. The optimal performance of a turbo-expander, characterized by its isentropic efficiency, is limited to a very narrow range of inlet operating conditions of pressure, temperature and mass flow rate. Slight deviations from the design conditions results in a sharp decrease in isentropic efficiency of the machine. As a result, pressure has to be regulated to the design conditions, either via the Joule-Thomson throttling process or using an expander that is capable of taking the time-varying pressure in the cavern and delivering a steady-state back pressure. This analysis employs the Joule-Thomson throttling. Previous works only consider an isothermal cavern [108], however here both adiabatic and isothermal conditions are investigated as they represent both extremes. Most importantly, the existence of an optimum operating pressure, leading to maximum roundtrip storage efficiency, is presented, which has not been formerly reported. Parametric studies, which illustrate the importance of the operating pressure and thermal storage temperature on the performance of both HT-CAES and AA-CAES systems, are presented. Moreover, the cyclic behavior and the existence of an asymptotic isentropic

condition in an adiabatic cavern are reported. Lastly, the performance of an HT-CAES system is compared with an AA-CAES system of the same power output.

## 4.2 Methods

While cost effective, traditional CAES systems suffer from heat losses during compression along with carbon emission due to combustion of fossil fuels. With AA-CAES systems, the heat of compression is stored in a thermal energy storage (TES) unit and returned to the compressed air during discharge. The higher overall efficiency of AA-CAES systems has made it an attractive alternative to traditional CAES. However, AA-CAES requires high storage and operating pressures for adequate energy densities and roundtrip efficiencies, as demonstrated in section 4.2. Of the only two compressed air energy storage plants in operation (Huntorf, Germany and McIntosh, United States) neither one employs AA-CAES.

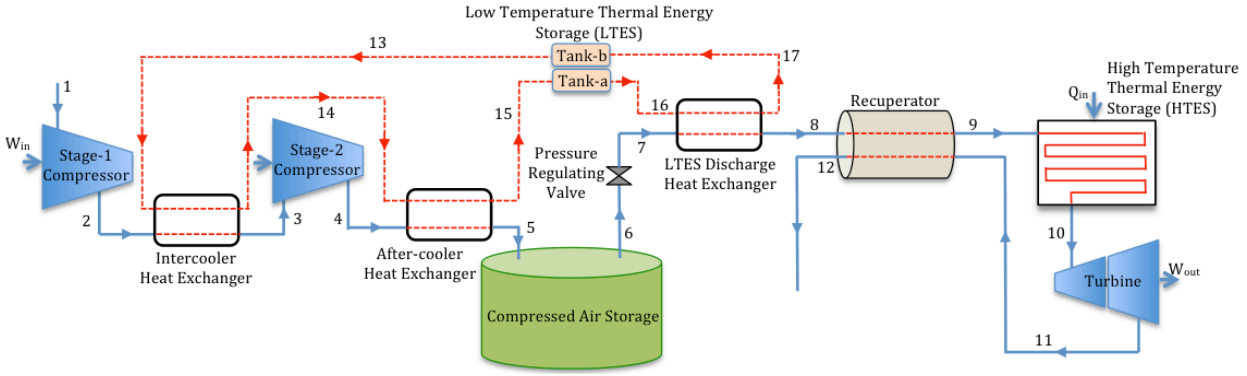


**Figure 4.1: Schematic of a High Temperature Hybrid Compressed Air Energy Storage (HT-CAES).**

The resolution between CAES and AA-CAES is the high temperature hybrid thermal CAES (HT-CAES). In an HT-CAES system the TES is replaced with a low and high temperature energy storage unit, as shown in Figure 1. As with TES in AA-CAES, the low temperature thermal energy storage (LTES) unit stores the heat of compression. But unlike TES in AA-

CAES, the high temperature thermal energy storage (HTES) unit in HT-CAES acts as a scalable energy reservoir without the complexity and limitations of a thermal transport fluid. The HTES unit takes advantage of the high thermal capacity of an inexpensive thermal medium to store heat that will later be used to heat up the compressed air out of the air storage. HT-CAES allows for direct conversion of electricity into heat through Joule heating. As a result, temperatures and volumetric energy densities well in excess of traditional CAES and AA-CAES can be achieved, while the size of the air storage can be reduced. The electricity could be supplied either from the grid or renewable source, e.g. wind and PV.

With the addition of a HTES unit, the workload is shifted from pure compression to investing partially in thermal storage. This separation of energy storage between compressed air and thermal storage has the effect of expanding the energy capacity of the compressed air system without the need to increase the air pressure or cavern capacity. HTES allows the system to be dynamically scaled up or down as the load leveling demand changes without any structural change in system configuration. Figure 2 is a sketch of the T-s diagram for both AA-CAES and HT-CAES, corresponding to the cycle in Figure 1, assuming isentropic components, an isothermal air reservoir and 100% heat exchanger and recuperator effectiveness. The process is summarized in Table 1. It should be noted that HTES is by nature a transient component as it depletes during the discharge process. However, it can be sized and designed to always heat up the discharging air to a constant temperature, thereby providing the expander with a steady-state steady flow. Under these conditions HTES can be thought of as a steady component.

**Table 4.1: Process Description Corresponding to the T-s Diagram in Figure 2**

| Process | Description |
|---|---|
| 1-2 | 1st stage isentropic compression for both HT-CAES and AA-CAES |
| 2-3 | Intercooling, at constant pressure, for both HT-CAES and AA-CAES |
| 3-4 | 2nd stage isentropic compression for both HT-CAES and AA-CAES |
| 4-5 | After-cooling for both HT-CAES and AA-CAES |
| 6 | This line represents the conditions of the isothermal cavern as it is depleted and throttled during the discharge process from pressures $P_{max}$ to the operating pressure, P', given by points 5 and 7 respectively. |
| 7-8 | Preheating the discharging air by the LTES from the generated heat of compression. Point 8 represents the maximum temperature achievable through AA-CAES |
| 8-8' | Isentropic expansion in AA-CAES (in Figure 1, this would correspond to 8-11) |
| 8-9 | Recuperator heat addition in HTH-CAES |
| 9-10 | Heat provided by the HTES in HTH-CAES |
| 10-11 | Isentropic expansion in HTH-CAES |

As evident in Figure, 2, the addition of an HTES dramatically increases the output power and the energy density of the storage system for a given size and pressure swing in the cavern, as the AA-CAES system is limited by the amount of energy stored purely during compression.

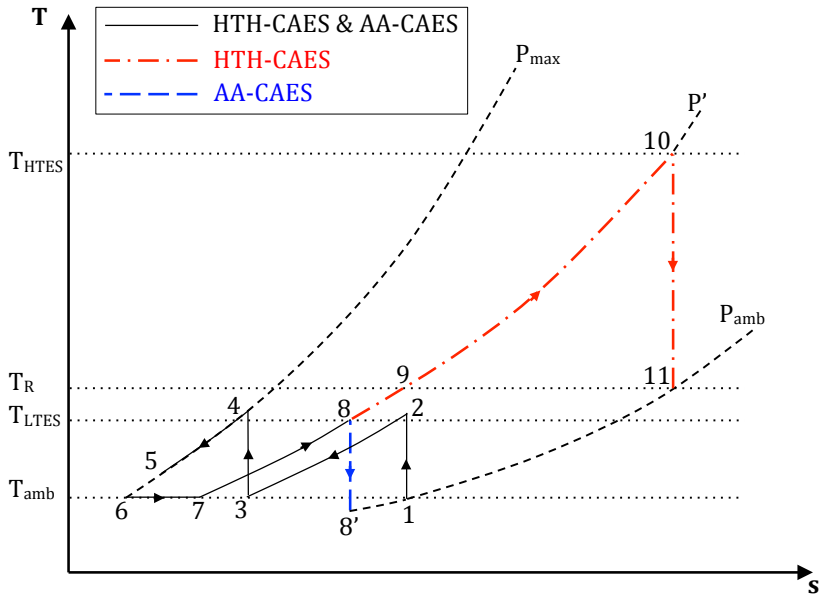


**Figure 4.2: T-s Diagram of both AA-CAES and HTH-CAES, assuming isentropic components, an isothermal cavern, and 100% heat exchanger effectiveness**

Assuming isentropic efficiencies of 100% for compressors and turbine, and an effectiveness of 100% for heat exchangers, Table 2 represents a snapshot of one such operational possibility for an isothermal cavern.

**Table 4.2: A specific example of the possible operational values corresponding to the T-s diagrams of Figure 2 and Figure3**

| Variable | Value | Variable | Value |
|---|---|---|---|
| $T_1$ | 300K | $T_8$ | 357K |
| $T_2$ | 460.25K | $T_9$ | 820.8K |
| $T_3$ | 300K | $T_{10}$ | 1300K |
| $T_4$ | 460.25K | $T_{8'}$ | 225.83K |
| $T_5$ | 332.05K | $T_{11}$ | 820.8K |
| $T_6$, $T_7$ | 300K | P’ | 5bar |
| $P_{amb}$ | 1bar | $P_{max}$ | 20bar |
| $P_i$ | 4.47bar | $C_r$ | 5 |

Where $P_i$ is the intercooling pressure, corresponding to minimum compression work, and $C_r=C_{LTES}/C_{air}$ is the heat capacity rate ratio, defined as the LTES heat transfer fluid (HTF) specific heat times its flow rate, over the specific heat of air, at constant pressure, times its flow rate. Data in Table 3 were also used.

Figure 3 involves an HTH-CAES T-s diagram under an adiabatic cavern, which is essentially the same as Figure 2 except for the treatment of the cavern. As a result all values given by Table 2 are applicable with the exception of temperatures $T_7$ and $T_6$, which are now time-dependent. Lines 6’ and 6 represent the instantaneous conditions in the cavern as it is charged and discharged respectively. Also, the isothermal line 7 represents the Joule-Thompson throttling, which brings the instantaneous condition of the discharging cavern air (a point along line 6) to the operating/prime pressure, P’. Where the prime pressure, P’, is defined as the minimum cavern pressure and the discharge process pressure, which is adjusted by the pressure regulating

valve. The cyclic conditions of an adiabatic cavern during the charge and discharge process, along with their operational values, are given in Appendix A. As shown there, the charge and discharge processes in the cavern (lines 6' and 6 respectively) tend to converge to an isentropic one after several charge and discharge cycles. All calculations presented for an adiabatic cavern in this paper, including Figure 3 represent the first charge and discharge cycle.

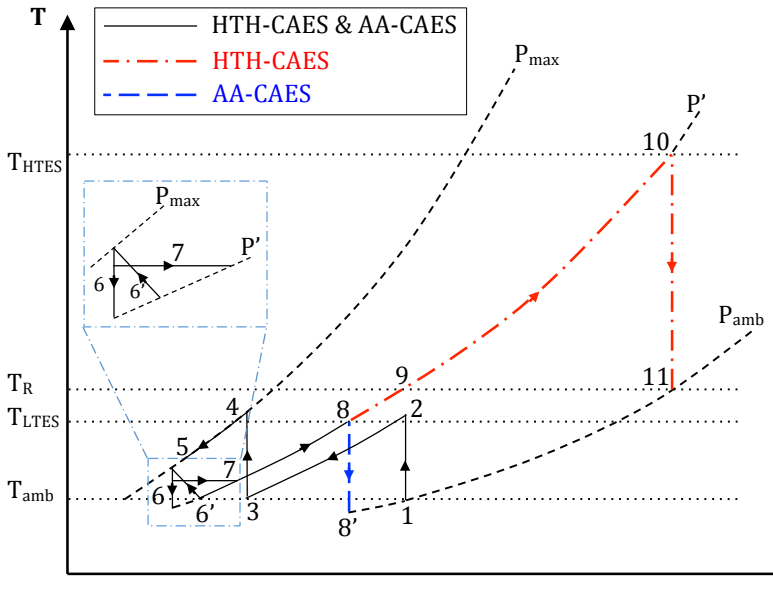


**Figure 4.3: T-s Diagram of both AA-CAES and HTH-CAES, assuming isentropic components, an adiabatic cavern, and 100% heat exchanger effectiveness**

## 4.3 Calculations

Figure 1 represents the HTH-CAES thermodynamic cycle that is analyzed here. During the charge process electricity from renewable sources, or the gird, is used to operate the compressor. Simultaneously or subsequently, depending on available power during the charge process, electricity is converted directly into thermal energy and is stored in the High Temperature Thermal Energy Storage (HTES). Conversion of electricity to thermal energy can result in very high temperatures and thus high energy densities when the energy is well contained. The

practical limit on how high a temperature can be reached in HTES is defined by the material properties of the storage and the electric wires. Alumina-based refractory provides service temperatures in excess of 1700C and Nichrome wires can have a continuously operating temperature of ~ 1680C. Considering that the heat of compression is absorbed during charge and is used during discharge, there is conceptually an AA-CAES built into the HTH-CAES cycle in Figure 1. The heat of compression is stored in a Low Temperature Thermal Energy Storage (LTES), which is essentially a two-tank system. Initially, tank "b" is filled with a cold Heat Transfer Fluid (HTF) in the charge process and tank "a" is empty. As the air being compressed, tank "b" is discharged and the HTF collects the heat of compression via the LTES charge heat exchanger. The hot HTF is then stored in tank "a" for later use during the discharge process. During the discharge process, air is released from the cavern and subsequently throttled through the pressure-regulating valve to a constant pressure, herein referred to as the prime pressure, *P'*. The temperature of the discharging air is then raised through three successive stages of heating before entering the expander: LTES, Recuperator, and HTES. Pressure losses within the pipes were not taken into account and all components besides the cavern are assumed to be quasi-steady. In addition, Table 3 summarizes the additional constants used in all studies presented here.

**Table 4.3: Assumed Constants**

| Constant | Value |
|---|---|
| Charge Time, $t_{charge}$ | 6 hours |
| Cavern Volume, $V_{cavern}$ | 300,000 $m^3$ |
| Compressor Isentropic Efficiency, $\eta_c$ | 75% |
| Turbine Isentropic Efficiency, $\eta_t$ | 80% |
| Heat Exchanger & Recuperator Effectiveness | 80% |
| Heat Capacity Rate Ratio of the LTES Heat Carrier Fluid to Air, $C_r=C_{LTES}/C_{air}$ | 5 |
| Specific Heat of Air at Constant Pressure, $C_p$ | 1 kJ/kg.K |

| | |
|---|---|
| Specific Heat of Air at Constant Volume, $C_v$ | 0.718 kJ/kg.K |
| Air Gas Constant, $R$ | 0.287 kJ/kg.K |
| Output Power, $\dot{W}_{Output}$ | 100MW |

A detailed outline of the calculations made for each component in the charge cycle is presented in this section. This includes all significant equations and any component specific assumptions.

### 4.3.1 Thermodynamic Equations

All components (compressors, heat exchangers and turbines) except for the cavern and HTES are assumed to operate quasi-steadily during charge and discharge. The rational is that the residence time within these components is much shorter than charge and discharge time scales, indicated in Table 3. Also, heat capacities are assumed to be temperature independent. The charging time is fixed, therefore, the cavern is charged to a peak pressure, corresponding to a specified flow rate, and is discharged till the cavern prime pressure, P', is reached.

#### *4.3.1.1 Compressor*

Considering Figure 2, the required first stage isentropic compression power is determined from the first law of thermodynamics as follows

$$\dot{W}_C = \dot{m}\,\frac{c_p T_1}{\eta_c}\left(\left(\frac{P_i}{P_1}\right)^{\frac{k-1}{k}} - 1\right) \tag{4.1}$$

Here $T_1$ and $P_1$ are the inlet temperature and pressure of the compressor at ambient conditions, respectively. The intercooling pressure, $P_i$, is given by $P_i = \sqrt{P_1 P_{max}}$, a well-known result corresponding to minimum compression power, and $P_{max}$ is the maximum cavern pressure at the end of the charge process. The second stage compression power is calculated similarly, for a pressure swing from $P_i$ to $P_{max}$. The inlet temperature of the 2nd stage compressor is determined

by a heat exchanger energy balance that takes into account the effectiveness and the LTES heat capacity rate ratio given by Table 3.

#### *4.3.1.2 Adiabatic Cavern*

The application of the mass and energy balance under temperature-independent specific heats and adiabatic boundary conditions results in the following transient thermodynamics for the cavern:

**Charge:**

$$M(t) = \dot{m}t + M' \tag{4.2}$$

$$T(t) = \frac{M'}{M(t)}T' + \frac{\dot{m}kT_5 t}{M(t)} \tag{4.3}$$

$$P(t) = P' + \frac{\dot{m}kRT_5 t}{V_{cavern}} \tag{4.4}$$

**Discharge:**

$$M(t) = M_{max} - \dot{m}t \tag{4.5}$$

$$T(t) = T_{max}\left(1 - \frac{\dot{m}t}{M_{max}}\right)^{(k+1)} \tag{4.6}$$

$$P(t)V_{cavern} = M(t)RT(t) \tag{4.7}$$

where *P'* is the cavern prime pressure and $T_5$ is the temperature of air into the cavern, as shown in Figure 1. Also, $M'$ is the mass of air in the cavern at the start of the charging process and $T'$ is its temperature. $T_{max}$ and $M_{max}$ are obtained by substituting $t_{charge}$ in equations (2) and (3). When the adiabatic assumption is made, $T' = T_5$ has been assumed, although it is shown in the appendix that there is a slight cycle-to-cycle variation within the first few cycles until an equilibrium is reached in the cavern. For general, though weak, temperature-dependent heat

capacities, numerical integration of mass and energy balance coupled with the equation of state will have to be resorted to determine the internal thermodynamics of the cavern.

#### *4.3.1.3 Isothermal Cavern*

Similarly, the following equations can be obtained for an isothermal cavern during charge and discharge:

**Charge:**

$$M(t) = \dot{m}t + M' \tag{4.8}$$

$$T(t) = \text{cte} \tag{4.9}$$

$$P(t) = P' + \frac{RT_5\dot{m}t}{V_{cavern}} \tag{4.10}$$

**Discharge:**

$$M(t) = M_{max} - \dot{m}t \tag{4.11}$$

$$T(t) = \text{cte} \tag{4.12}$$

$$P(t)V_{cavern} = M(t)RT(t) \tag{4.13}$$

#### *4.3.1.4 LTES and Recuperator*

The LTES working fluid storage tanks are assumed to be adiabatic. The final LTES temperature during the charge process is calculated through a heat exchanger analysis using the effectiveness and the heat capacity rate ratio given by Table 3. Similarly the recuperation analysis is performed assuming the effectiveness given in Table 3.

#### *4.3.1.5 Joule-Thomson Throttling*

The air pressure is reduced to the process pressure via the Joule-Thomson throttling. It is essentially an iso-enthalpic process when the valve is fully insulated. The Joule-Thomson

coefficient, $\mu_{JT} = \frac{\partial T}{\partial P}\Big]_h$, drops continuously for a given pressure as the temperature increases for air. It takes the value of $\mu_{JT} = 0.2143\ C.\text{bar}^{-1}$ at $0.0C$, 60 bar and $0.0161\ C.\text{bar}^{-1}$ at $280C$, 60 bar [109]. The former translates into a $\Delta T = 12.85C$ across the valve while the latter results in $\Delta T = 0.966C$. Considering the narrow range of variations of the Joule-Thomson coefficient, therefore, the real gas effects have been neglected and the throttling process has further assumed to be isothermal. Consequently, $T_6 = T_7$ in Figure 1

#### *4.3.1.6 HTES and Turbo-expander*

As mentioned earlier, the HTES is inherently a transient component. However, it can be designed to deliver a constant temperature necessary for optimal operation of the turbo-expander. Since the plant is assumed to deliver a constant power output, $\dot{W}_{Output}$, the necessary HTES exit air temperature, $T_{10}$, can be determined through an energy balance of the turbo-expander as follows:

$$T_{10} = \frac{\dot{W}_{Output}}{\eta_t \dot{m}\, c_p \left[1 - \left(\frac{P_{12}}{P'}\right)^{\frac{k-1}{k}}\right]} \tag{4.14}$$

Note that $P_{12} = P_1$ in equation (14). The necessary heat addition by the HTES to air is therefore given by

$$\dot{Q}_{HTES} = \dot{m}\, c_p (T_{10} - T_9) \tag{4.15}$$

One way of designing the HTES for a constant exhaust temperature is through bypassing the cold air and mixing it with the hot air out of HTES, as shown in Figure 4. Part of the incoming air is bypassed around the HTES while the rest goes through it. It is assumed that the HTES length is designed for 100% effectiveness. Nonetheless, since the maximum temperature of

HTES drops, so does the exhaust air temperature out of it, hence $T_{hot}(t)$. Applying the energy balance to the point where the bypass line mixes with the hot flow out of the HTES, the bypass mass flow rate, $\dot{m}_{bp}(\mathrm{t})$, can be obtained as a function of $T_{hot}(t)$ and $T_{10}$:

$$\dot{m}_{bp}(t) = \dot{m}\left(\frac{T_{hot}(t) - T_{10}}{T_{hot}(t) - T_9}\right) \tag{4.16}$$

Therefore, fixing $T_{10}$ in equation (16) reduces the control problem to determining $T_{hot}(t)$.

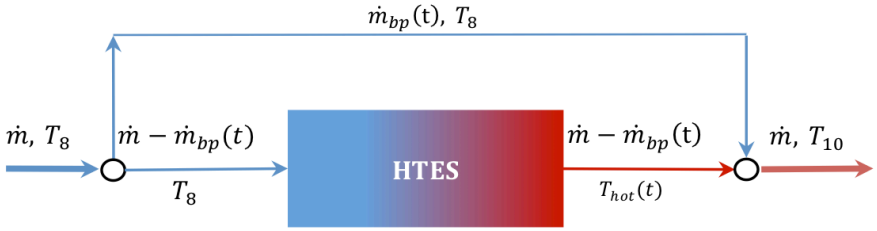


**Figure 4.4: A control strategy to keep the temperature of the air out of the HTES constant.**

Finally, the round trip efficiency of the system is calculated on an energy basis as follows

$$\eta_{Round\ trip} = \frac{\int_0^{t_{discharge}} \dot{W}_{Output}\, dt}{\int_0^{t_{discharge}} \dot{Q}_{HTES} dt + \int_0^{t_{charge}} \dot{W}_c dt} \tag{4.17}$$

## 4.4 Results

The effects of the prime pressure, P', defined as the minimum cavern pressure and the discharge operating pressure, are investigated in the HTH-CAES. The studies are done for an isothermal and an adiabatic cavern. The isothermal and adiabatic cavern assumptions represent the two possible extreme cavern conditions. An isothermal cavern is realized when the heat transfer between the cavern and its surroundings occurs much more rapidly than the heating or cooling due to charging and discharging. Conversely, an adiabatic cavern assumption depicts the case of small thermal equilibration time scales within the cavern, over which the heat flow across the cavern boundary is negligible. In reality, the cavern thermodynamic conditions lie somewhere

between the two extremes. Finally, similar parametric studies are presented for an AA-CAES system, with the same output power of 100MW, and the results are compared with the HTH-CAES system.

### *4.4.1 HTH-CAES Results*

For a fixed power output of 100MW, and for the constant parameters given in Table 3, the prime pressure is varied and the corresponding roundtrip efficiency of the hybrid energy storage system is calculated for various flow rates, under the assumption of an isothermal and adiabatic cavern. As shown in Figure 5, for a specified mass flow rate out of the cavern there is an optimum prime pressure for which the efficiency is a maximum.

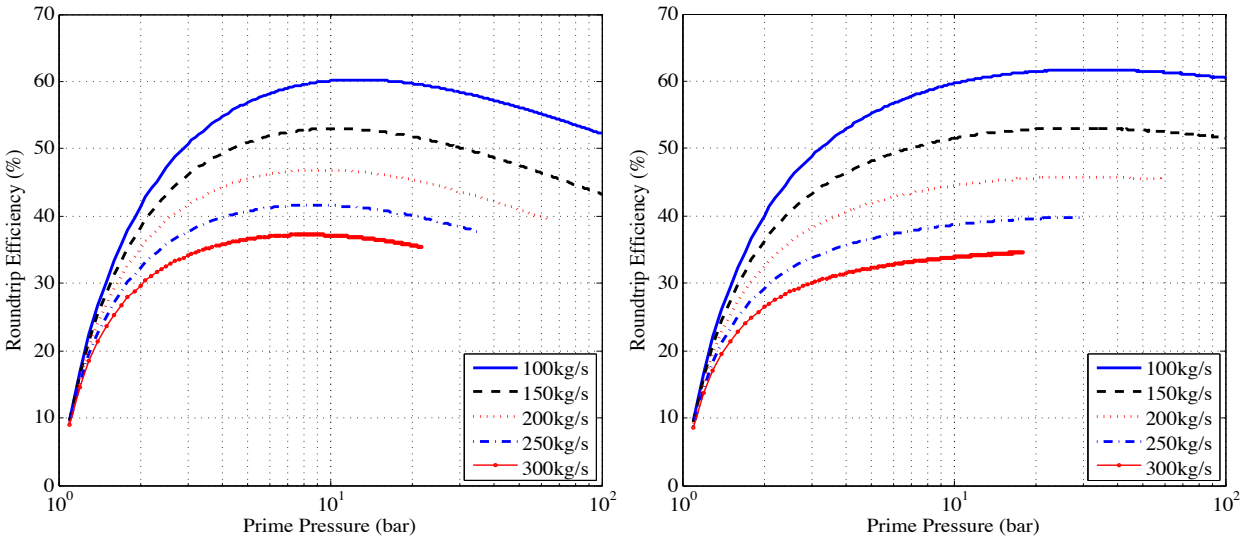


**Figure 4.4: Roundtrip efficiency as a function of the prime pressure for an isothermal cavern (a), adiabatic cavern (b), and a 100MW power output**

As compared with the isothermal cavern, given by Figure 5(a), the maximum efficiency in an adiabatic cavern, Figure 5(b), occurs at a higher prime pressure for a similar mass flow rate in both cases. Nevertheless, the maximum round trip efficiencies for both adiabatic and isothermal

caverns are not significantly different. For an isothermal case, the optimum prime pressure is near 10 bar, whereas for an adiabatic case it is near 20 bar. Also, the flatness of the efficiency curves around the optimum prime pressure covers a considerably wider range in an adiabatic cavern compared to an isothermal cavern.

Although distinct, nominal peak efficiencies in an isothermal cavern, given by Figure 5(a), occur within a narrow prime pressure range of about 8 to 15 bar. Also, an interesting observation in Figure 5 is that the efficiency curves are quite flat around the optimum prime pressure, particularly at higher mass flow rates, which could be of considerable significance when the cost of the plant is to be optimized. The curves in Figure 5 terminate when the temperature of air into the recuperator exceeds the turbine exhaust temperature. In this case recuperation becomes ineffective.

With a constant output power enforced throughout this paper, the efficiency of the system, given by equation (17), is only a function of the HTES and compressor power requirements. Therefore, the point of maximum efficiency occurs when the sum of both HTES and compressor power reach a minimum. The optimum prime pressure leading to maximum efficiency, in Figure 5, is caused by the competing power requirements of the compressor and HTES. The reason behind the optimum point of operation in Figure 5 is best described through Figure 6, which is a plot of the HTES and compressor power requirement, given by equations (1) and (15), along with their sum. As the prime pressure increases, the HTES heat requirement drops however the compression power requirement increases, and their sum reaches a minimum at precisely the optimum efficiencies in Figure 5. Figure 6 illustrates this point for a 100MW isothermal-cavern HTH-CAES, in which the mass flow rate is 150kg/s, and through the specified constants in Table 3.

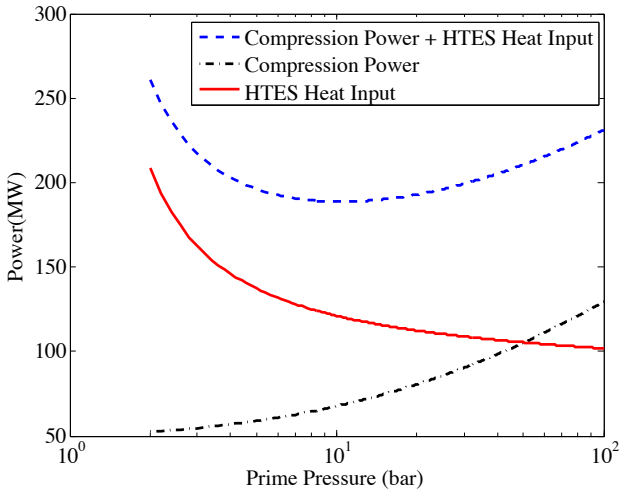


**Figure 4.5: The input power of the HTH-CAES compressor and HTES along with their sum as a function of the prime pressure, with a mass flow rate of 150kg/s, illustrating the reason leading to an optimum efficiency in Figure 5**

Fixing the prime pressure and the mass flow rate fixes the turbine inlet temperature, i.e. the HTES exit temperature, for the specified power output. Figure 7 contains such data corresponding to Figure 5, for both an isothermal and adiabatic cavern. The necessary HTES exit temperature decreases with increasing mass flow rate and increasing operating pressure. The region above the dotted horizontal line in Figure 7 entails currently infeasible turbine inlet temperatures dictated by the metallurgical limits associated with turbine blade materials [110]. The HTES exit temperatures in an adiabatic cavern, given by Figure 7(b), is identical to those corresponding to the isothermal case, Figure 7(a), with the exception that the temperatures are terminated at lower prime pressures for the adiabatic case when recuperation becomes ineffective.

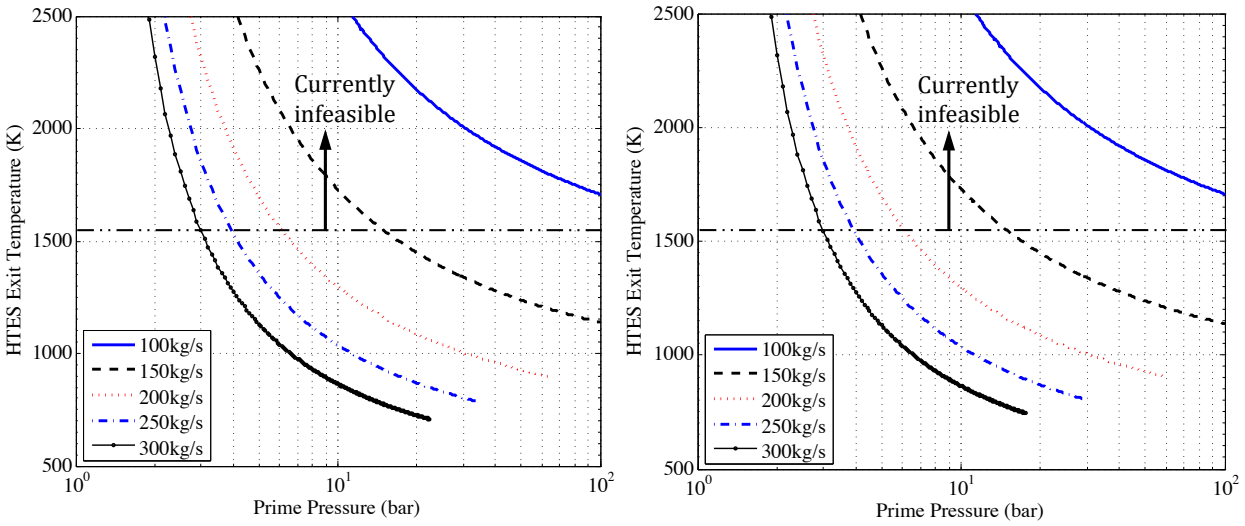


**Figure 4.6: HTES exit temperature versus the prime pressure for an isothermal cavern (a), an adiabatic cavern (b), and a 100MW output power**

The corresponding maximum cavern pressure as a function of the prime pressure is shown in Figure 8. The maximum pressure increases with prime pressure and flow rate.

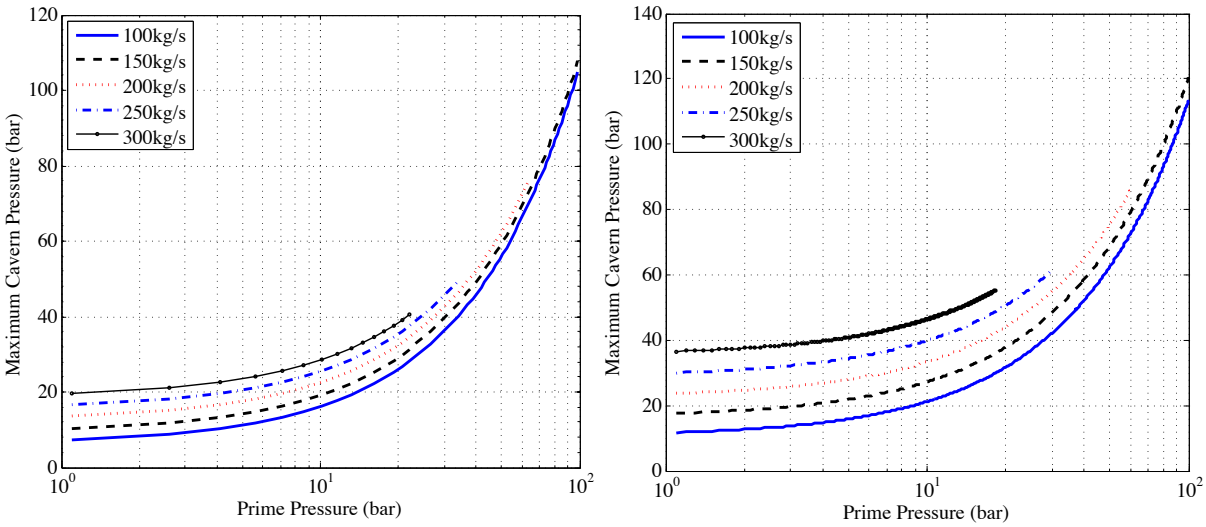


**Figure 4.7: Maximum cavern pressure as a function of the prime pressure for an isothermal cavern (a), and an adiabatic cavern (b)**

As compared with an isothermal cavern, given by Figure 8(a), an adiabatic cavern, Figure 8(b), leads to a higher maximum pressure for the same amount of stored mass.

### 4.4.2 Advanced-Adiabatic CAES Results

A similar formulation was utilized for the calculations of an advanced-adiabatic design, however without an HTES and a recuperation component. In other words, the air out of the LTES discharge heat exchanger goes directly into the power turbine, i.e. where points 8 and 10 in Figure 1 coincide. In this analysis, the output power is also fixed at 100MW, and the same constants provided by Table 3 are used. The output power is a function of the LTES temperature, the prime pressure, and the mass flow rate as illustrated by equation (14). However, without an HTES the turbine inlet temperature cannot be as easily adjusted. The LTES temperature is a function of the maximum cavern pressure, which is a function of the flow rate and the prime pressure as shown by equations (4) and (10). Therefore, the output power is ultimately only a function of the flow rate and the prime pressure.

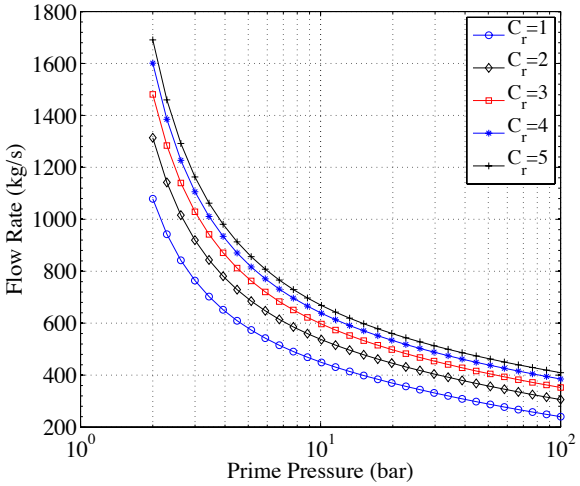


**Figure 4.8: Flow rates versus the prime pressure for an AA-CAES system of 100MW power output power, with the assumption of an isothermal cavern for various heat capacity rate ratios The heat capacity rate ratio, $C_r$, is defined as**

**$C_r = \frac{\dot{m}_{LTES}\, c_{LTES}}{\dot{m}_{air} c_{p,air}}$, where $\dot{m}_{LTES}$ is the LTES heat transfer fluid mass flow rate and $c_{LTES}$ is its specific heat, $\dot{m}_{air}$ is the air mass flow rate and $c_{p,air}$ is its specific heat at constant pressure, as defined in Table 3.**

The required flow rate as a function of prime pressure is shown in Figure 9 for various heat rate ratios under the assumption of an isothermal cavern. As the prime pressure increases, the required flow rate to achieve a constant output power of 100MW decreases. Curves of different LTES heat capacity rate ratios are shown in Figure 9. For higher LTES temperatures, achieved through lower heat rate capacity ratios, lower flow rates are required to achieve the constant output power. The maximum cavern pressure, given by equation (10), is a function of both the prime pressure and the flow rate. Figure 10 maps the maximum cavern pressure as a function of the cavern prime pressure. Evidently, a minimum value exists. The reason is that the maximum pressure is proportional to the prime pressure, as given by equation (10), and the flow rate given by Figure 9 and the rate at which the flow rate decreases leads to the minimum cavern pressure value in Figure 10.

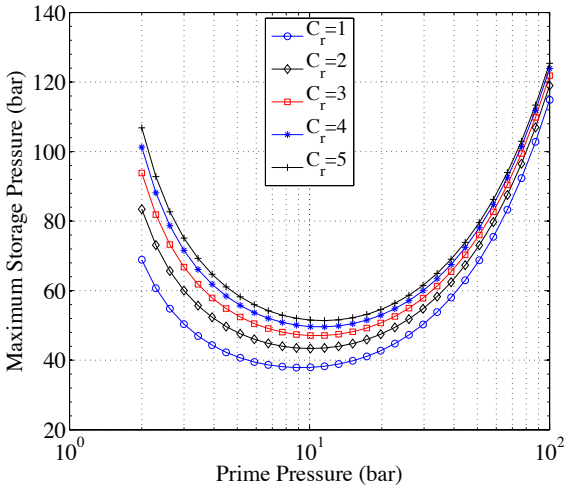


**Figure 4.9: The maximum cavern pressure versus the prime pressure for an AA-CAES of a constant 100MW power output and an isothermal cavern assumption**

The associated LTES temperature, which is a function of the maximum cavern pressure, is shown in Figure 11. The LTES temperature increases with decreasing heat capacity rate ratio. A minimum LTES temperature value exists as the LTES is largely influenced by the trend given by the storage pressure shown in Figure 10.

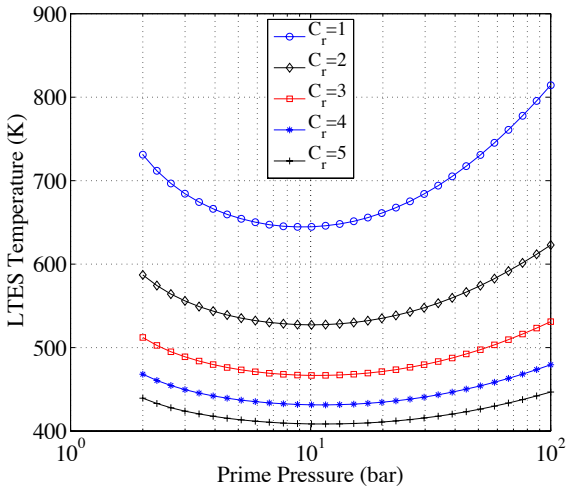


**Figure 4.10: The LTES temperature versus the prime pressure of an AA-CAES for a constant 100MW output power and an isothermal cavern**

Finally, the associated round trip efficiency of the AA-CAES storage system as a function of prime pressure is shown in Figure 12. Curves for various LTES heat capacity rate ratios are plotted to illustrate the dependence of the round trip efficiency on the LTES temperature. Lower LTES heat capacity rate ratios correspond to higher LTES temperatures and higher round trip efficiencies.

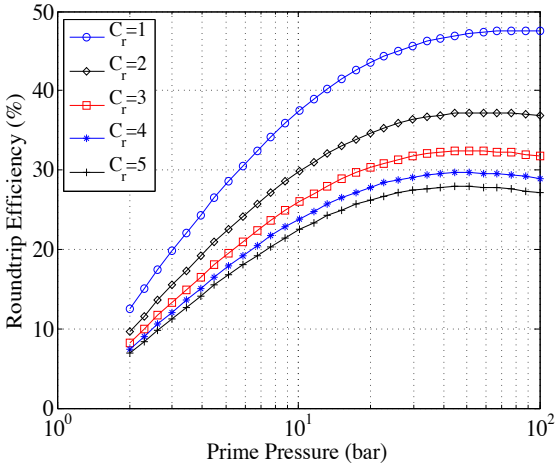


**Figure 4.11: The round trip efficiency versus the prime pressure of an AA-CAES system for a constant 100MW output power and an isothermal cavern assumption**

In the limiting case when $C_r$=1, i.e. when the LTES can reach the highest possible temperatures, the round efficiency for the prime pressure of 50 bar is approximately 47%. Comparing results in Figure 12 with those in Figures 5, it is evident that the AA-CAES has lower efficiencies compared to HTH-CAES. There are two reasons for that: 1) throttling the cavern pressure to the constant turbine operating pressure kills the available energy between the two pressures even though the enthalpic content of the air remain constant. This energy could have otherwise been extracted via an expander, and 2) the maximum temperature of the throttled process is higher in HTH-CAES compared to AA-CAES. Throttling is often a restriction imposed by the narrow range of optimal operation of a turbo-expander. While a positive displacement machine with proper valve-timing control can adjust to a time-varying inlet pressure and maintain an optimal performance, a turbo-expander performs optimally over a narrow range of inlet operating conditions of pressure, temperature and mass flow rate. Slight deviations from the design conditions results in a sharp decrease in isentropic efficiency of the machine. As a result, pressure has to be regulated to the design conditions, either via a Joule-Thomson throttling process or using an expander that is capable of taking the time-varying pressure in the cavern and

delivering a steady-state back pressure. The studies presented above quantify the performance envelope under throttling for both CAES's.

### 4.5 Cyclic Cavern Analysis

In this section, a brief analysis of the specific entropy, and its cyclic variations, corresponding to an adiabatic and isochoric cavern is presented. We begin the analysis by presenting the governing equations, followed by the charge, discharge and cycle-to-cycle variations of the cavern.

#### 4.5.1 Governing Equations:

The general mass, energy and entropy balance equations together with the calorically perfect gas equations of state for are given below:

$$\frac{dM}{dt} = \dot{m}_{in} - \dot{m}_{out} \tag{4.18}$$

$$\frac{dE}{dt} = \dot{m}_{in}h_{in} - \dot{m}_{out}h_{out} + \dot{Q} \tag{4.19}$$

$$\frac{dS}{dt} = \dot{m}_{in}s_{in} - \dot{m}_{out}s_{out} \tag{4.20}$$

$$PV = MRT \tag{4.21}$$

Where

$$E = Me \tag{4.22}$$

$$S = Ms \tag{4.23}$$

$$e = C_vT \tag{4.24}$$

$$h = C_pT \tag{4.25}$$

Where $e$, $h$ and $s$ are the specific energy, enthalpy and entropy, and $M$ is the mass of air in the cavern.

***Charge: ($\dot{m}_{out} = 0$)***

Expanding equation (20) and employing (18) results in the following equation for the specific entropy in the cavern:

$$M\frac{ds}{dt} = \dot{m}_{in}(s_{in} - s) \tag{4.26}$$

with the initial condition of

$$s(t = 0) = s(T_o, P_o) = s_o \tag{4.27}$$

Where the subscript *"o"* indicates initial properties of the cavern.

***Discharge: ($\dot{m}_{in} = 0$)***

Similarly expanding equation (20) and employing (18), results in the following governing equation for the discharge process:

$$-\dot{m}_{out}s + M\frac{ds}{dt} = -\dot{m}_{out}s \tag{4.28}$$

which, upon simplifying, yields

$$\frac{ds}{dt} = 0 \quad \rightarrow \quad s = constant \tag{4.29}$$

Therefore, the specific entropy of the cavern remains constant during the discharge process.

#### *4.5.1.1 Cyclic Variations*

Coupled integration of equations (18) through (25) along with equations (26), (27), and (29) results in cycle-to-cycle variations of the isochoric cavern. The assumed constants in this analysis are provided in Table 4.

**Table 4.4: Cyclic Cavern Assumed Constants**

| Constant | Value |
|---|---|
| Cavern Volume, $V_{cavern}$ | 300,000 $m^3$ |
| Specific Heat of Air at Constant Pressure, $C_p$ | 1 kJ/kg.K |
| Specific Heat of Air at Constant Volume, $C_v$ | 0.718 kJ/kg.K |
| Air Gas Constant, $R$ | 0.287 kJ/kg.K |
| Minimum Pressure, $P_{min}$ | 5 bar |
| Maximum Pressure, $P_{max}$ | 20bar |
| Cavern Initial Temperature, $T_o$ | 300K |
| Cavern Inlet Temperature, $T_{in}$ | 300K |
| Mass Flow Rate, $\dot{m}$ | 200kg/s |

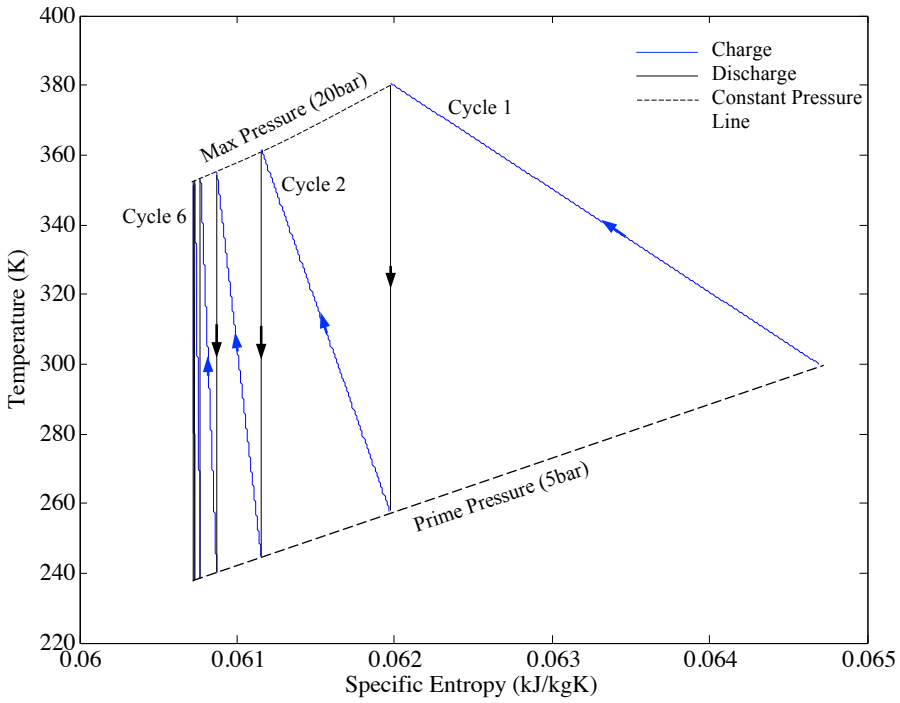


**Figure 4.12: T-s diagram of an adiabatic cavern cyclic process. The first 6 cycles of the charge and discharge process are shown.**

The result, which illustrates the cyclic variations of the cavern specific entropy, is shown in Figure 4. As shown, the specific entropy of the cavern decreases during the charge process and remains constant during the discharge process. This trend continues until the specific entropy in the cavern during the charge process, becomes isentropic, beyond which point the cavern

specific entropy does not change between cycles. As the cavern charges and discharges between the specified minimum and maximum pressures, the temperature of the cavern reaches a final range after approximately 6 cycles, under the constraints specified.

### 4.6 Discussion

The analyses presented so far are based on the assumption that pressure in the cavern monotonically increases to the peak pressure during the charge phase and monotonically drops to the prime pressure during the discharge phase. However, coupling the HTH-CAES with renewables, wind and/or solar PV for example, may invalidate this assumption, as the available power is intermittent in nature. This fact may cause the plant to discharge before reaching the peak pressure in cavern or charge before reaching the prime pressure in cavern. This consideration raises the following question: if an HTH-CAES system is designed for an optimum operating pressure condition given by Figure 5, what would be the repercussions on the roundtrip efficiency if only a portion of the total storage capacity is used? More specifically, what is roundtrip efficiency if the storage pressure swings around $P \pm x$ where $P_{nin} < P \pm x < P_{max}$? The answer to this question depends on the assumption/condition of the storage cavern (isothermal or adiabatic). In the case of an isothermal cavern all components and operating conditions of the cycle are time independent, with the exception of mass and pressure in cavern. However, the discharge operating pressure is adjusted by the pressure-regulating valve, which maintains constant pressure conditions. Therefore, regardless of the cavern state of charge, as long as the same amount of mass is charged and discharged, which is the case for a given pressure swing x, the roundtrip efficiency remains the same as the designed optimum. In the case of an adiabatic cavern however, the answer to the question is not so obvious. The time dependent temperature of the discharging cavern air is carried downstream, affecting all discharge components (LTES heat

exchanger, recuperator, HTES and turbine). With constant compression and expansion power, enforced throughout the paper, the roundtrip efficiency, equation (17), is a function of the HTES power consumption, equation (15), which is ultimately only a function of the HTES inlet temperature, $T_9$. The two constant temperature streams, provided by the LTES heat exchanger, $T_{16}$, and the recuperator, $T_{11}$, heat the discharging cavern air prior to their entrance into the HTES, and have the effect of drastically reducing the time dependent HTES inlet temperature variations, $T_9$. To demonstrate this effect, discharge temperatures are plotted as a function of time in Figure 13 for a 30bar prime pressure and a 150kg/s mass flow rate, corresponding to an optimum design given by Figure 5. In this example, the corresponding constant HTES exit temperature is $T_{10}$=1340K, as demonstrated by Figure 7. The constant turbine exhaust temperature is $T_{11}$=674K, and the constant LTES temperature is $T_{16}$=370.5K.

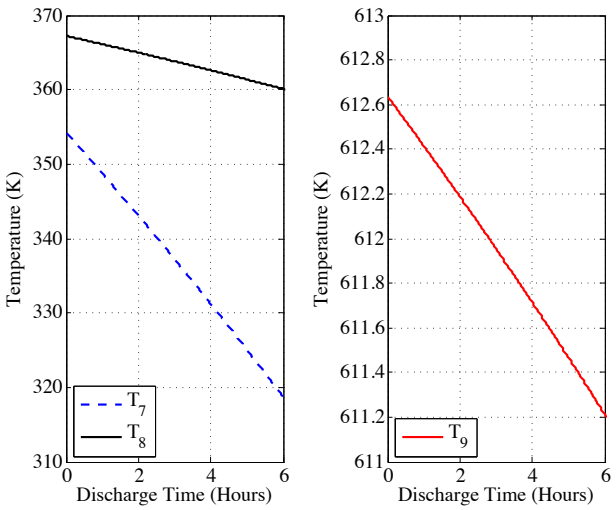


**Figure 4.13: Transient discharge temperatures in the case of an adiabatic cavern, corresponding to a prime pressure of 30bar and a mass flow rate of 150kg/s. Where the HTES exit temperature is $T_{10}$=1340K, the turbine exhaust temperature is $T_{11}$=674K, and the LTES temperature is $T_{16}$=370.5K. $T_7$ is the discharging cavern air temperature, $T_8$ is the exit air temperature of the LTES discharge heat exchanger, and $T_9$ is the HTES inlet air temperature. All subscripts correspond to the process diagram points given in Figure 1.**

The cavern discharge air temperature, $T_7$, has a relatively high temperature variation throughout the process, as shown in Figure 14(a). However, the constant temperature heating, provided by the LTES, $T_{16}$, reduces the temperature variations entering the recuperator, $T_8$, as demonstrated by its shallower slope in Figure 14(a). Subsequently, the constant temperature heating, provided by the recuperator, $T_{11}$, further reduces the temperature transients entering the HTES, as demonstrated by $T_9$ in Figure 14(b). As a result, the HTES inlet temperature variations lead to a maximum temperature difference of about 1 kelvin, a negligible change. Therefore, the energy consumption of the HTES remains essentially constant throughout the cycle, and the roundtrip efficiency, again in the case of an adiabatic cavern, remains approximately the same as the designed optimum. The calculations performed to produce Figure 14 assumed an effectiveness of 80%, as given in Table 3. It is important to note however, that the time dependent temperature variations, $T_8$ and $T_9$ in Figure 13, become identically zero at 100% heat exchanger effectiveness, where the cold exit streams become equal in temperature to the hot, and constant, inlet streams.

Another point in the analysis presented in this paper is that even though all calculations were done for a 100 MW system, the scale of utilization of the proposed HTH-CAES and the findings of the paper remains scalable and size independent. The proposed system can be integrated with a wind or PV farm, given the local wind statistics, the solar irradiation data (TMY3, for example) and the total daily, monthly and annual energy consumption of the end users. Evidently, the farm has to be oversized to account for times of insufficient or unavailable renewable power. It should be noted that since the HTES operates entirely based on resistive heating (Joule heating), it accepts any kind of electric power signal – smooth or fluctuating. It, therefore best lends itself to integration with the intermittently available wind and solar power. When the fluctuating electric

power is below the compressor power requirement, it is entirely converted to heat and stored in the HTES. When it is above that threshold, the HTES acts as a filter that absorbs the fluctuations in the form of heat and provides the compressor with a smooth power signal for proper operation. Figure 15 schematically illustrates the idea. A proper control system would therefore be necessary alongside the HTH-CAES system to properly distribute the intermittent input power signal between the HTES and the compressor within an HTH-CAES plant.

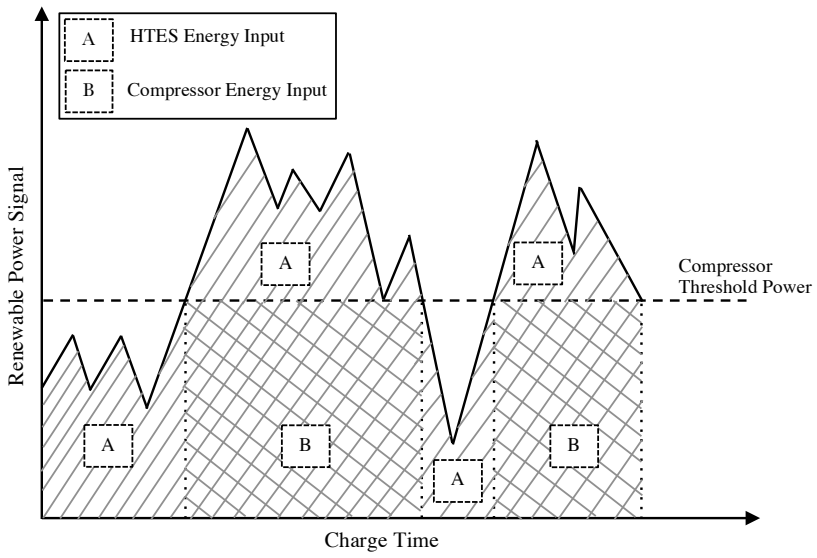


**Figure 4.14: The distribution of an intermittent renewable power signal between thermal and compressed air storage for proper operation of the HTH-CAES system and effective utilization of the available power**

## 4.7 Conclusion

A 100MW power output HTH-CAES system, with specified isentropic component efficiencies given by Table 3, was investigated. The sliding-pressure cavern is throttled in the discharge process to a constant pressure, i.e. the prime pressure, under both isothermal and adiabatic cavern conditions. The two assumptions were investigated as they demonstrate the two possible extreme cavern conditions. Parametric studies of the prime pressure were investigated for both cavern

conditions. Through the parametric study, the existence of an optimum prime pressure leading to maximum roundtrip efficiency was found. For both isothermal and adiabatic cavern conditions, the maximum round trip efficiency is within the same proximity, although the associated optimum prime pressure for an adiabatic cavern is considerably higher. A 100MW AA-CAES system was also modeled as a comparison with a throttled, isothermal, sliding pressure cavern employing the same isentropic component efficiencies used for the HTH-CAES system. It was found that the roundtrip efficiency of the AA-CAES system is highly dependent on the storage temperature. In the limiting case when the heat rate capacity ratio is unity, $C_r$=1, i.e. when the LTES can reach the highest possible temperatures, the roundtrip efficiency for a practical yet high prime pressure of 50 bar is approximately 47%. The roundtrip efficiency of an HTH-CAES system with same output power of 100MW, a flow rate of 150kg/s and a prime pressure of 15bar is about 53%. The implication of this result is that even in the case of maximum LTES temperature, 725K, which is higher than what can be provided by currently available compressors [111], an HTH-CAES system is more efficient by 6.5%. Future works should include proper account of HTES heat losses during charge and discharge to quantify the roundtrip efficiency of thermal energy storage. In addition, future works should account for pressure losses throughout the cycle.

**Table 4.5: Chapter 4 Nomenclature**

| Nomenclature | | | |
|---|---|---|---|
| LTES | Low Temperature Thermal Energy Storage | $\dot{m}$ | Air Discharge and Charge Flow Rate [kg/s] |
| HTES | High Temperature Thermal Energy Storage | m | Cavern Air Mass [kg] |
| $\eta_c$ | Compressor Isentropic Efficiency | $\dot{Q}_{HTES}$ | HTES Heat Input [kW] |
| $\eta_t$ | Turbine Isentropic Efficiency | $P_{max,adiabatic}$ | Maximum Adiabatic Cavern Pressure [bar] |
| $V_{cavern}$ | Cavern Volume [$m^3$] | $P_{max,isothermal}$ | Maximum Isothermal Cavern Pressure [bar] |
| P | Pressure [bar] | k | Ratio of Specific Heats |
| T | Temperature [bar] | $\dot{W}_{Output}$ | Output Power [kW] |
| s | Specific Entropy [kJ/kgK] | $\dot{W}_c$ | Compression Power [kW] |
| $t_{chaarge}$ | Charge Time | u | Specific Internal Energy in Cavern [kJ/kg] |
| $c_v$ | Specific Heat of Air at Constant Volume [kJ/kgK] | R | Specific Ideal Gas Constant of Air [kJ/kgK] |
| $c_p$ | Specific Heat of Air at constant pressure [kJ/kgK] | P’ | Prime Pressure [bar], Minimum Cavern Pressure and Throttling Pressure |
| $c_{,LTES}$ | Specific heat of the LTES Heat Carrier [kJ/kgK] | $\eta_{Roundtrip}$ | Round Trip Storage Efficiency |
| $C_{LTES}$ | LTES Heat Capacity Rate [kW/K] | $\Delta t$ | Time Step (Seconds) |

# Chapter 5: Thermodynamic Performance and Cost Optimization of a Modified Hybrid Thermal-Compressed Air Energy Storage System Design

## 5.1 Introduction

The hybrid thermal and compressed air energy storage system is intended to provide a means of enabling a larger fraction of renewable energy utilization, while maintaining our environmental integrity. However, to fully utilize the hybrid energy storage system an optimization study is necessary to maximize its performance and minimize its cost. In this chapter a modified Hybrid Thermal and Compressed Air Energy Storage (HT-CAES) configuration is presented which has the potential of eliminating the necessary combustion emissions in conventional CAES, and mitigating some technical issues in the otherwise attractive CAES derivatives, such as: 1) high storage pressures, 2) large storage volumes, 3) increased complexity, 4) strict geological locations, 5) low energy density, and 6) high costs. In HT-CAES, part of the available energy is spent on compressing the air, and the rest is directly converted to heat and stored in a High temperature Thermal Energy Storage (HTES) medium. The HTES can be charged either electrically from the grid, by the surplus of photovoltaic or wind electricity through Joule heating, or by a high temperature fluid stream. The high temperature fluid stream could also be either hot exhaust waste heat recovery or high temperature output of a CSP plant. Therefore the HTES eliminates the necessary combustion in conventional CAES plants and provides a means of substantially heating the air prior to expansion. The modified HT-CAES configuration presented here also includes a turbocharger, on the discharge side, which provides supplementary mass flow rate alongside the air storage. The addition of a turbocharger has the potential of

drastically reducing the storage volume and pressure, which reduces the system complexity and cost, in addition to eliminating the need for multistage compression and expansion.

In generally, the cost of thermal storage is substantially lower than the cost of air storage, per kilowatt-hour [112]-[122]. However, a heat engine is theoretically lower in efficiency than a CAES plant. Therefore, with increased reliance on thermal storage, through the turbocharger, the HT-CAES system cost and efficiency are anticipated to decrease. The goal of this chapter is to provide an efficiency and cost map of the HT-CAES system versus both the operating pressure and the distribution of energy, between thermal and compressed air storage. This chapter will illustrate and properly quantify a tradeoff that exists between the HT-CAES system cost and performance. Both roundtrip energy and exergy efficiencies are quantified, presented, and compared. Lastly, a local optimum-line of operation, which results in a local maximum in efficiency and a local minimum in cost, is presented.

## 5.2 Methods

Figure 1 represents the HT-CAES thermodynamic cycle that is analyzed here. During the charge process electricity from renewable sources, or the gird, is used to operate the compressor. Simultaneously or subsequently, depending on available power during the charge process, electricity is converted directly into thermal energy, through joule/resistive heating, and is stored in the High Temperature Thermal Energy Storage (HTES) unit. In addition to the direct electricity-to-heat conversion and storage, accomplished by the HTES, the heat of compression is also stored separately in a Low Temperature Thermal Energy Storage (LTES), which is essentially a two-tank system. Initially during the charge process, tank “a” is filled with a cold Heat Transfer Fluid (HTF) and tank “b” is empty, shown in Figure 1. As the air is being

compressed, tank "a" is discharged and the HTF collects the heat of compression via the LTES charge heat exchanger. The hot HTF is then stored in tank "b" for later use during the discharge process. During the discharge process, air is released from the cavern/tank and subsequently maintained at a constant process pressure, via Joule-Thomson throttling, through the pressure-regulating valve. The process pressure is herein referred to as the prime pressure. The temperature of the discharging air is then raised through three successive stages of heating before entering the expander: LTES, regenerator, and HTES. Additionally during the discharge process, a turbocharger is utilized which provides supplementary mass flow rate alongside the air storage. This has multiple advantages: 1) the storage system does not purely rely on the mass flow rate provided by the cavern 2) the necessary storage volume can be significantly reduced, which alleviates the restriction on geological locations 3) storage pressures can be drastically reduced, which has profound impacts on the lifetime, reliability and practicality of implementation 4) the cost of the system can be considerably reduced, as the system cost becomes leveraged by the price of thermal storage, which is typically cheaper than CAES [123].

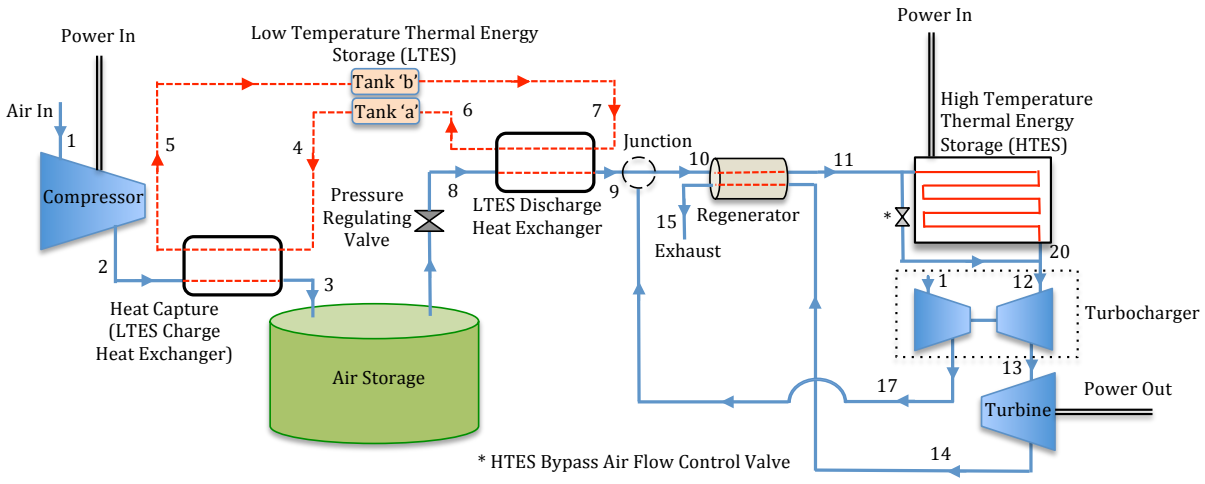


**Figure 5.1: Patented Hybrid Thermal and Compressed Air Energy Storage Process Diagram [124]**

Throughout this paper, the prime pressure, $P_{prime}$, is defined as the minimum air storage

pressure and the discharge operating/process pressure, adjusted by the pressure-regulating valve. Hence, the prime pressure delineates the expansion and compression ratios of the turbine and turbocharger compressor, which dictates their exhaust temperatures $T_{14}, T_{17}$ shown in Figure 1. Therefore, the placement order of the regenerator, LTES discharge heat exchanger, and turbocharger junction on the discharge side of Figure 1 is one possible configuration. In this analysis however, depending on the chosen prime pressure, the configuration order of the LTES discharge heat exchanger, regenerator, and junction, is rearranged such that successive heating is always attained.

### 5.2.1 Problem Statement

As described, the novel hybrid storage system presented here allows a portion of the available energy, from the grid or renewable sources, to operate a compressor and the remainder to be converted and stored directly in the form of heat by the HTES. The premise of this paper is to optimize this distribution of energy between compressed air energy storage and thermal energy storage for maximum efficiency, and for minimum cost. To properly quantify the distribution of energy between thermal and compressed air energy storage we define the variable β, which represents the fraction of energy converted and stored in the form of heat through the HTES, $\mathrm{Q_{HTES}}$, over the total amount of energy stored in the system; the energy of compression, $\mathrm{W_{Comp}}$, plus electricity-to-heat conversion and storage, $\mathrm{Q_{HTES}}$.

$$\beta = \frac{\mathrm{Q_{HTES}}}{\mathrm{W_{Comp}} + \mathrm{Q_{HTES}}} \tag{5.1}$$

The optimization analysis is achieved through a parametric study of the energy allocation fraction, defined by β, and examining its affects on the performance, cost, component sizing, and various other parameters that characterize the hybrid storage system. In addition to β, the prime

pressure is also investigated as its variation leads to important and conclusive design guidelines.

### 5.2.2 Assumptions

Pressure losses within the pipes were not taken into account and all components, besides the air storage and HTES, are assumed to operate quasi-steadily during charge and discharge. The rational is that the residence time within these components is much shorter than charge and discharge time scales, indicated in Table 1. Also, heat capacities are assumed to be temperature independent and isentropic component efficiencies are incorporated. Table 1 summarizes the additional constants used throughout the investigation presented here.

**Table 5.1: Thermodynamic Constants**

| Property | Value | Units | Description |
|---|---|---|---|
| $P_1$ | 1 | Bar | Atmospheric Pressure |
| $T_1$ | 300 | K | Atmospheric Temperature |
| $P_2$ | 20 | Bar | Maximum Air Storage Pressure |
| $T_4$ | 300 | K | LTES Inlet HX Temperature During Charge |
| $T_{12}$ | 1000 | K | Turbocharger Inlet Temperature |
| $T_{min}$ | 1000 | K | HTES Primed/Initial/Minimum Temperature |
| $T_{max}$ | 1600 | K | HTES Maximum Temperature (End of Charge) |
| $t_{charge}$ | 6 | Hours | Charge Time |
| $t_{discharge}$ | 6 | Hours | Discharge Time |
| $W_{output}$ | 100 | MW | Power Output Provided by the System |
| $\varepsilon_{d,LTES}$ | 0.8 | - | LTES Discharge Heat Exchanger Effectiveness |
| $\varepsilon_{c,LTES}$ | 0.8 | - | LTES Charge Heat Exchanger Effectiveness |
| $\eta_c$ | 0.75 | - | Compressor Isentropic Efficiency |
| $\eta_{Dcomp}$ | 0.75 | - | Turbocharger Compressor Isentropic Efficiency |
| $\eta_t$ | 0.8 | - | Turbine Isentropic Efficiency |
| $\eta_r$ | 0.8 | - | Regenerator Effectiveness |
| $c_{HTES}$ | 0.88 | kJ/kg K | Specific Heat Capacity of HTES |
| $R$ | 0.287 | kJ/kg K | Specific Gas Constant of Air |
| $c_v$ | 0.718 | kJ/kg K | Specific Heat Capacity of Air at Constant Volume |
| $c_p$ | 1 | kJ/kg K | Specific Heat Capacity of Air at Constant Pressure |

It is imperative to note that the maximum air storage pressure, $\mathbf{P_2}$=20bar, assumed in this analysis is considerably lower than that of conventional (~70bar) and advanced adiabatic (>70bar) compressed air energy storage systems. A detailed outline of the calculations made for each component in the cycle is presented next; this includes all significant equations and any component specific assumptions.

### 5.3 Calculations

The general mass and energy balance equations together with the calorically perfect gas equations of state are given below:

$$\frac{dM}{dt} = \dot{m}_{in} - \dot{m}_{out} \tag{5.2}$$

$$\frac{dE}{dt} = \dot{m}_{in}h_{in} - \dot{m}_{out}h_{out} + \dot{Q} - \dot{W} \tag{5.3}$$

$$PV = MRT \tag{5.4}$$

Where

$$E = Me \tag{5.5}$$

$$e = c_v T \tag{5.6}$$

$$h = c_p T \tag{5.7}$$

Where $e$ and $h$ are the specific energy and enthalpy, and $M$ is the mass of air. The isentropic relation, for an ideal and calorically perfect gas, relating pressure and temperature is below

$$\frac{T_2}{T_1} = \left(\frac{P_2}{P_1}\right)^{\frac{k-1}{k}} \tag{5.8}$$

### 5.3.1 Compressor

A constant compression ratio and flow rate is assumed in the compressor model. Additionally, adiabatic conditions are assumed, which result in a constant compression power with a mass flow rate given by equation (9). The compression mass flow rate, given by equation (9), is obtained by utilizing an energy balance, equation (3), and the calorically perfect and ideal gas relation given by equations (7) and (8).

$$\dot{m}_{charge} = \frac{\eta_c}{c_p T_1 \left( \left( \frac{P_2}{P_1} \right)^{\frac{k-1}{k}} - 1 \right) t_{charge}} W_{comp} \tag{5.9}$$

Where $\eta_c$ is the isentropic compressor efficiency, k is the ratio of specific heats for air, $P_2$ and $P_1$ are the maximum air storage and ambient pressures respectively, $T_1$ is the ambient temperature, $c_p$ is the specific heat of air at constant pressure, and $t_{charge}$ is the charge time. Lastly, $W_{comp}$ is the total allocated compression energy, which is a function of β; therefore the charge mass flow rate, given by equation (9), is also a function of β. The coefficient of $W_{comp}$ in equation (9) is a constant, the value of which can be obtained through the constants in Table 1. The compressor exhaust temperature is obtained by utilizing the isentropic compressor efficiency, defined as the ratio of isentropic work over actual work, the isentropic relation given by equation (8), and the calorically perfect gas equation (7), resulting in equation (10)

$$T_2 = \frac{T_1 \left( \left( \frac{P_2}{P_1} \right)^{\frac{k-1}{k}} - 1 \right)}{\eta_c} + T_1 \tag{5.10}$$

### 5.3.2 LTES

The Low Temperature Thermal Energy Storage (LTES), as explained previously, is a two-tank

system containing and circulating a Heat Transfer Fluid (HTF), which collects the heat of compression during charge, and withdraws the heat during the discharge process. Tank 'a' is assumed in thermal equilibrium with the environment and tank 'b' is assumed adiabatic, shown in Figure 1. Utilizing the constant heat exchanger effectiveness, $\varepsilon_{c,LTES}$, provided by Table 1, and an energy balance, through equation (3) and (7), the inlet and exit LTES heat exchanger temperature streams, corresponding to points 3 and 5 in Figure 1, can be obtained and are given by equations (11) and (12)

$$T_3 = T_2 - \varepsilon_{c,LTES}(T_2 - T_4) \tag{5.11}$$

$$T_5 = \frac{\dot{m}_{charge} c_p}{\dot{m}_{c,LTES} c_{LTES}} (T_2 - T_3) + T_4 \tag{5.12}$$

Where $\dot{m}_{c,LTES}$ is the LTES charge mass flow rate and $c_{LTES}$ is the specific heat of the HTF. All subscripts correspond to the process diagram in Figure 1. The heat capacity rate of the air and LTES HTF are assumed equal. Moreover, tank 'b' is assumed adiabatic, therefore $T_5$=$T_7$ in Figure 1. The temperatures in the vicinity of the LTES discharge heat exchanger and the regeneration component are calculated similarly, by applying an energy balance, assuming adiabatic conditions, and considering the heat exchanger effectiveness provided in Table. 1.

### 5.3.3 Air Storage

The air storage volume is calculated through an energy balance assuming an adiabatic, ideal, and calorically perfect gas. Utilizing equations (3)-(6) it can be shown that during the charge process the necessary air storage volume, which operates at a specified pressure swing, $\Delta P = P_2 - P_{prime}$, is

$$V_{Air\ Storage} = \frac{kRT_3 t_{charge}}{P_2 - P_{prime}} \dot{m}_{charge} \tag{5.13}$$

Where $P_{prime}$ is the minimum storage pressure and $P_2$ is the maximum storage pressure, given in Table 1. The calculated results given by equations (9) and (11) are used to determine the air storage volume in equation (13). The mass flow rate, given by equation (9), is a function of the energy fraction, β, therefore the air storage volume, specified by equation (13), is also a function of β. The air storage discharge mass flow rate is determined through an energy balance assuming an adiabatic, ideal, and calorically perfect gas. Utilizing equation (3)-(6), where $M_o$ is the initial stored air mass determined through the ideal gas equation (4), it can be shown that

$$\dot{m}_{discharge} = \frac{M_o + t_{charge}\dot{m}_{charge}}{t_{discharge}} \left[ 1 - \left( \frac{P_{prime}}{P_2} \right)^{\frac{1}{k}} \right] \tag{5.14}$$

The air storage is initially assumed at a specified prime pressure, $P_{prime}$, and ambient temperature. The air storage is inherently transient therefore the time dependent temperatures and pressures must be calculated as the discharging air passes through the various downstream components. Through the mass and energy balance, equations (2) and (3), together with the calorically perfect gas equations of state, given by equations (4)-(7), the following discretized equations are used to determine the time dependent temperature and pressure of the discharging air

$$u(t + \Delta t) = \frac{M(t)u(t)}{M(t + \Delta t)} + \frac{M(t + \Delta t) - M(t)}{M(t + \Delta t)} h(t) \tag{5.15}$$

$$T(t + \Delta t) = \frac{u(t + \Delta t)}{c_v} \tag{5.16}$$

$$P(t + \Delta t) = \rho(t + \Delta t) \cdot R \cdot T(t + \Delta t) \tag{5.17}$$

The initial temperature of the discharging air is found by incorporating the ideal gas law given the specified maximum pressure in Table 1, the calculated volume from equation (13), and the total stored mass. The air storage is discharged until the specified prime pressure, $P_{prime}$, is reached.

### 5.3.4 Turbocharger

The purpose of the turbocharger is to provide supplementary mass flow rate, at the junction in Figure 1, in addition to the discharging cavern/tank flow rate. The total discharge flow rate, which enters the HTES and turbine, is therefore the sum of both discharging cavern/tank mass flow rate plus supplementary mass flow rate provided by the turbocharger. Through an energy and mass balance, on a control volume containing the turbocharger and power turbine, the total necessary discharge mass flow rate is obtained and is given by equation (18)

$$\dot{m}_t = \frac{\dot{W}_{output} - \dot{m}_{discharge} c_p (T_{17} - T_1)}{c_p (T_{12} - T_{14}) - c_p (T_{17} - T_1)} \tag{5.18}$$

Where $\dot{W}_{output}$, $T_{12}$, $T_1$ and $c_p$ are constants specified by Table 1, and $\dot{m}_{discharge}$ is given by equation (14). The compressor and turbine exhaust temperatures, $T_{14}$ and $T_{17}$, are obtained by employing the isentropic compressor and turbine efficiencies given in Table 1, similar to the procedure which arrived at equation (10).

### 5.3.5 HTES

The high temperature thermal energy storage (HTES) is inherently a transient component. However, the HTES can be designed to deliver a constant temperature, necessary for optimal operation of a turbo-expander, through bypassing a portion of the cold inlet air with the hot flow

exiting the HTES, as shown in Figure 1. Applying the energy and mass balance to the point where the bypass line mixes with the hot flow out of the HTES, the bypass mass flow rate, $\dot{m}_{bp}(\mathrm{t})$, can be obtained as a function of $T_{20}(t)$ and $T_{12}$:

$$\dot{m}_{bp}(t) = \dot{m}_t \frac{T_{20}(t) - T_{12}}{T_{20}(t) - T_{11}(t)} \tag{5.19}$$

Where $T_{20}(t)$ is the time dependent temperature of the HTES. For simplicity, and as a first order approximation, a lumped capacitance approximation is used to model the HTES, where no temperature gradients exist within the HTES. Additionally it is assumed that at each instant of time during the discharge process the exit air temperature is equal to the instantaneous HTES temperature. The amount of energy allocated to the HTES, $Q_{\beta,HTES}$, is used to size its mass such that its maximum specified temperature is reached at the end of charge as follows

$$M_{HTES} = \frac{Q_{\beta,HTES}}{c_{HTES}(T_{max} - T_{min})} \tag{5.20}$$

The total energy that must be stored by the hybrid storage system, to deliver the constant energy output specified in Table 1, must be iteratively solved at each specified β. This is because the sought-after efficiency of the system is inherently a function of β as made clear by equation (21)

$$E_{input}(\beta) = \frac{E_{output}}{\eta_I(\beta)} \tag{5.21}$$

The first law efficiency, or equivalently the roundtrip energy efficiency, $\eta_I$, is defined as the total output energy over the total input energy, thermal plus compression. $E_{input}$ and $E_{output}$ are the total input and output energies. The bisection method is used to iteratively solve for the necessary input energy, such that the final HTES temperature, at the end of discharge, reaches

precisely the minimum value specified in Table 1.

### 5.3.6 Roundtrip Energy and Exergy Efficiencies

The roundtrip energy efficiency (1st law efficiency) of the system is defined on an energy basis as the total output over total input energy as shown by equation (22).

$$\eta_I = \frac{\int \dot{W}_{output}\, dt}{\int \dot{W}_{comp} dt + \int \dot{Q}_{HTES}\, dt} \tag{5.22}$$

Similarly, the roundtrip exergy efficiency (2nd law efficiency) is defined as the total output over total input exergy, as shown by equation (23).

$$\eta_{II} = \frac{\int \dot{W}_{output}\, dt}{\int \dot{W}_{comp} dt + \int (1 - T_o/T_{HTES}) \dot{Q}_{HTES}\, dt} \tag{5.23}$$

The exergy associated with compression and expansion is equivalent to their energy values, assuming adiabatic conditions. However, the exergy associated with heat transfer in the HTES is determined by the second term in the denominator of equation (23). For simplicity, assuming no temperature gradients within the HTES and a constant input electrical signal, the exergy associated with heat transfer can be calculated by first determining the HTES temperature, $T_{HTES}$, during the charge process using the energy balance equation (3). Performing the Integration in equation (23) and utilizing the 1st law efficiency and β definitions, through equation (22) and (1), results in equation (24)

$$\eta_{II} = \frac{\eta_I}{1 - T_o \beta \ln\left(1 + \delta/T_{\min}\right)/\delta} \tag{5.24}$$

Where $T_o$ is the ambient temperature, $T_{\min}$ is the minimum HTES temperature, and $\delta$ is the maximum HTES temperature difference, $\delta = T_{\max} - T_{\min}$. The 2nd law efficiency of the system, equation (24), is presented conveniently as a function of the 1st law efficiency, $\eta_I$, the energy distribution fraction, $\beta$, and the HTES periphery temperatures. By observing the 2nd law efficiency, equation (24), it becomes immediately apparent that all variables in the denominator are positive. Therefore, the 2nd law efficiency is always greater than or equal to the 1st law efficiency, $\eta_{II} \geq \eta_I$, which is consistent with the exergy efficiency of heat engines.

### 5.3.7 Cost Functions

The following cost functions, based on thermodynamic variables, are used to determine the purchase price of the compressors and turbines [125], [126].

$$\Xi_{\text{compressor}} = \mathrm{c}_1 \frac{39.5\,\dot{m}}{0.9 - \eta_c} r_c \ln(r_c) \tag{5.25}$$

$$\Xi_{\text{turbine}} = \mathrm{c}_1 \frac{266.3\,\dot{m}}{0.92 - \eta_t} \ln(r_e)(1 + \exp(0.036 T_{\text{inlet}} - 54.4 c_2)) \tag{5.26}$$

Where $r_c$ and $r_e$ are the compression and expansion pressure ratios and the constants, $\mathrm{c}_1$=1.051 $c_2$=1.207, reflect costs reported by the Gas Turbine World Handbook [125], [126]. The cost of air storage through an above ground tank typically scales with volume and pressure, however, with a fixed maximum pressure throughout this study, the cost function for a tank as a function of volume, based on multiple vendors (Fjords Processing, KS Industries, Modern Custom Fabrication Inc.), is below

$$\Xi_{\text{Air Storage}} = 1000\, V_{tank} \tag{5.27}$$

The cavern cost function, based on volume, is shown below [23]

$$\Xi_{\text{Air Storage}} = 3.75\times10^{7} + 62\, V_{cavern} \tag{5.28}$$

In this analysis the cheapest air storage architecture, based on the above cost functions, is utilized. Lastly, the HTES is an alumina-based refractory with a material purchase cost, based on mass and determined through various vendors (Resco Products, Harbison-Walker Refractories), given by the cost function below

$$\Xi_{\text{HTES}} = 2.2 M_{HTES} \tag{5.29}$$

In addition to the above cost functions, a factor of 1.25 is multiplied to account for the remaining heat exchangers, pipes, valves, LTES HTF and tanks. The total system capital cost per kilowatt-hour is given below

$$Cost\left[\frac{\$}{kWh}\right] = \frac{(\Xi_{\text{compressor}-1} + \Xi_{\text{compressor}-2} + \Xi_{\text{turbine}-1} + \Xi_{\text{turbine}-2} + \Xi_{\text{Air Storage}} + \Xi_{\text{HTES}})\times1.25}{E_{output}} \tag{5.30}$$

Where two compressor and turbine cost functions are considered, as evident by Figure 1. The denominator represents the total delivered energy, obtained by multiplying the total discharge time by the constant output power, as specified in Table 1.

### 5.4 Results

As stated in the Problem Statement section 2.1, the premise of this study is to investigate the performance and cost of the hybrid energy storage system as the energy distribution between thermal and compressed air energy storage is varied. The distribution of energy is quantified

through the variable β, equation (1). The extreme case of β=100% results in pure thermal energy storage, as no energy is allocated towards compression, and the air storage does not receive or provide any air mass flow. Therefore, in the case where β=100% the process diagram, in Figure 1, becomes a regenerative brayton cycle. Conversely, the case of β=0% results in pure compressed air energy storage, with no energy allocated to the HTES. In addition to analyzing the ramifications of β on the performance and cost of the system, the prime pressure is also investigated. The prime pressure, $P_{prime}$, represents the minimum air storage pressure and the discharge operating pressure, which is adjusted through the pressure-regulating valve, as shown in Figure 1. The two variables under investigation β and $P_{prime}$ are of particular interest as their variation lead to noteworthy and definitive design guidelines.

### 5.4.1 Roundtrip Energy and Exergy Efficiencies

The roundtrip energy efficiency (1$^{st}$ law efficiency) map of the HT-CAES system, and its corresponding contour plot, is provided in Figure 2. As stated previously, in the extreme limit of β=100%, where the energy is stored purely in the form of heat through the HTES, the hybrid storage system becomes a regenerative brayton cycle. Moreover, in a regenerative brayton cycle, with a constant power output and turbine inlet temperature, there exists an optimum operating pressure (prime pressure, $P_{prime}$) leading to maximum energy efficiency. This is equivalent to, and validates, the profile in Figure 2 at β=100%.

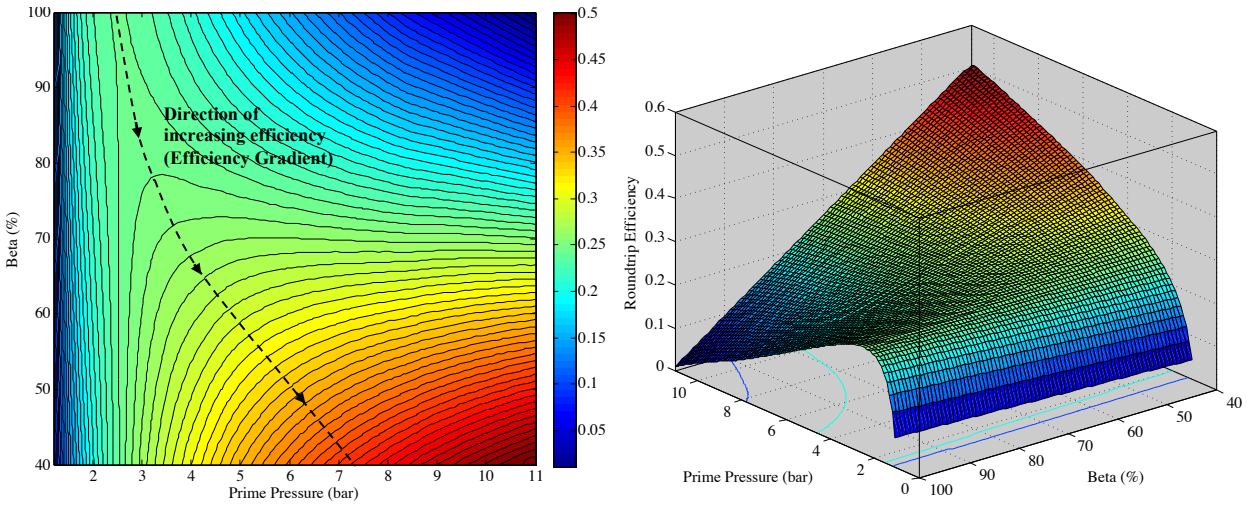


**Figure 5.2: HT-CAES roundtrip energy efficiency map as a function of the energy distribution fraction, β, and the prime pressure, $P_{prime}$. The dotted line represents the direction of increasing efficiency (efficiency gradient, $\nabla\eta(\beta, P_{prime})$), which begins at the optimum design point of a regenerative brayton cycle (at $\beta = 100\%$).**

As the operating pressure increases, at β=100%, eventually regeneration becomes ineffective as the turbine exhaust temperature falls below the turbocharger compressor exhaust temperature. At which point regeneration is disengaged and a classical brayton cycle is employed at higher operating pressures, resulting in slightly higher efficiencies, nevertheless, eventually leading to zero efficiency. A brayton cycle at a constant turbine inlet temperature of 1000K, power output of 100MW, and isentropic efficiencies corresponding to the constants in Table 1, reaches an efficiency of zero at an operating pressure of 11.3bar and is not operational for higher operating pressures. In general, the efficiency of the hybrid storage system increases with decreasing β; as the reliance on compressed air storage increases. This is because a hybrid CAES system is theoretically more efficient than its corresponding brayton cycle counter part. Additionally, CAES systems are generally not bound by the Carnot efficiency, as is the case for heat engines. Furthermore, as β increases, a larger fraction of the discharge flow rate is provided by the turbocharger, which introduces additional isentropic component efficiencies that impede the roundtrip energy efficiency of the system. The efficiency of the hybrid storage system increases

with the operating pressure at the lower end of the β spectrum, corresponding to higher compressed air storage dependence, as illustrated in Figure 2. The reason behind the monotonic increase in efficiency with operating pressure, at lower β values, stems from the accompanying decrease in throttling losses and exhaust temperatures.

At β values below 40%, the amount of energy allocated towards the HTES becomes too low for proper operation. This is because the HTES mass, which is calculated based on the specified temperature swing in Table 1, decreases with decreasing β; as the energy allocated for thermal storage decreases. Eventually, the HTES mass becomes too low and drops below the minimum specified temperature at the end of discharge, and therefore cannot bear the total discharging flow rate. Hence, β values below 40% are not investigated. Beginning with the optimum prime pressure of a regenerative brayton cycle, at β=100% in Figure 2, and moving along the direction of increasing efficiency or efficiency gradient, results in the dotted line shown in Figure 2. Any perpendicular deviation along this efficiency gradient results in a lower efficiency than otherwise achievable. The significance of this efficiency gradient curve will be demonstrated and revisited when discussing the capital cost of the system, in section 4.3.

The roundtrip exergy efficiency ($2^{nd}$ law efficiency) contour map of the HT-CAES system is provided in Figure 3.

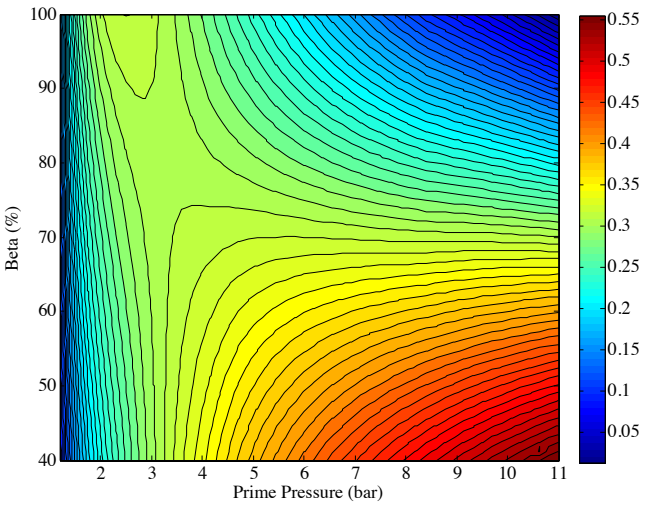


**Figure 5.3: HT-CAES roundtrip exergy efficiency contour map as a function of the energy distribution fraction, β, and the prime pressure.**

The HT-CAES exergy efficiency is always greater than its energy efficiency, a result that is consistent with heat engines. The energy and exergy efficiencies become coincident in the limiting case of a very large HTES temperature swing, $\delta = T_{max} - T_{min}$, as indicated by equation (31).

$$\lim_{\delta \to \infty} \eta_{II} = \eta_I \tag{5.31}$$

Therefore, the minimum exergy efficiency is equal to its corresponding energy efficiency, $\eta_{II,min} = \eta_I$. This is due to the increase in internal irreversibilities associated with mixing losses in the HTES at a high temperature swing; a result that is undetected through the first law analysis and efficiency. Conversely, the largest difference in 1st and 2nd law efficiencies (in other words, the maximum exergy efficiency for a given energy efficiency) occurs in the limit of a very low HTES temperature difference, meaning the HTES remains isothermal, and internal irreversibilities associated with mixing losses are eliminated, as shown by equation (32)

$$\lim_{\delta \to 0} \eta_{II} = \frac{\eta_I}{1 - \beta \frac{T_o}{T_{\min}}} \tag{5.32}$$

Further increase in their difference occurs for 1) high $\beta$ values, and 2) at lower HTES temperatures. Since the exergy efficiency is defined as a comparison of the system performance to the ideal case, at high $\beta$ values the system is utilizing a lower quality of energy (heat), therefore for the same energy efficiency the result is higher exergy efficiencies. In the limit that $\delta = T_{max} - T_{min} = 0$, by definition this means the HTES remains isothermal, $T_{min} = T_{max} = T_{HTES}$. As a mathematical consequence, with a lower HTES temperature the second term in the denominator of equation (23) is at a minimum, which leads to maximum exergy efficiency for a given energy efficiency. However, the physical meaning can be explained as follows: at a low HTES temperature the system is utilizing a lower quality of heat, therefore for the same energy efficiency the result is higher exergy efficiencies.

### 5.4.2 Component Sizing

The various mass flow rates of the system, the air storage volume, and the thermal storage mass are presented in this section. The charge and discharge mass flow rates into and out of the cavern/tank are plotted, in Figure 4, as functions of the prime pressure and the energy distribution fraction. The charging mass flow rate, into the air storage, is identically zero at β=100% as no energy is allocated and stored in the form of compression, Figure 4. In general, the charge mass flow rate increases with decreasing β as more energy is allocated towards compressing and storing air. In addition, at higher roundtrip efficiencies the amount of output power per kilogram of air is also higher; meaning, for a constant power output the necessary mass flow rate is lower. Consequently, at the lower end of the β spectrum, the charge mass flow rate decreases with prime pressure, as a result of the increase in efficiency, as evident by Figure

2 and 3. The discharging mass flow rate provided by the air storage is nearly identical to the charge mass flow rate, as the air storage is assumed adiabatic. Therefore, the trends of the discharging mass flow rate, as a function of β and the prime pressure, are the same as those described previously for the charging flow rate. The analysis performed here is of the first cycle, however after several cycles the air storage no longer experience cyclic variations, at which point the charge and discharge mass flow rates become identical.

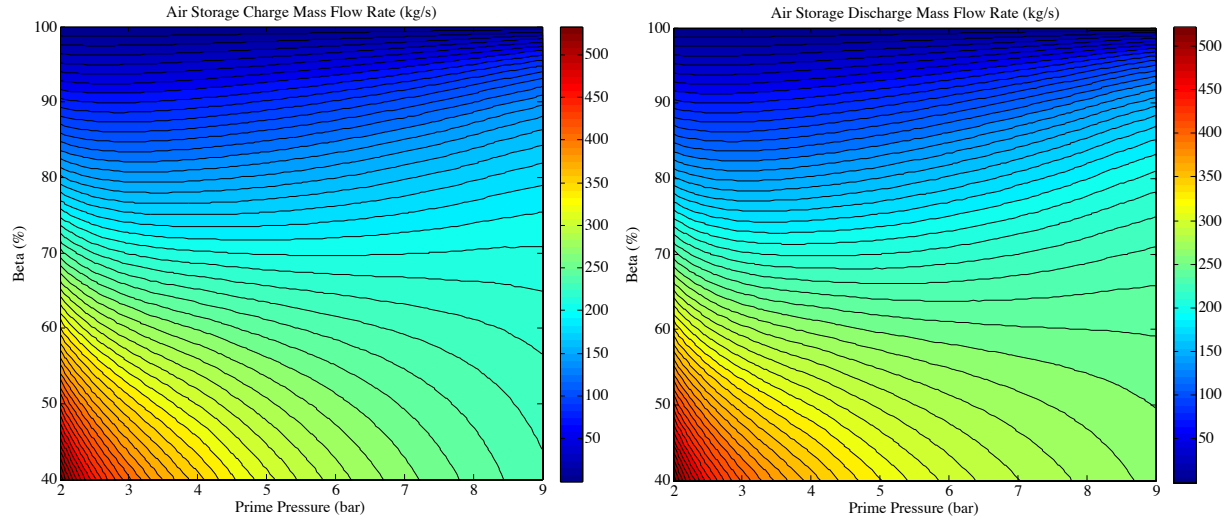


**Figure 5.4: HT-CAES air storage, charge and discharge, mass flow rates as a function of the energy distribution, β, and the prime pressure**

The turbine and turbocharger mass flow rates are plotted in Figure 5 as functions of the energy distribution fraction and the prime pressure. As depicted by Figure 5, the turbine mass flow rate generally decreases with decreasing β. Moreover, the turbine mass flow rate, at the higher β spectrum, reaches a minimum value as a function of the prime pressure and decreases with increasing prime pressure at the lower β spectrum. The turbine mass flow rate resembles the opposite trend depicted by the roundtrip efficiency. This is because the total and necessary mass flow rate through the turbine is largely influenced by the roundtrip efficiency of the system. The total mass flow rate is inversely proportional to the roundtrip storage efficiency, since the total

power output per kilogram of air is higher at regions of higher efficiency, which for a constant power output results in lower mass flow rates. Conversely, the total power output per kilogram is lower at regions of lower efficiency, which for a constant power output results in higher necessary mass flow rates.

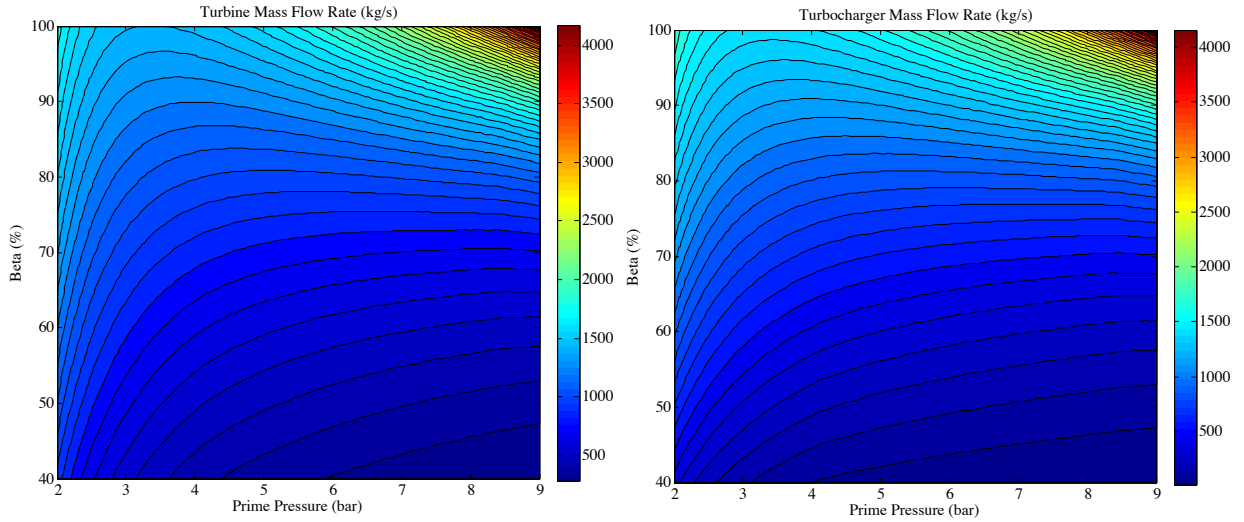


**Figure 5.5: HT-CAES turbine and turbocharger, mass flow rates as a function of the energy distribution, β, and the prime pressure**

The necessary turbocharger mass flow rate, in general, decreases with decreasing β values. By definition, as β decreases the reliance of the flow rate on the turbocharger decreases as the air storage provides a larger fraction of the total flow rate. The turbocharger mass flow rate map is largely influenced by the total turbine mass flow rate, as it is defined as the difference between the total and the stored air discharge mass flow rate.

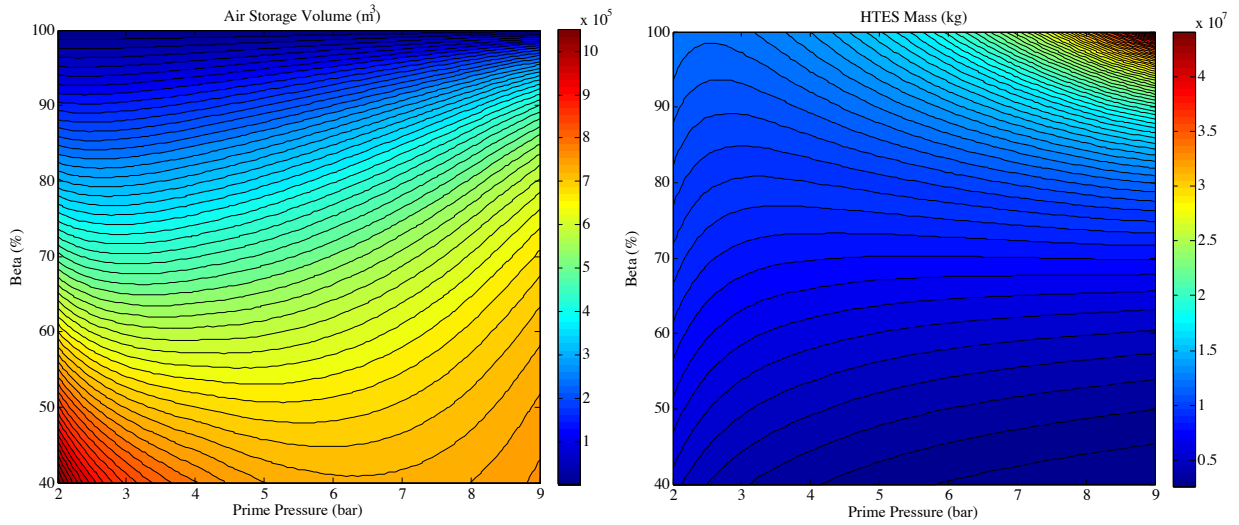


**Figure 5.6: HT-CAES air storage volume and thermal storage mass as a function of the energy distribution, β, and the prime pressure**

The air storage volume, Figure 6, generally increases with decreasing β; this is because the reliance on the compression energy increases with decreasing β. At β=100%, the air storage volume is identically zero, as the system evolves into a regenerative brayton cycle. As β values decrease from 100%, the volume increases with the prime pressure and the total compression energy, as depicted by equation (13). The compression energy, for a fixed β value, is inversely proportional to the roundtrip efficiency of the system. Therefore the air storage volume, at constant β, is proportional to the prime pressure and inversely proportional to the roundtrip efficiency of the system. The competition between the efficiency of the system and its prime pressure leads to a minimum air storage volume illustrated in Figure 5, for a fixed β value, particularly at the lower β spectrum.

The HTES mass is plotted in Figure 6 as functions of the prime pressure and β. More energy is allocated towards thermal storage with increasing β. Therefore in general, the HTES mass increases with β in order to achieve the specified and constant HTES temperature swing in each

cycle, as shown in Figure 6. For a fixed value of β, at the higher end of its spectrum, the HTES mass given in Figure 6 reaches a minimum as a function of the prime pressure. The prime pressure leading to a minimum HTES mass coincides with that of maximum efficiency, in Figure 2. As the prime pressure increases, the HTES mass also increases due to the decrease in system efficiency; therefore more energy must be stored as higher turbine mass flow rates are employed to obtain the constant output energy during each cycle. Inversely, at the lower end of the β spectrum, the efficiency of the system increases with prime pressure, therefore the total discharge flow rate and the total necessary HTES mass decrease with increasing prime pressure.

### 5.4.3 Capital Cost

The total cost of the storage system per unit of delivered energy, equation (27), is shown in Figure 7. The roundtrip efficiency and air storage price have a dominant influence on the system capital cost, as the air storage price per unit volume is much higher than the HTES cost per unit mass, and the efficiency dictates the necessary storage sizes. Therefore in general, the cost increases with decreasing efficiency and increasing storage volume. At β=100%, where the air storage volume is identically zero, the cost is purely that of the HTES and its corresponding machinery cost per kilowatt-hour. As the system efficiency decreases, with increasing prime pressure at β=100%, the necessary HTES mass and flow rates, Figure 4 & 5, increase drastically resulting in higher cost. As β decreases, the air storage price begins to influence the system cost as its necessary volume increases. At β values very near 100%, a tank is more cost effective than a cavern, however caverns become more cost effective very quickly as β is decreased from 100%.

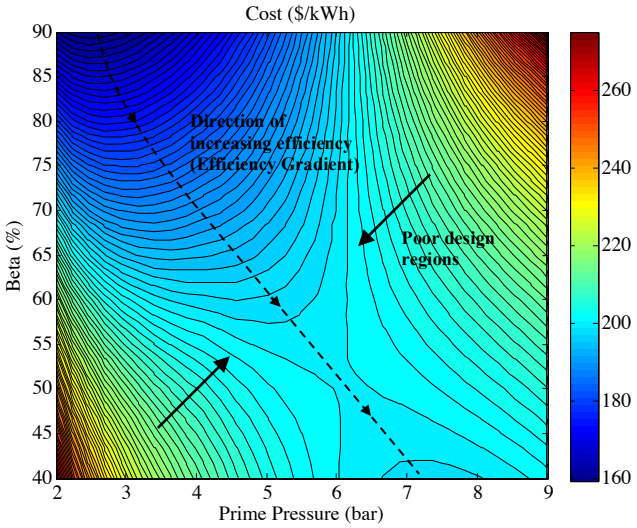


**Figure 5.7: HT-CAES cost ($/kWh), equation (27), as a function of the energy distribution, β, and the prime pressure. The dotted line represents the direction of increasing efficiency (given in Figure 2), which begins at the optimum prime pressure of a regenerative brayton cycle (at $\boldsymbol{\beta = 100\%}$).**

Revisiting the efficiency gradient in Figure 2, and overlapping the efficiency gradient on the cost map results in the dotted line, labeled "Efficiency gradient", in Figure 6. As was demonstrated by Figure 2, any perpendicular deviation from this efficiency gradient results in a lower efficiency than otherwise achievable. Additionally however, the cost map given by Figure 6 demonstrates that perpendicular deviations from this efficiency gradient also result in a higher cost. Therefore, the efficiency gradient provides a local optimum design region resulting in maximum efficiency and minimum cost. Any deviation perpendicular to the efficiency gradient line results in a higher cost and lower efficiency than otherwise achievable, therefore areas away from this line can be regarded as poor design regions that should be avoided.

In general, the cost of the hybrid storage system increases along the efficiency gradient, or along the local optimum line of operation. In other words, as the reliance on thermal energy storage is increased the cost of the system is decreased, as the system cost becomes leveraged by the cheap

thermal energy storage cost. The addition of the turbocharger provides a means of heavily relying on thermal storage, as its additional mass flow rate reduces the reliance on the air storage. Therefore, there exists an inherent trade-off in the hybrid storage cost and efficiency as a function of the energy distribution. The desired point of operation along the efficiency gradient, or the local optimum line of operation, depends on the specific energy application, which the hybrid storage system must integrate with. Energy application priorities are not unique; these priorities may include cost, efficiency and footprint. The efficiency gradient line provides a means of adjusting the system characteristics to meet various application priorities without a change in system capacity. However, tradeoffs between efficiency, cost, and footprint are inherent in the system and quantified through the efficiency, size, and cost maps provided by Figures 2, 5, and 6. A lower system cost and footprint results in a lower efficiency, corresponding to higher thermal energy storage allocation (large β values). On the contrary, higher system efficiency requires a higher capital cost and a larger footprint, corresponding to higher compressed air energy storage allocation (lower β values).

It is imperative to note the existence of a local minimum and maximum in cost along the efficiency gradient, at the lower end of the β spectrum, given by Figure 7. This is caused by the local minimum in storage volume, shown in Figure 5, as a function of the prime pressure at lower β values. The slopes in the vicinity of the local minimum and maximum in cost are quite gradual. Additionally, any further increase in efficiency at β=40%, at the lower end of the efficiency gradient in Figure 7, would require an increase in the prime pressure which would further increase the cost of the system. Therefore, the optimal global maximum and minimum in cost and efficiency reside at the ends of the local optimum line of operation.

## 5.5 Discussion

The capital costs of various grid-scale energy storage systems are widely available in the literature. Table.2 provides a summary of the minimum, average, and maximum reported capital cost values of various available grid-scale energy storage technologies, along with the calculated HT-CAES system cost for comparison.

**Table 5.2: Reported capital costs of various grid-scale energy storage systems, from the literature [127]**

| Energy Storage Technology | Capital cost, per unit of storage capacity ($/kWh) | | |
|---|---|---|---|
| | **Minimum** | **Average** | **Maximum** |
| CAES | 249 | 312 | 330 |
| Flywheel | 2,201 | 5,701 | 29,808 |
| Li-ion battery | 546 | 649 | 666 |
| Supercapacitors | 822 | 910 | 1,018 |
| Hydrogen | 474 | 642 | 927 |
| **HT-CAES** | **65** | **-** | **200** |

The minimum hybrid thermal-compressed air energy storage (HT-CAES) system capital cost, in Table 2, corresponds to β=100%, which results in pure thermal storage. The maximum HT-CAES capital cost value corresponds to β=40%, where the turbocharger is essentially turned off and the system resembles that of a conventional CAES design. Moreover, the performance of a conventional CAES system is identical to that of an HT-CAES system at β=40%, assuming a similar storage pressure and turbine inlet temperature. As evident through Table 2, the HT-CAES system is reasonably competitive from a capital cost perspective, as the HT-CAES system cost is leveraged by the cheap thermal storage. The CAES capital cost range in Table 2 is that of a conventional design. The cost of an advanced adiabatic CAES system is typically higher than that of a conventional system due to its need for multistage compression and expansion [38]. Additionally, the performance of an AA-CAES is typically lower in efficiency than that of

hybrid system, assuming throttling losses exist, due to its strong dependence on the temperatures captured by the generated heat of compression. In the presence of throttling losses and internal irreversibilities, realistic AA-CAES efficiencies range from 28%-47% depending on the temperature limit provided by the generated and stored heat of compression [38]. Therefore, the HT-CAES system provides a competitive design compared to conventional CAES systems and its advanced adiabatic derivative. Moreover, HT-CAES provides a means of adjusting to various footprint and cost requirements, without compromising the storage capacity. It is important to note that further performance improvements, in the HT-CAES system, are possible. As noted in the capital cost section 4.3, the HT-CAES system cost is dominated by the air storage price. Therefore, incorporating intercooling and reheating components can reduce the necessary compression power and increase the potential for regeneration. Thereby improving the performance of the HT-CAES system without a substantial increase in its capital cost per unit of storage capacity.

Although batteries, flywheels, and supercapacitors generally have higher energy efficiencies, their costs are substantially higher than CAES systems. In addition, their lifetime, energy capacity and discharge times are typically lower than CAES systems. These parameters, among others, play a key role in determining the suitable applications that an energy storage technology may provide within the electrical grid. With their unique strengths and weaknesses, it is unlikely that a sole energy storage technology will provide a universal solution. On the contrary, each available energy storage technology may provide an exclusive solution to a specific grid/renewable-integration application. A good metric for comparing various forms of energy storage is the levelized cost of electricity (LCOE), as it considers the energy efficiency, lifetime,

capital cost, and maintenance cost of the system. Therefore, in future work, further insight can be gained by comparing the HT-CAES system with various other forms of energy storage from an LCOE perspective.

## 5.6 Conclusion

A novel hybrid thermal and compressed air energy storage configuration is developed which has the potential of eliminating combustion emissions and drastically reducing the storage pressure, volume, and cost as compared with conventional CAES and its derivatives. The addition of both thermal energy storage and a turbocharger have the effect of significantly leveraging the cost of the system, as supplementary mass flow rate is provided along side the stored air, and the cost of thermal storage is considerably cheaper than air storage. The reduced system cost, however, comes at the expense of a reduced efficiency, as the performance of heat engines are bound by the Carnot limit and compressed air energy storage, theoretically, has no such constraint. The hybrid system provides the flexibility of adjusting to a myriad of storage volumes based on available geological restrictions. In addition, the hybrid storage system performs best at low storage pressures, which reduces the complexity as it alleviates the need for multistage compression and expansion. The thermodynamic optimization results provide the operational efficiency, cost and storage sizing (thermal and air volume) maps, which can be used as a reference in future development endeavors. In addition all mass flow rate maps are provided, which dictate the necessary machinery sizes. The operational flexibility of HT-CAES is particularly useful as the priorities of various energy applications are not unique, these priorities may include cost, efficiency, and footprint. The hybrid CAES system possesses a wide range of possible operations, without a compromise in its storage capacity, which may prove useful as we move towards a sustainable future.

**Table 5.3: Chapter 5 Nomenclature**

| Nomenclature | | | |
|---|---|---|---|
| HT-CAES | Hybrid Thermal Compressed Air Energy Storage | LTES | Low Temperature Thermal Energy Storage |
| HTES | High Temperature Thermal Energy Storage | HTF | LTES Heat Transfer Fluid |
| $r_e$ | Expansion Pressure Ratio | $r_c$ | Compression Pressure Ratio |
| $\beta$ | Energy Distribution (equation 1) | $\eta$ | Component Efficiency |
| $W$ | Energy of Compression or Expansion | $\varepsilon$ | Heat Exchanger Effectiveness |
| $\dot{W}$ | Power of Compression or Expansion | $k$ | Ratio of Specific Heat of Air |
| $Q$ | Heat Energy | $V$ | Volume |
| $\dot{Q}$ | Heat Power | $R$ | Ideal Gas Constant of Air |
| $P$ | Pressure | $E$ | Energy |
| $T$ | Temperature | $e$ | Specific Energy |
| $\rho$ | Density | $h$ | Specific Enthalpy |
| $M$ | Mass | $u$ | Specific Internal Energy |
| $\dot{m}$ | Mass Flow Rate | $\Xi$ | Component Cost Function |
| $t$ | Time of Charge or Discharge | $c_p$ | Specific Heat of Air at Constant Pressure |
| $c_v$ | Specific Heat of Air at Constant Volume | $c_{HTES}$ | Specific Heat of the HTES |
| $c_{LTES}$ | Specific Heat of the LTES HTF | $t$ | Charge or Discharge Time |
| $\eta_I$ | Roundtrip Energy Efficiency (1st Law Efficiency) | $\eta_{II}$ | Roundtrip Exergy Efficiency (2nd Law Efficiency) |

# Chapter 6: Performance of The Hybrid Compressed Air Energy Storage System at Minimum Entropy Generation

## 6.1 Introduction

The optimization of a hybrid thermal-compressed air energy storage system, unlike heat engines, has not been devoted any attention. Conversely, the optimization of heat engines has been investigated quite extensively [128]-[146]. Numerous optimization criterions have been examined to analyze the performance of common heat engines [147-151]. However such analysis has not been employed on a hybrid thermal-compressed air energy storage system. Common optimization variables investigated in the literature for power cycles are thermal efficiency, output power, entropy generation, and ecological function [152]. The Gouy-Stodola theorem states that maximum output work coincides with minimum entropy generation. For heat engines, the maximum efficiency and maximum output power do not necessarily coincide. In a regenerative Brayton cycle, maximum work and maximum efficiency correspond to the same design point only at recuperator effectiveness of fifty percent. [153].

The main objective of this chapter is to investigate the performance of an isobaric hybrid thermal and compressed air energy storage system at the point of minimum entropy generation, which has not been formerly reported. Both the energy and exergy efficiencies are examined and the optimum design points leading to their maxima is compared with the design point corresponding to minimum entropy generation. The premise is to determine whether minimization of entropy production is equivalent to optimal performance conditions. Additionally, a discussion is provided that demonstrates the criterion at which the maximum energy efficiency and maximum

exergy efficiency become coincident with the design point of minimum entropy generation. Throughout the analysis, it is assumed that external irreversibility's are present. The effects of both internally reversible and irreversible processes are examined and compared. Additionally, the thermal energy storage efficiency is taken into consideration and its effects on the optimum design points, leading to maximum energy efficiency, maximum exergy efficiency, and minimum entropy generation, are examined.

## 6.2 HT-CAES Thermodynamic Cycle

Fig. 1 represents the HT-CAES thermodynamic cycles that are analyzed here.

The thermodynamic models assume an adiabatic and constant pressure air storage, which can be either underwater air storage or a cavern constructed in underground rock formation with a water-equalizing pit, in order to maintain isobaric conditions [154]. The air storage under this assumption remains isothermal, therefore reduces to just a delay time in the operation of the plant. Fig. 1(a) and (b) show the described HT-CAES system with and without regeneration.

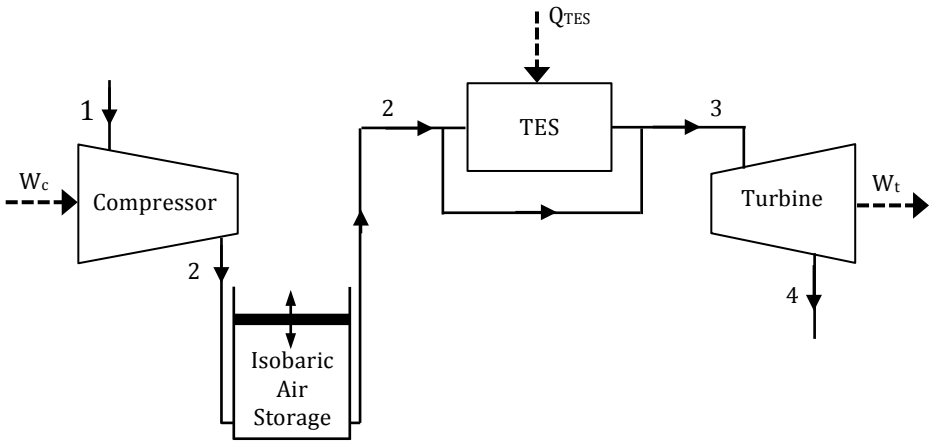


**(a)**

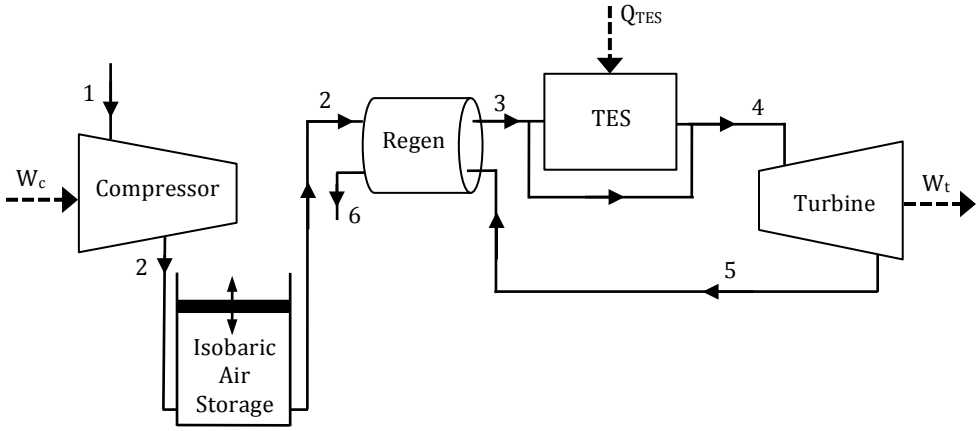


**(b)**

**Figure 6.1: (a) HT-CAES Thermodynamic Cycle Configuration Without Regeneration (b) HT-CAES Thermodynamic Cycle Configuration With Regeneration**

The sensible thermal energy storage unit, shown in Fig. 1, is inherently a transient component. However, the TES can be designed to deliver a constant temperature, necessary for optimal operation of an expander, through bypassing a potion of the cold inlet air with the hot flow exiting the TES, as demonstrated by Fig. 1. Throughout the analysis it is assumed that the TES has a minimum temperature, $T_{min}$, which is equivalent to the constant turbine inlet temperature ($T_{min} = T_3$ in the case without regeneration in Fig. 1(a), and $T_{min} = T_4$ with regeneration in Fig. 1(b)) at the beginning of charge and end of discharge. The TES maximum temperature, $T_{max}$, is reached at the end of the charge process and beginning of the discharge process, which must be set larger than the turbine inlet temperature. A zero order model of the TES is assumed, in which no temperature gradients within the TES exist during the charge or discharge process. However, thermal storage efficiency is taken into consideration and its value represents the percentage of

irretrievable energy loss within a full cycle. Additionally, the following analysis is based on the simplifying assumptions of a calorically perfect gas, ideal gas, and negligible pressure drops.

## 6.3 Internally Reversible HT-CAES

Considering the internally reversible HT-CAES system without regeneration, followed by a similar analysis of an internally reversible HT-CASES system with regeneration. In this section it is also assumed that the thermal energy storage is 100% energy efficient. In section 4 the thermal energy storage efficiency along with internal irreversibilities are analyzed. The following analysis is composed of a calculation of the energy efficiency, exergy efficiency and the entropy generation as the pressure ratio is varied. The pressure ratio is defined as the maximum to minimum pressure ratio in the system ($r = P_2/P_1 = P_4/P_5$).

### 6.3.1 HT-CAES Without Regeneration

#### *6.3.1.1 First Law Efficiency*

The roundtrip energy storage efficiency of the HT-CAES system, defined as the output power over the total input power, is given by equation (1)

$$\eta_I = \frac{\dot{W}_t}{\dot{W}_C + \dot{Q}_{TES}} \tag{6.1}$$

Assuming constant specific heats for air, isentropic compressor and turbine, and constant inlet turbine temperature, $T_3$, the energy efficiency can be rewritten to equation (2).

$$\eta_I = \frac{1 - T_1/T_2}{1 - T_1/T_3} = \frac{1 - r^{-\alpha}}{1 - r_T^{-1}} \tag{6.2}$$

Where, $\propto = (\gamma - 1)/\gamma$, $\gamma$ is the ratio of specific heats for air, and $r_T$ is the maximum to minimum temperature ratio in the cycle, $r_T = \frac{T_3}{T_1}$. By examining equation (2), and considering a Brayton cycle with a heat source provided by the TES, it becomes evident that the numerator represents

the Brayton cycle efficiency, in the case of pure thermal energy storage and no air storage. Similarly, the denominator of equation (2) represents the Carnot efficiency of the associated Brayton cycle. Therefore, equation (2) can be written as shown in equation (3)

$$\eta_I = \frac{\eta_{Brayton}}{\eta_{Carnot}} \tag{6.3}$$

Equation (3) provides an interesting result, which illustrates that the process is 100% efficient when there is no heat addition provided by the thermal storage, $T_3 = T_2$, and the compression and expansion processes are along the same isentropic line. The addition of heat through the thermal storage takes the process off the compression isentrope and introduces the Carnot limit into the cycle. In the extreme of very high temperatures of thermal storage, i.e. when the balance between heat and isentropic work of compression shifts predominantly toward heat, the cycle is dominated by the Brayton cycle as the Carnot efficiency approaches unity. In another extreme where the energy allocated into thermal energy storage approaches zero and $T_3 = T_2$, HT-CAES reduces to an advanced adiabatic system with a theoretical round-trip efficiency of unity, as evident from equation (3). In this limit, where advanced adiabatic CAES aims to operate, the expansion isentrope coincides with the compression isentrope. When there is economic and technological justification, this limit is theoretically the most desirable zone of operation for energy storage/retrieval. One can therefore conclude that the efficiency of a non-regenerative HT-CAES cycle is 1) always greater than the efficiency of the corresponding Brayton cycle, in the case of pure thermal energy storage, and 2) is not bound by the Carnot efficiency.

#### *6.3.1.2 Second Law Efficiency*

The roundtrip exergy efficiency of the HT-CAES system, which is defined as the total output exergy over the total input exergy, is given by equation (4)

$$\eta_{II} = \frac{\int \dot{W}_t \, dt}{\int \dot{W}_c \, dt + \int (1 - T_1/T_{TES}) \dot{Q}_{TES} \, dt} \tag{6.4}$$

Where $\dot{Q}_{TES}$ is the TES input joule heating power. The total energy stored in the TES is calculated through an energy balance which results in: $Q_{TES}=\dot{Q}_{TES}t = Mc(T_{max} - T_{min}) = Mc(T_{max} - T_3) = \dot{m}c_p t(T_3 - T_2)$, where $M$, $c$, $\dot{m}$ and $c_p$ are the TES mass, TES specific heat, air mass flow rate, and specific heat of air at constant pressure, respectively. Lastly, the instantaneous temperature of the TES during the charge process is calculated through an energy balance, which results in $T_{TES} = \frac{\dot{Q}_{TES}}{Mc} t + T_{min}$, where $T_{min} = T_3$. Evaluating the integrals in equation (4) results in equation (5)

$$\eta_{II} = \frac{T_3 - T_4}{T_2 - T_1 + \frac{Mc}{\dot{m}c_P t}(T_{\max} - T_3) - T_1 \frac{Mc}{\dot{m}c_P t} \ln\left(\frac{T_{\square ax}}{T_3}\right)} \tag{6.5}$$

Further simplification of equation (5), while substituting temperature ratios, $r_T = \frac{T_3}{T_1}$ and $r_H = \frac{T_{max}}{T_3}$, leads to equation (6)

$$\eta_{II} = \frac{\eta_{Brayton}}{\eta_{Carnot} - r_T^{-1}(1 - r_T^{-1} r^{\alpha}) \frac{\ln(r_H)}{(r_H - 1)}} \tag{6.6}$$

Equation (6) reveals that the exergy efficiency of the HT-CAES system is always higher than its energy efficiency given by equation (3), provided the TES increases the temperature of the discharging air, $T_2 < T_3$. This result is consistent with heat engines, in which their exergy efficiencies are generally higher than their associated energy efficiencies.

#### *6.3.1.3 Entropy Generation*

The total entropy generation associated with the operation of the HT-CAES system is evaluated through an entropy balance and is given in equation (7)

$$S_{gen} = \int \frac{\dot{Q}_{out}}{T_{out}} dt - \int \frac{\dot{Q}_{in}}{T_{in}} dt \tag{6.7}$$

The second integral in equation (7), associated with the TES heat input, is calculated through a similar approach that arrived at equation (5), resulting in the following expression

$$S_{gen} = \frac{\dot{m} c_P t (T_4 - T_1)}{T_1} - Mcln\left(\frac{T_{max}}{T_3}\right) \tag{6.8}$$

Normalizing the entropy generation with the total stored air mass times its specific heat, $\dot{m}c_P t$, and relating temperature ratios with pressure ratios through isentropic relations, results in equation (9)

$$\frac{S_{gen}}{\dot{m} c_P t} = (r_T r^{-\alpha} - 1) + (r_T^{-1} r^{\alpha} - 1) \frac{\ln(r_H)}{r_H - 1} \tag{6.9}$$

Plotting the energy efficiency, exergy efficiency, and the normalized entropy generation given by equations (3), (6) and (9) respectively results in Fig. 2.

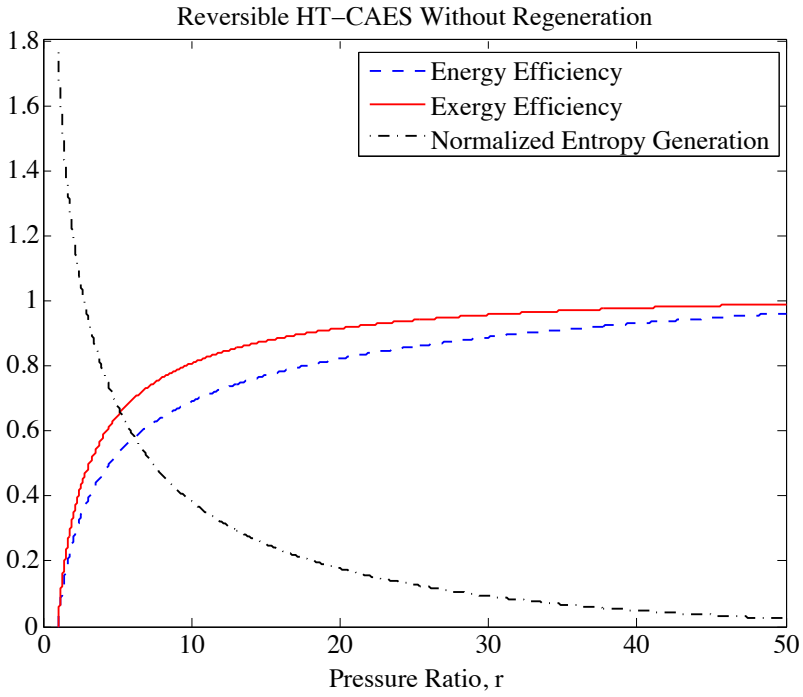


**Figure 6.2: Energy efficiency, exergy efficiency and normalized entropy generation of the internally reversible, and 100% energy efficient TES, HT-CAES system without regeneration as a function of the pressure ratio, r.**

In the case of an internally reversible HT-CAES system without regeneration, all performance indices monotonically improve with increasing operating pressure, as shown by Fig. 2. Therefore, in this specific case, an increase in the energy and exergy efficiency does in fact correlate with a decrease in entropy generation. It is also imperative to note that in an HT-CAES system the output power increases with the pressure ratio, as the turbine and compressor are decupled in contrast to a Brayton cycle. Therefore, a decrease in entropy generation also correlates with an increase in output power. In section 4, it will be shown that this is not necessarily the case in the presence of internal irreversibility's, and a discussion explaining the reason behind the phenomenon is provided in section 5.

### 6.3.2 With Regeneration

We undertake a similar procedure to arrive at the energy efficiency, exergy efficiency, and entropy generation in the case of internally reversible HT-CAES system, however including regeneration, Fig. 1(b). Similarly, the pressure ratio is varied, and the performance indices are examined and compared to determine whether minimization of entropy production may lead to conclusive design guidelines.

#### *6.3.2.1 First Law Efficiency*

The energy efficiency, as defined in equation (1) and assuming constant specific heat, leads to equation (10).

$$\eta_I = \frac{T_4 - T_5}{T_2 - T_1 + T_4 - T_3} \tag{6.10}$$

Rearranging equation (10) and relating temperature ratios to pressure ratios through isentropic relations leads to equation (11)

$$\eta_I = \frac{1}{2 - \eta_{Brayton,R}} \tag{6.11}$$

Where $\eta_{Brayton,R}$ is the energy efficiency of the corresponding regenerative Brayton cycle, in the case of pure thermal energy storage and no air storage. Equation (11) is analogous to equation (3), however including regeneration. The regenerative brayton cycle efficiency is given by equation (12)

$$\eta_{Brayton,R} = 1 - r_T^{-1} r^{\alpha} \tag{6.12}$$

The temperature ratios $r_T = \frac{T_4}{T_1}$ and $r_H = \frac{T_{max}}{T_4}$ are defined as the maximum to minimum temperature ratios that the air and TES experience in the regenerative cycle. Equation (11)

illustrates that the 1st law efficiency of a regenerative HT-CAES system is always higher than its Brayton cycle counter part, as was the case in the non-regenerative system shown by equation (3).

#### *6.3.2.2 Second Law Efficiency*

The 2nd law efficiency of the HT-CAES system with regeneration, Fig. 1(b), is obtained through a similar procedure, which arrived at the exergy efficiency without regeneration, given by equation (6). The result is given by equation (13)

$$\eta_{II} = \frac{\eta_I}{1 - \eta_I \frac{\ln(r_H)}{r_T(r_H - 1)}} \tag{6.13}$$

Where $\eta_I$ is the first law efficiency given by equation (11). Through an energy balance, the following relation given by equation (14) was used to relate the mass and specific heats of the air and TES with their temperature differences

$$\frac{Mc}{\dot{m}c_P t} = \frac{T_4 - T_3}{T_{max} - T_4} = \frac{(1 - r^{-\alpha})}{r_H - 1} \tag{6.14}$$

Again, notice that the second law efficiency of the HT-CAES system, given by equation (13), is always higher than its first law efficiency. The gap between the energy and exergy efficiency increases with increasing energy efficiency and decreasing temperature ratios ($r_T$ and $r_H$). Meaning it is more effective, exergetically, to reduce the TES temperature swing and air temperature swing throughout the cycle, as a result of the associated decrease in mixing irreversibility's.

### *6.3.2.3 Entropy Generation*

The normalized entropy generation associated with the operation of a regenerative HT-CAES system, Fig. 1(b), is evaluated through an entropy balance, equation (7), undertaking a similar procedure which arrived at equation (9), The result is given in equation (15).

$$\frac{S_{gen}}{\dot{m}c_p t} = (r^{\alpha} - 1) + (r^{-\alpha} - 1)\frac{\ln(r_H)}{r_H - 1} \tag{6.15}$$

Plotting the energy efficiency, exergy efficiency, and the normalized entropy generation given by equations (11), (13) and (15) respectively results in Fig. 3.

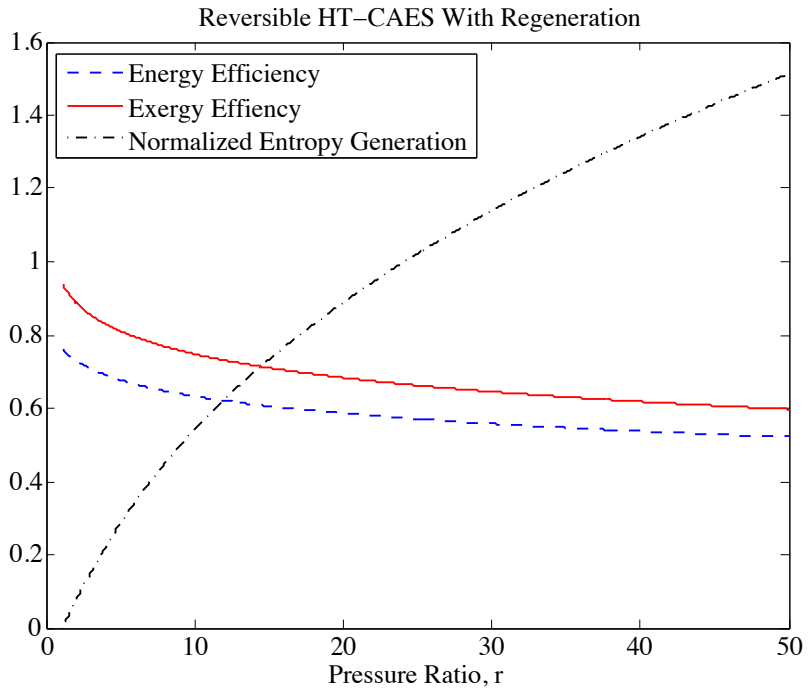


**Figure 6.3: Energy efficiency, exergy efficiency and normalized entropy generation of the internally reversible, and 100% energy efficient TES, HT-CAES system with regeneration as a function of the pressure ratio, r.**

In the case of an internally reversible HT-CAES system with regeneration, the optimum operating pressure occurs at unity, as measured by the maximum energy and exergy efficiencies along with the coincident minimum entropy generation. However, at a pressure ratio of unity the power output is zero. Therefore in order to achieve finite time processes, and for the system to become operational, entropy must be generated. This contradicts the Gouy-Stodola theorem of heat engines, which demonstrates that maximum output power correlates with minimum entropy generation. In section 4, internal irreversibility's and thermal energy storage efficiencies are taken into consideration to determine whether minimization of entropy generation may lead to optimal performance.

### 6.4 Internally Irreversible HT-CAES With Regeneration

Let us now consider the regenerative HT-CAES system, Fig. 1(b), with internal irreversibilies and TES inefficiencies. The analysis is similar to the procedures involved in the reversible case. However, the temperatures, $T_2$, $T_5$, $T_3$, and $T_6$ need to be determined as functions of other operating parameters. Utilizing isentropic component efficiencies, regenerator effectiveness, and an energy balance of the regenerator, results in the following temperatures corresponding to Fig. 1(b)

$$T_2 = T_1\left(1 + \frac{1}{\eta_c}(r^{\alpha} - 1)\right) \tag{6.16}$$

$$T_5 = T_4\left(1 - \eta_T(1 - r^{-\alpha})\right) \tag{6.17}$$

$$T_3 = T_2 + (T_5 - T_2)\eta_R \tag{6.18}$$

$$T_6 = T_5 + T_2 - T_3 \tag{6.19}$$

Where $\eta_c$, $\eta_T$ and $\eta_R$ are the compressor, turbine and regenerator efficiencies, respectively.

### 6.4.1 First Law Efficiency

Starting with equation (1) and undertaking a similar procedure, which arrived at equation (3) and (11), results in equation (20), where $\eta_H$ is the TES retrieval efficiency.

$$\eta_I = \frac{T_4 - T_5}{T_2 - T_1 + (T_4 - T_3)/\eta_H} \tag{6.20}$$

Utilizing temperatures (16) through (19) results in equation (21)

$$\eta_I = \frac{\eta_T \eta_H \eta_C (1 - r^{-\alpha})}{(\eta_H + \eta_R - 1)\, r_T^{-1}(r^{\alpha} - 1) + \eta_C \eta_R \eta_T (1 - r^{-\alpha}) + \eta_{Carnot} \eta_C (1 - \eta_R)} \tag{6.21}$$

Where $\eta_{Carnot}$ is the Carnot efficiency of the corresponding Brayton cycle, analogous to the HT-CAES cycle of Fig. 1(b), and is given by equation (22)

$$\eta_{Carnot} = 1 - \frac{T_1}{T_4} = 1 - r_T^{-1} \tag{6.22}$$

We can find an optimum compression ratio, which would result in a maximum energy efficiency by applying $(\partial \eta_I / \partial r) = 0$ whose solution gives

$$r_{opt}(\eta_{I,max}) = \left( 1 + \sqrt{\frac{r_T \eta_C (1 - \eta_R) \eta_{Carnot}}{(\eta_R + \eta_H - 1)}} \right)^{\frac{1}{\alpha}} \tag{6.23}$$

Interestingly, the optimum pressure ratio, which leads to maximum energy efficiency, is independent of the turbine isentropic efficiency. In addition, when the regenerator effectiveness is unity, the optimum pressure ratio is also unity, matching that of Fig. 3.

### 6.4.2 Second Law Efficiency

Starting with equation (4) and undertaking a similar procedure that arrived at equations (6) and (13), results in equation (24)

$$\eta_{II} = \frac{T_4 - T_5}{T_2 - T_1 + \frac{Mc}{\dot{m}c_p t}(T_{max} - T_4) - T_1 \frac{Mc}{\dot{m}c_p t} \ln\left(\frac{T_{max}}{T_4}\right)} \tag{6.24}$$

Where the mass and specific heats of the air and TES medium are related by equation (25)

$$\frac{Mc}{\dot{m}c_P t} = \frac{T_4 - T_3}{\eta_H (T_{max} - T_4)} \tag{6.25}$$

Substituting equations (16) through (19) and equation (25) into equation (24) and simplifying results in equation (26)

$$\eta_{II} = \frac{\eta_T \eta_{\square} \eta_C (1 - r^{-\alpha})}{(r^{\alpha} - 1) r_T^{-1} (\eta_H - A + A\eta_R) + A\eta_T \eta_C \eta_R (1 - r^{-\alpha}) + \eta_{Carnot} A \eta_C (1 - \eta_R)} \tag{6.26}$$

Where

$$A = 1 - \frac{\ln(r_H)}{r_T (r_H - 1)} \tag{6.27}$$

We can find an optimum compression ratio, which would result in a maximum exergy efficiency by applying $(\partial \eta_{II} / \partial r) = 0$ whose solution gives

$$r_{opt}(\eta_{II,max}) = \left(1 + \sqrt{\frac{\eta_C(1-\eta_R)\eta_{Carnot}[r_T(r_H-1)-\ln(r_H)]}{(r_H-1)(\eta_R+\eta_H-1)+(1-\eta_R)r_T^{-1}\ln(r_H)}}\right)^{\frac{1}{\alpha}} \quad (6.28)$$

Similar to the optimum pressure ratio leading to maximum energy efficiency, equation (23), the optimum pressure ratio, which leads to maximum exergy efficiency, is independent of the turbine isentropic efficiency. In addition, when the regenerator effectiveness is unity, the optimum pressure ratio is also unity, matching that of Fig. 3.

### 6.4.3 Entropy Generation

Starting with equation (7), and undertaking a similar procedure, which arrived at equations (9) and (15), however with an additional heat loss term associated with the TES irretrievable energy efficiency, results in equation (29).

$$\frac{S_{gen}}{\dot{m}c_p t} = \left(\frac{T_6}{T_1}-1\right) - \frac{T_4-T_3}{\eta_H(T_{max}-T_4)}\ln\left(\frac{T_{max}}{T_4}\right) + \frac{\frac{2(T_4-T_3)(1-\eta_H)}{\eta_H}}{T_{max}(1+\eta_H)+T_4(1-\eta_H)} \quad (6.29)$$

Utilizing the temperatures in equation (16) through (19) and finding an optimum compression ratio, which would result in minimum entropy generation by applying $(\partial S_{gen}/\partial r) = 0$, results in equation (30) as the solution

$$r_{opt}(S_{gen,min}) = \left(\frac{\eta_T\eta_H\eta_C(1-\eta_R)r_T + \eta_C\eta_T\eta_R B}{\eta_R\eta_H + r_T^{-1}(1-\eta_R)B}\right)^{\frac{1}{2\alpha}} \quad (6.30)$$

Where

$$B = \frac{\ln(r_H)}{r_H - 1} - \frac{2}{r_H \frac{(1+\eta_H)}{(1-\eta_H)} + 1} \tag{6.31}$$

Typical trends of the energy efficiency, exergy efficiency and normalized entropy generation as functions of the pressure ratio, given by equations (21), (26) and (29), are illustrated in Fig. 4.

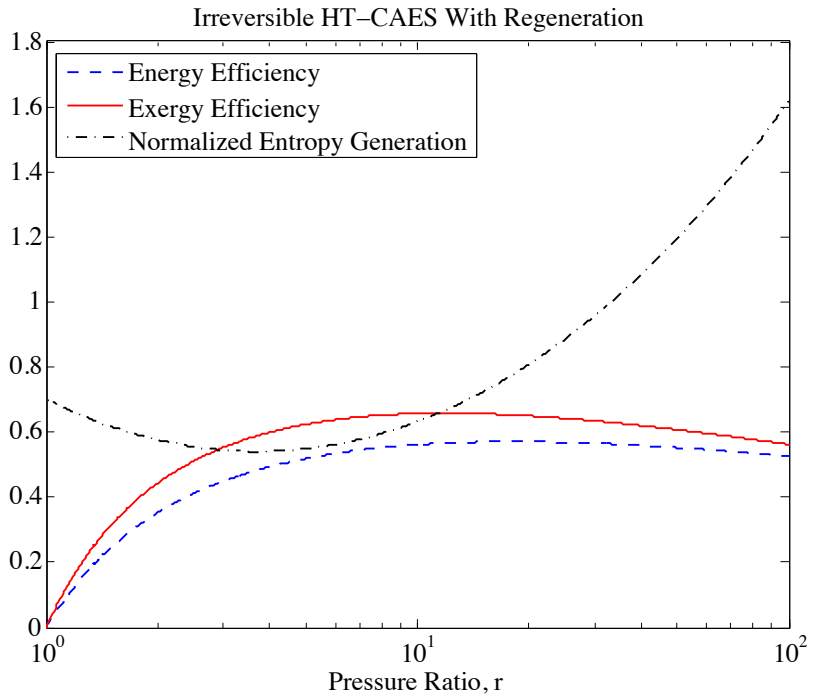


**Figure 6.4: Energy efficiency, exergy efficiency and normalized entropy generation of the regenerative HT-CAES cycle corresponding to Fig. 1(b). With $\eta_R = 0.6$, $\eta_c = \eta_T = \eta_H = 0.9$, $r_T = 3.33$, and $r_H = 1.5$**

The results provided in Fig. 4 are for $\eta_R = 0.6$, $\eta_c = \eta_T = \eta_H = 0.9$, $r_T = 3.33$, and $r_H = 1.5$. Since the HT-CAES system is essentially a broken Brayton cycle, where the compressor is decoupled from the turbine, the turbine power is entirely available for useful work. Therefore, the power output increases monotonically with increasing pressure ratio. Consequently, Fig. 4 offers a design region in terms of the pressure ratio: the pressure ratio of a real HT-CAES system

must be larger than $r(\eta_{I,max})$. The rational being that the system efficiency should only be compromised for a higher output power, depending on the specific applications of use and their priorities i.e., cost, size, performance, etc. Fig. 4 reveals that the operational regime at minimum entropy generation is different from that at maximum exergy efficiency, maximum energy efficiency, and maximum work output. Indicating that a real HT-CAES system designed based on a minimum entropy generation criterion, in general, would not operate at maximum work output, maximum energy efficiency, or maximum exergy efficiency. It will be further shown, in a forthcoming discussion, that in an HT-CAES system, the regime of minimum entropy generation may become equivalent to the regime of maximum energy and exergy efficiency only under certain conditions.

The optimum pressure ratios corresponding to the maximum energy efficiency, exergy efficiency and minimum entropy generation, given by equations (23), (28) and (30), are plotted as a function of the regenerator effectiveness, in Fig. 5. The results in Fig. 5 are plotted assuming $\eta_c = \eta_T = \eta_H = 0.9$ , $r_T = 3.33,$ and $r_H = 1.5$ . Fig. 5 reveals that the design regime corresponding to minimum entropy generation occurs at a lower pressure ratio than that which corresponds to maximum energy efficiency and/or maximum exergy efficiency, more specifically $r\left(S_{gen,min}\right) < r\left(\eta_{II,max}\right) < r(\eta_{I,max})$. In addition, as the regenerator effectiveness decreases the optimum pressure ratios, corresponding to all performance indices, increase and the gaps between them also increase. As evident by equations (23), (28) and their plots in Fig. 5, the optimum pressure ratio leading to maximum energy and exergy efficiencies, at a regenerator effectiveness of unity, is unity. Moreover, the optimum pressure ratio corresponding to minimum entropy generation, at $\eta_R = 1$ and as given by equation (30), leads to a calculated value of 0.49,

which is a nonoperational value. However, restricting the pressure ratios to values above unity, results in an optimum of unity. Therefore, at a regenerator effectiveness of unity, all optimum design conditions converge, which is in agreement with the reversible case, as given by Fig. 3. In contrast, a regenerator effectiveness of 0.5 leads to a convergence in the optimum pressure ratios leading to maximum output power, maximum energy efficiency, and minimum entropy generation, in a Brayton cycle [153].

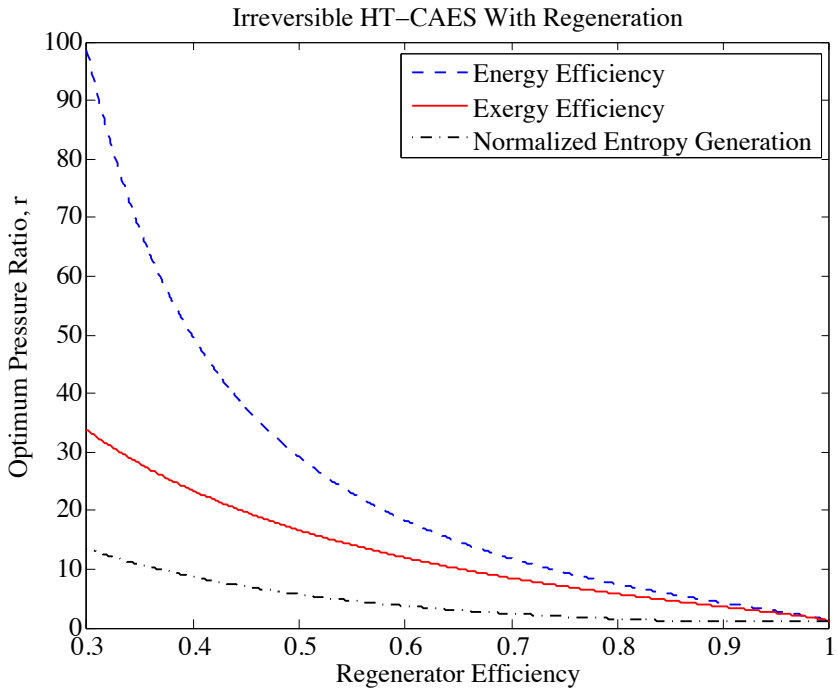


**Figure 6.5: The optimum pressure ratios corresponding to maximum energy efficiency, maximum exergy efficiency and minimum normalized entropy generation, of the regenerative HT-CAES cycle, corresponding to Fig. 1(b), as the regenerator effectiveness is varied, with $\eta_c = \eta_T = \eta_H = 0.9$, $r_T = 3.33$, and $r_H = 1.5$**

A plot of the optimum pressure ratios as a function of the temperature ratio, $r_T$, is given in Fig. 6. The result in Fig. 6 was plotted for $\eta_R = \eta_c = \eta_T = \eta_H = 0.9$, and $r_H = 1.5$. The results provided by Fig. 6 further demonstrate that optimum design criterions do not necessarily coincide. More specifically, as in the case with varying regenerator effectiveness, $r(S_{gen,min}) < r(\eta_{II,max}) < r(\eta_{I,max})$.

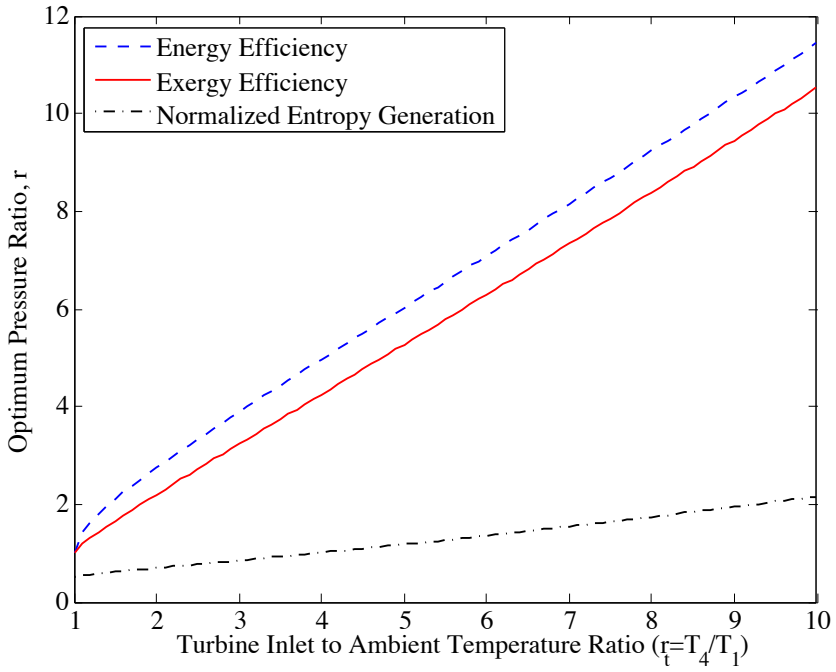


**Figure 6.6: The optimum pressure ratios corresponding to maximum energy efficiency, maximum exergy efficiency and minimum normalized entropy generation, of the regenerative HT-CAES cycle, corresponding to Fig. 1(b), as the turbine inlet to ambient temperature ratio is varied, with $\eta_R = \eta_c = \eta_T = \eta_H = 0.9$, and $r_H = 1.5$**

The effect of the thermal energy storage efficiency on the optimum pressure ratio design is illustrated by Fig. 7, assuming $\eta_R = \eta_c = \eta_T = 0.9$, $r_H = 1.5$, and $r_T = 3.33$, for all performance indices given by equations (23), (28) and (30). The optimum pressure ratios for all indices increase with decreasing thermal storage efficiency. Additionally, Fig. 6 reveals that the optimum pressure is again observed in the same order, $r(S_{gen,min}) < r(\eta_{II,max}) < r(\eta_{I,max})$, as that in Fig. 5 and Fig. 6. Equation (30) is unbiased to the pressure ratio range, therefore although the optimum pressure ratio values corresponding to minimum entropy generation, at thermal storage energy efficiencies greater than 0.5, are below unity, this indicates that the actual optimum and realistic value, although non-operational, is in fact unity.

Lastly, the compressor isentropic efficiency is varied, and its effects on the optimal pressure ratios are investigated, as shown in Fig. 8, assuming $\eta_R = \eta_H = \eta_T$, $r_H = 1.5$ and, $r_T = 3.33$. The trends exhibited by the optimal pressure ratios, as the compressor isentropic efficiency is decreased in Fig. 8, are quite the opposite as those observed when the thermal energy storage efficiency is decreased, Fig. 7. Nonetheless, the optimal pressure ratio deign ranking remains consistent, namely, $r(S_{gen,min}) < r(\eta_{II,max}) < r(\eta_{I,max})$. Equation (30) is unbiased to the pressure ratio range. Therefore, although the optimum pressure ratio values corresponding to minimum entropy generation are below unity, at compressor isentropic efficiencies less than 0.95, this indicates that the actual optimum and realistic value, although non-operational, is in fact unity.

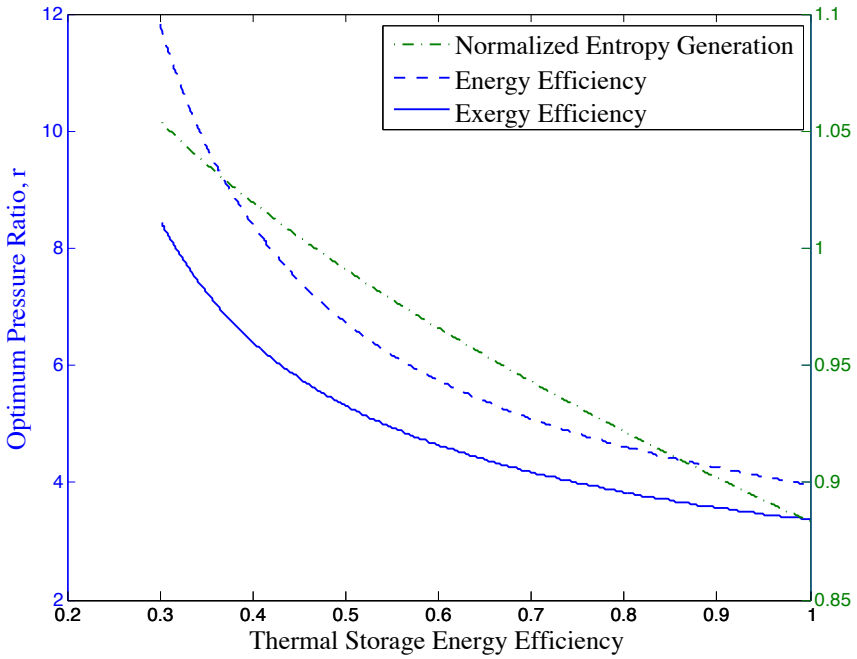


**Figure 6.7: The optimum pressure ratios corresponding to maximum energy efficiency, maximum exergy efficiency and minimum normalized entropy generation, of the regenerative HT-CAES cycle, corresponding to Fig. 1(b), as the thermal storage energy efficiency is varied, with $\eta_R = \eta_c = \eta_T = 0.9$, $r_H = 1.5$, and $r_T = 3.33$**

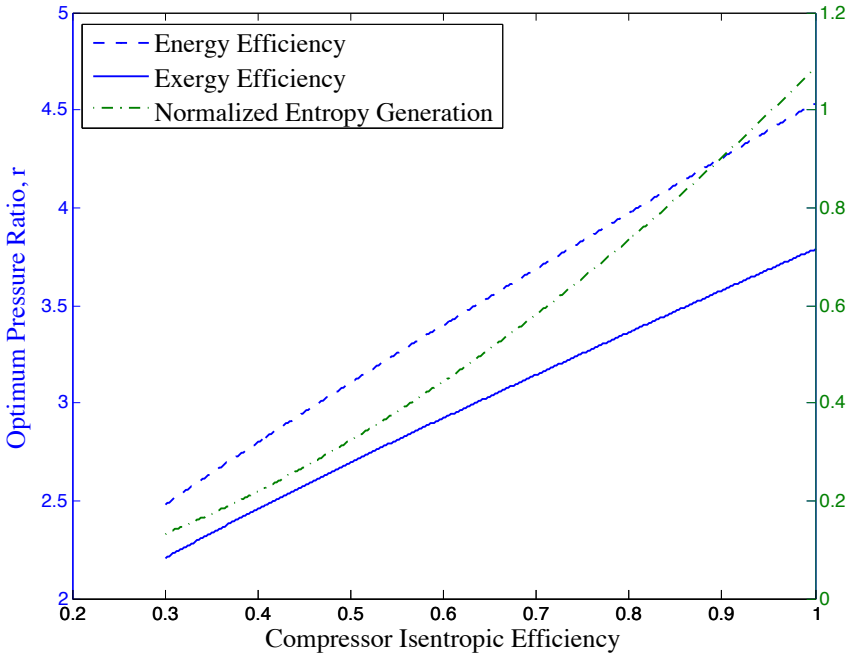


**Figure 6.8: The optimum pressure ratios corresponding to maximum energy efficiency, maximum exergy efficiency and minimum normalized entropy generation, of the regenerative HT-CAES cycle, corresponding to Fig. 1(b), as the compressor isentropic efficiency is varied, with $\eta_R = \eta_H = \eta_T = 0.9$, $r_H = 1.5$, and $r_T = 3.33$**

## 6.5 Discussion

As demonstrated by the results in this chapter, it is not always the case that minimum entropy is coincident with maximum power and efficiency, which is also the case for heat engines [153]. However, Its important to note that in certain conditions the minimization of entropy generation may correlate with the maximization of energy efficiency, exergy efficiency, and power output. This was demonstrated in the case of an internally reversible and non-regenerative HT-CAES system, as shown in Fig. 2. In the case of an internally reversible regenerative HT-CAES system, the maximum energy and exergy efficiencies did correlate with minimum entropy generation, however this was not the case for the maximum output power, Fig. 3. In practical applications it is almost unavoidable to neglect internal irreversibility's, and the additional energy retrieval

benefit provided by a regenerator far outweighs its cost. Therefore, the more realistic results are those provided by the regenerative HT-CAES cycle with internal irreversibility's. It was observed, for a regenerative HT-CAES system with internally irreversibilies, that only in the case of a regenerative effectiveness of 100% did the minimum entropy generation correlate with maximum energy and exergy efficiencies, however not with maximum output power. In contrast to heat engines, where optimum design condition become coincident at a regenerator effectiveness of 50% [153]. It was also observed that the optimum pressure ratio corresponding to minimum entropy generation occurs at generally lower values than those corresponding to maximum exergy and energy efficiencies. Furthermore, the optimum pressure ratio corresponding to maximum energy efficiency was generally the largest. More specifically, the following order, $r(S_{gen,min}) < r(\eta_{II,max}) < r(\eta_{I,max})$, was a consistent trend throughout the analysis.

Combining the first and second laws of thermodynamics can provide further insights on the criterions necessary for coincident optimal design conditions. The turbine output energy is given simply by equation (32)

$$W_T = W_C + Q_{in} - Q_{out} \tag{6.32}$$

Eliminating the output heat $Q_{out}$ from equations (7) and (32) and dividing by the total input energy, $E_{input}$, results in equation (33)

$$\eta_I = 1 - \frac{T_1}{E_{input}}\left[Mcln(r_h) + S_{gen}\right] \tag{6.33}$$

Similarly, eliminating the output heat $Q_{out}$ from equations (7) and (32) and dividing by the total input exergy, $\mathbf{E}_{input}$, results in equation (34)

$$\eta_{II} = 1 - \frac{T_1}{\mathbf{E}_{input}} S_{gen} \tag{6.34}$$

The first and second law efficiencies, given by equations (33) and (34), reveal the specific conditions upon which the minimum generation of entropy becomes coincident with the maximization of the energy and exergy efficiencies. Only in the particular case where the input energy, thermal energy storage mass, specific heat, and maximum to minimum temperature ratio, $r_h$, are a constant does the minimum entropy generation coincide with maximum energy efficiency. Similarly, only the specific case where the total input exergy is a constant, does the minimum entropy generation coincide with maximum exergy efficiency. Otherwise, the entire term in the vicinity of the entropy generation variable, $S_{gen}$, must reach a minimum for the energy and exergy efficiencies to reach a maximum, in equation (33) and (34). This is precisely the reason why optimal conditions corresponding to minimum entropy generation did not correlate with maximum energy or maximum exergy efficiencies in the irreversible hybrid thermal and compressed air energy storage system.

## 6.6 Conclusion

A regenerative and non-regenerative hybrid thermal and compressed air energy storage system is designed based on the objective of minimum entropy generation. The cases of both internally reversible and irreversible conditions were investigated. It was illustrated that a hybrid compressed air energy storage system optimized through this criterion is likely to perform at an energy and exergy efficiency that is lower than that which is otherwise achievable. This work illustrated that for a hybrid compressed air energy storage system, minimization of entropy generation does not always correlate with minimization of energy losses. Only under specific

conditions does the minimum entropy generation coincide with maximum energy and exergy efficiencies. Moreover it was generally observed that the optimum operating pressure conditions based on maximum energy efficiency, maximum exergy efficiency, and minimum entropy generation can be ordered in the following manner: $r(S_{gen,min}) < r(\eta_{II,max}) < r(\eta_{I,max})$.

**Table 6.1: Chapter 6 Nomenclature**

| Nomenclature | | | |
|---|---|---|---|
| CAES | Compressed Air Energy Storage | TES | Thermal Energy Storage |
| HT-CAES | Hybrid Thermal - CAES | AA-CAES | Advanced Adiabatic - CAES |
| $r$ | Pressure Ratio | $r_H$ | Maximum TES Temperature Ratio |
| $r_T$ | Maximum Cycle Temperature Ratio | $\eta_c$ | Compressor Isentropic Efficiency |
| $\dot{W}_t$ | Turbine Output Power | $\eta_R$ | Regenerator Effectiveness |
| $\dot{W}_c$ | Compressor Input Power | $\eta_T$ | Turbine Isentropic Efficiency |
| $\dot{Q}_{TES}$ | TES Power/Heat input | $\eta_H$ | TES Efficiency |
| $W_c$ | Compression Energy | $\eta_{Brayton}$ | Brayton Cycle Efficiency |
| $Q_{TES}$ | TES Energy Input | $\eta_{Brayton,R}$ | Regenerative Brayton Cycle Efficiency |
| $W_t$ | Turbine Energy Output | $\eta_{Carnot}$ | Carnot Efficiency |
| $P$ | Pressure | $S_{gen}$ | Entropy Generation |
| $T$ | Temperature | $r_{opt}$ | Optimum Pressure Ratio |
| $\gamma$ | Ratio of Specific Heat for Air | $E_{input}$ | Input Energy |
| $M$ | TES Mass | $\mathbf{E}_{input}$ | Input Exergy |
| $\dot{m}$ | Mass Flow Rate | $\mathrm{Q_{in}}$ | Input Heat |
| $R$ | Ideal Gas Constant of Air | $\mathrm{Q_{out}}$ | Output Heat |
| $c_v$ | Specific Heat of Air at Constant Volume | $c_p$ | Specific Heat of Air at Constant Pressure |
| $c$ | TES Specific Heat | t | Total Charge or Discharge Time |
| $\eta_I$ | HT-CAES Roundtrip Energy Efficiency (1st Law Efficiency) | $\eta_{II}$ | HT-CAES Roundtrip Exergy Efficiency (2nd Law Efficiency) |

# Chapter 7: Exergy Analysis of the Modified Hybrid Thermal-Compressed Air Energy Storage System

## 7.1 Introduction

Exergy is defined as the theoretical maximum amount of work possible by a system, as the system comes into equilibrium with the environment. Alternatively, exergy can be defined as the minimum amount of power necessary to remove a system from equilibrium to a specified state. Exergy is an extension of the second law of thermodynamics, and it provides a more meaningful investigation to energy systems, as it considers the quality of energy, with the environment as a reference point [155]-[176]. An exergy efficiency is often more useful and provides better insight of the performance of a system, as it measures the system to the ideal/reversible case. The objective of this chapter is to continue the thermodynamic investigation effort of the hybrid thermal and compressed air energy storage system presented in chapter 5, however from an exergy perspective. The exergetic component efficiencies and the exergy destructions of each component are presented. This chapter is an attempt to pin point the largest sources of internal irreversibilities in the hybrid thermal-compressed air energy storage system. Through this analysis, a means of improving the storage performance is naturally established and presented.

## 7.2 Thermodynamic Analysis

The exergy of a system, $\boldsymbol{E}$, at a specified state is given by the expression

$$\boldsymbol{E} = (E - U_o) + P_o(V - V_o) - T_o(S - S_o) \tag{7.1}$$

Where *E, V,* and *S* denote, respectively, the energy, volume, and entropy of the system. The energy, *E*, is the sum of internal kinetic and potential energies. $U_o, V_o,$ and $S_o$ are the values of

the same properties id the system were at the dead state. The dead state is that corresponding to the conditions of the environment. When mass flows across the boundary of a control volume, there is an exergy transfer accompanying mass flow. Additionally, there is an exergy transfer accompanying flow work. The specific flow exergy accounts for both of these, and is given by

$$e_f = h - h_o - T_o(s - s_o) + \frac{V^2}{2} + gz \tag{7.2}$$

Where *h* and *s* represent the specific enthalpy and entropy, respectively, at the inlet or exit under consideration; $h_o$ and $s_o$ represent the respective values of these properties when evaluated at the dead state. The change in specific entropy of an ideal gas with constant specific heat is given by

$$s_2 - s_1 = c_p \ln T_2 / T_1 - R ln\, P_2/P_1 \tag{7.3}$$

The exergy rate balance for control volumes is given below

$$\frac{d\boldsymbol{E}_{cv}}{dt} = \sum_j \left(1 - \frac{T_o}{T_j}\right)\dot{Q}_j - \left(\dot{W}_{cv} - P_o \frac{dV_{cv}}{dt}\right) + \sum_i \dot{m}_i\, e_{fi} - \sum_e \dot{m}_e\, e_{fe} - \dot{E}_d \tag{7.4}$$

Where the first term on the left represents the time rate of change of the exergy of the control volume. The first term on the right side of the equation represents the rate of exergy transfer rate accompanying heat. The second term is the accompanying exergy transfer rate accompanying work, other than flow work. The third and forth terms are the exergy transfer rates accompanying mass flow at the inlet, i, and exit, e. finally the last term, $\dot{E}_d$, accounts for the time rate of exergy destruction due to irreversibilities within the control volume.

### 7.2.1 Exergy Destruction

The destruction of exergy in each component in the HT-CAES system is provided through the exergy balance equation. Assuming an adiabatic and steady state process, the exergy destruction of a compressor or turbine is given by

$$\dot{E}_d = \sum_i \dot{m}_i \, e_{fi} - \sum_e \dot{m}_e \, e_{fe} - \dot{W}_{cv} \tag{7.5}$$

Similarly, the exergy destruction of heat exchangers, pressure regulating valve, and junctions are calculated assuming adiabatic and steady processes, and are given by

$$\dot{E}_d = \sum_i \dot{m}_i \, e_{fi} - \sum_e \dot{m}_e \, e_{fe} \tag{7.6}$$

The exergy destruction of the air storage is inherently time dependent and calculated assuming an adiabatic process through

$$\dot{E}_d = \sum_i \dot{m}_i \, e_{fi} - \sum_e \dot{m}_e \, e_{fe} - \frac{d\boldsymbol{E}_{cv}}{dt} \tag{7.7}$$

The total exergy destruction throughout the charge and discharge processes is calculated by integrating the time rate of exergy destruction of each component throughout the charge and discharge time. In addition the total exergy destruction is normalized by the total output energy, which is specified in chapter 5, defined as $W_{output}$. The total normalized exergy destruction of each component is therefore given by

$$\boldsymbol{E}_{norm} = \frac{\int \dot{E}_d \, dt}{W_{output}} \tag{7.8}$$

### 7.2.2 Component Exergy Efficiency

The mathematical definitions of the exergy efficiency of each component are presented here. In every instance, the efficiency is derived by the use of the exergy rate balance. Each of the cases considered involves a control volume at steady state, and it is assumed that there is no heat transfer between the control volumes its surroundings. For a turbine operating at steady state with no heat transfer with its surroundings, the steady state form of the exergy rate balance reduces as follows.

$$e_{f1} - e_{f2} = \frac{\dot{W}_{cv}}{\dot{m}} + \frac{\dot{E}_d}{\dot{m}} \tag{7.9}$$

The term on the left of the side of the equation represents the decrease in the flow exergy from turbine inlet to exit. The equation shows that the flow exergy decreases because the turbine develops work, and the exergy is destroyed. A parameter that gauges how effectively the flow exergy decreases is converted to the desired product is the exergetic turbine efficiency, given below

$$\varepsilon_{Turbine} = \frac{(\dot{W}_{cv}/\dot{m})}{e_{f1} - e_{f2}} \tag{7.10}$$

This particular exergetic efficiency is sometimes referred to as the turbine effectiveness. It is important to note that the exergetic turbine efficiency is defined differently from the isentropic turbine efficiency. For the compressor operating at steady state with no heat transfer with its surroundings, the effectiveness of the conversion from work to input or flow exergy increase is gauged, similarly, by the exergetic compressor efficiency

$$\varepsilon_{Compressor} = \frac{(e_{f2} - e_{f1})}{-(\dot{W}_{cv}/\dot{m})} \tag{7.11}$$

The heat exchanger shown in Figure 1, operating at steady state with no heat transfer with their surroundings, and both streams at temperature above $T_o$, the exergy balance of which reduces to

$$\dot{m}_h(e_{f1} - e_{f2}) = \dot{m}_c(e_{f4} - e_{f3}) + \frac{\dot{E}_d}{\dot{m}} \tag{7.12}$$

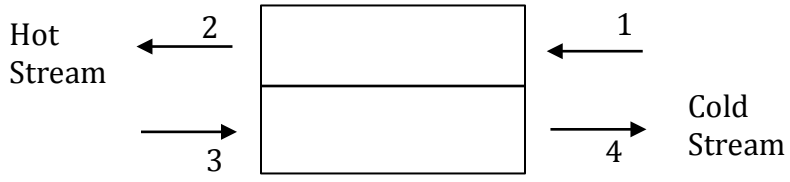


**Figure 7.1: Counter flow heat exchanger schematic**

The term on the left side of the equation accounts for the decrease in the exergy of the hot stream. The first term on the right accounts for increase in exergy of the cold stream. The hot stream, in Figure 1, can be regarded as supplying the exergy increase of the cold stream as well as the exergy destroyed, therefore we can write the exergetic heat exchanger efficiency as

$$\varepsilon_{HX} = \frac{\dot{m}_c(e_{f4} - e_{f3})}{\dot{m}_h(e_{f1} - e_{f2})} \tag{7.13}$$

The same equation is utilized for the exergetic efficiency of the regenerator. The exergetic efficiency of the pressure regulative valve is given by

$$\varepsilon_{PRV} = \frac{e_{fe}}{e_{fi}} \tag{7.14}$$

The exergetic efficiency of the air storage medium is defined similarly as the total flow exergy output over the total inlet flow exergy. A schematic of the junction, which is applicable to the HTES bypass line and the turbocharger junction, illustrated by Figure 1.5, in chapter 5, is in Figure 2 below.

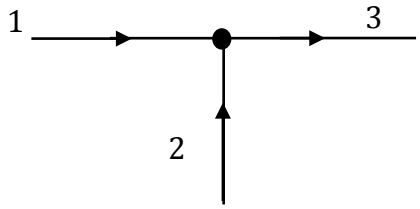


**Figure 7.2: Mass Flow Junction Schematic**

The exergetic efficiency of the junction is defined as

$$\varepsilon_J = \frac{\dot{m}_3 e_{f3}}{\dot{m}_1 e_{f1} + \dot{m}_2 e_{f2}} \tag{7.15}$$

The three components prior to the HTES (LTES, regenerator and Junction) are placed such that successive heating is always attained, and the configuration is dependent on the prime pressure. In order to obtain a general expression for the exergetic efficiency of these components, independent of the prime pressure, all three components are treated as one, as illustrated by the schematic in Figure 4.

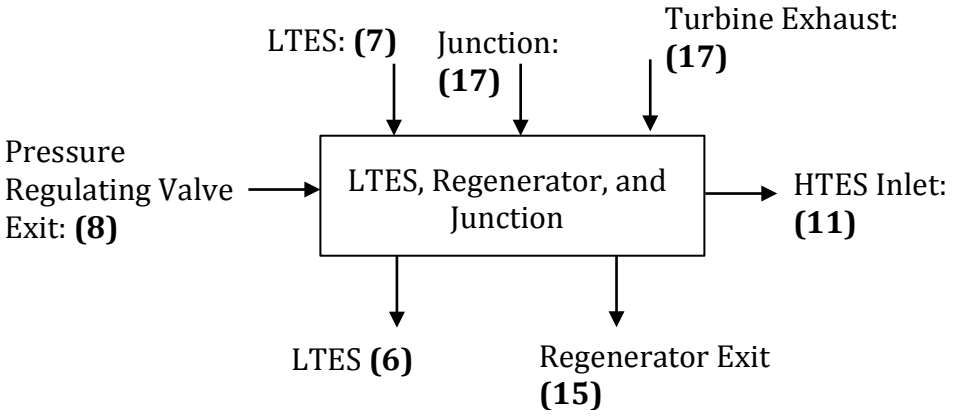


**Figure 7.3: A control volume containing the LTES discharges heat exchanger, the regenerator, and the turbocharger junction.**

The exergetic efficiency of the control volume containing the 2 stage heating and junction shown in Figure 3a, can be expressed as follows

$$\varepsilon_{CV} = \frac{\dot{m}_{11}e_{f11} - \dot{m}_{8}e_{f8}}{\dot{m}_{t}\left(e_{f14} - e_{f15}\right) + \dot{m}_{LTES}\left(e_{f7} - e_{f6}\right) + \dot{m}_{17}e_{f17}} \tag{7.16}$$

The roundtrip exergy efficiency of the high temperature thermal energy storage is defined as the total output over total input exergies. The input and output exergies are ultimately defined by

$$\boldsymbol{E_{HTES}} = \int (1 - T_o/T)\dot{Q}_{HTES}dt \tag{7.17}$$

Assuming a zero order model of the thermal storage, where no temperature gradient exist within the medium, the temperature of the HTES during the charge process is calculated through an energy balance and is given by

$$T = \frac{\dot{Q}_{in}}{Mc} t + T_{min} \tag{7.18}$$

Where M, c, t, and $T_{min}$, are the HTES mass, specific heat, time of charge, and minimum temperature at the beginning of charge. Evaluating the exergy transfer integral, during the charge process, accompanying heat transfer and noting that the total input energy into the HTES is $Q_{HTES} = Mc(T_{max} - T_{min})$, results in

$$\boldsymbol{E_{input}} = Mc(T_{max} - T_{\min}) - T_o Mcln\frac{T_{max}}{T_{min}} \tag{7.19}$$

The output exergy is calculated similarly, however incorporating energy efficiency and assuming the HTES is perfectly effective, meaning the air temperature exiting the HTES is equal to the instantaneous HTES temperature. Through an energy balance, on a control volume containing the HTES, the instantaneous temperature of the HTES during the discharge is given by

$$T = \left[\eta_{I,HTES}(T_{max} - T_{min}) + \left(T_{min} - \frac{T_{in}}{\varepsilon_{HTES}}\right)\right] e^{-\frac{\dot{m}c_p}{Mc}\varepsilon_{HTES}t} + \frac{T_{in}}{\varepsilon_{HTES}} \tag{7.20}$$

Where $\eta_{HTES} = Q_{out}/Q_{in}$ is the energy efficiency of the HTES, and $\varepsilon_{\square TES}$ is the heat transfer effectiveness of the HTES. Utilizing the time dependent temperature and evaluating the exergy transfer accompanying heat transfer results in the following second law roundtrip efficiency of the HTES

$$\eta_{II,HTES} = \frac{\eta_{\square,HTES} T_m - \ln\left(\eta_{I,HTES} T_m T_n + 1\right)}{T_m - \ln\left(T_m T_n + 1\right)} \tag{7.21}$$

Where $T_m=(T_{max}-T_{min})/T_{min}$, and $T_n=T_o/T_{min}$. Notice when the first law efficiency is unity or zero, the second law efficiency of the HTES becomes identical to the first law efficiency. However,

deviations between the first and second law efficiencies occur when the first law efficiency is nonzero and non-unity.

The roundtrip exergy efficiency of the hybrid thermal and compressed air energy storage is calculated through a control volume containing the entire hybrid storage system, as shown in Figure 5.

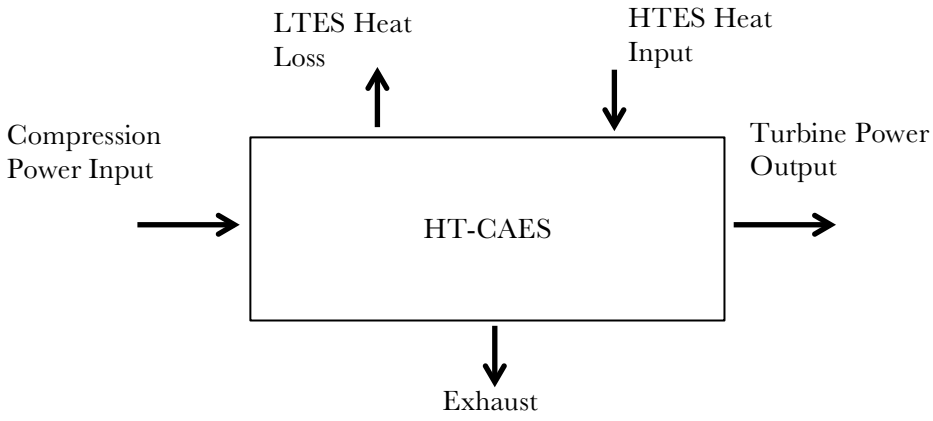


**Figure 7.4: a control volume containing the HT-CAES system illustrating all energy streams through the control volume**

The second law roundtrip efficiency of the system is defined as the total output exergy over the total input exergy into the system

$$\eta_{II} = \frac{\int \dot{W}_t \, dt}{\int \dot{W}_c dt + \int (1 - T_o/T) \dot{Q}_{HTES} dt} \tag{7.22}$$

With the first law efficiency defined as the total input energy over the total output energy, as shown below

$$\eta_I = \frac{W_t}{W_c + Q_{HTES}} \tag{7.23}$$

and utilizing the same energy distribution variable, which quantifies the allocation of storage energy between thermal and compressed air storage, as shown below

$$\beta = \frac{Q_{HTES}}{W_C + W_t} \tag{7.24}$$

Evaluating the second law efficiency integral results in the following

$$\eta_{II} = \frac{\eta_I}{1 - \frac{\ln\left(T_{max}/T_{min}\right)}{T_{max} - T_{min}} T_o \beta} \tag{7.25}$$

Which can be further reduced to

$$\eta_{II} = \frac{\eta_I}{1 - \frac{\ln\left(1 + \delta/T_{min}\right)}{\delta} T_o \beta} \tag{7.26}$$

Where

$$\delta = T_{max} - T_{min} \tag{7.27}$$

The HT-CAES exergy efficiency is always greater than its energy efficiency, a result that is consistent with heat engines. The energy and exergy efficiencies become coincident in the limiting case of a very large HTES temperature swing, $\delta = T_{max} - T_{min}$, as indicated below

$$\lim_{\delta \to \infty} \eta_{II} = \eta_I \tag{7.28}$$

Therefore, the minimum exergy efficiency is equal to its corresponding energy efficiency, $\eta_{II,min} = \eta_I$. This is due to the increase in internal irreversibilities associated with mixing losses in the HTES at a high temperature swing; a result that is undetected through the first law analysis and efficiency. Conversely, the largest difference in 1st and 2nd law efficiencies (in other words, the maximum exergy efficiency for a given energy efficiency) occurs in the limit of a very low

HTES temperature difference, where the HTES temperature remains isothermal and internal irreversibilities associated with mixing losses are eliminated, as shown below

$$\lim_{\delta \to 0} \eta_{II} = \frac{\eta_I}{1 - \beta \frac{T_o}{T_{\min}}} \tag{7.29}$$

Further increase in their difference occurs for 1) high $\beta$ values, and 2) at lower HTES temperatures. Since the exergy efficiency is defined as a comparison of the system performance to the ideal case, at high $\beta$ values the system is utilizing a lower quality of energy (heat), therefore for the same energy efficiency the result is higher exergy efficiencies. In the limit that $\delta = T_{max} - T_{min} = 0$, by definition this means the HTES remains isothermal, $T_{min} = T_{max} = T_{HTES}$. As a mathematical consequence, with a lower HTES temperature the second term in the denominator of equation (23) is at a minimum, which leads to maximum exergy efficiency for a given energy efficiency. However, the physical meaning can be explained as follows: at a low HTES temperature the system is utilizing a lower quality of heat, therefore for the same energy efficiency the result is higher exergy efficiencies.

### 7.3 Results

Figure 6 below demonstrates the configuration of the LTES, regenerator, and turbocharge junction, as a function of the energy distribution and prime pressure, such that successive heating is always attained during the discharge process. The configuration, as depicted by Figure 6, is independent of the energy distribution and only a function of the prime pressure. This is because the prime pressure dictates the temperatures of the storage cycle, however the energy distribution ultimately determines the mass flow rates and size of the system. Configuration 1 represents the discharge process in the following order: turbocharger junction, LTES discharge heat exchanger, than regenerator. Configuration 2 represents the turbocharger junction, regenerator, than LTES

discharge heat exchanger. Lastly, configuration 5 represents the regenerator, turbocharger junction, than LTES discharge heat exchanger. This configuration map was also the case in the optimization chapter.

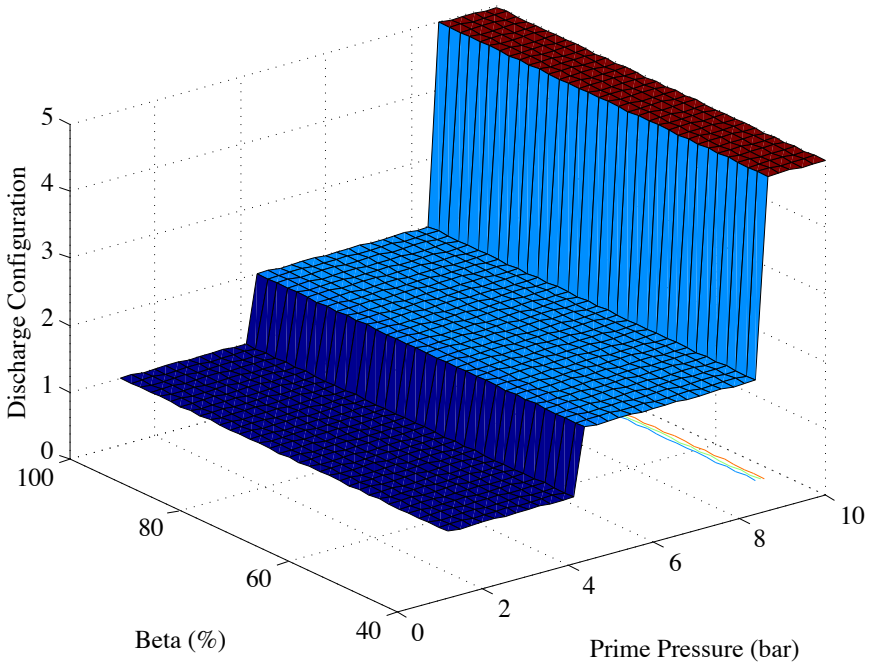


**Figure 7.5: The configuration order of the LTES discharge heat, turbocharger junction, and regenerator, such that successive heating is always attained. Where the configuration number represent: 1) Junction → LTES → Regenerator 2) Junction → Regenerator → LTES and 5) Regenerator → Junction →LTES, respectively.**

The discontinuity in the cycle configuration translates to discontinuities in the exergetic efficiencies and calculated components exergy destructions. The component exergy destruction calculations are presented next, followed by the exergetic component efficiencies.

### 7.3.1 Exergy Destruction

The normalized exergy destruction of the pressure-regulating valve is plotted in Figure 5 as a function of the energy distribution fraction and the prime pressure. As the prime pressure is

increased, the necessary change in pressure through throttling is decreased; therefore irreversibilities or exergy losses are decreased. This trend is more pronounced at the lower end of the beta spectrum, as more energy is allocated towards compression, since more mass flow is provided by the air storage, which must be throttled.

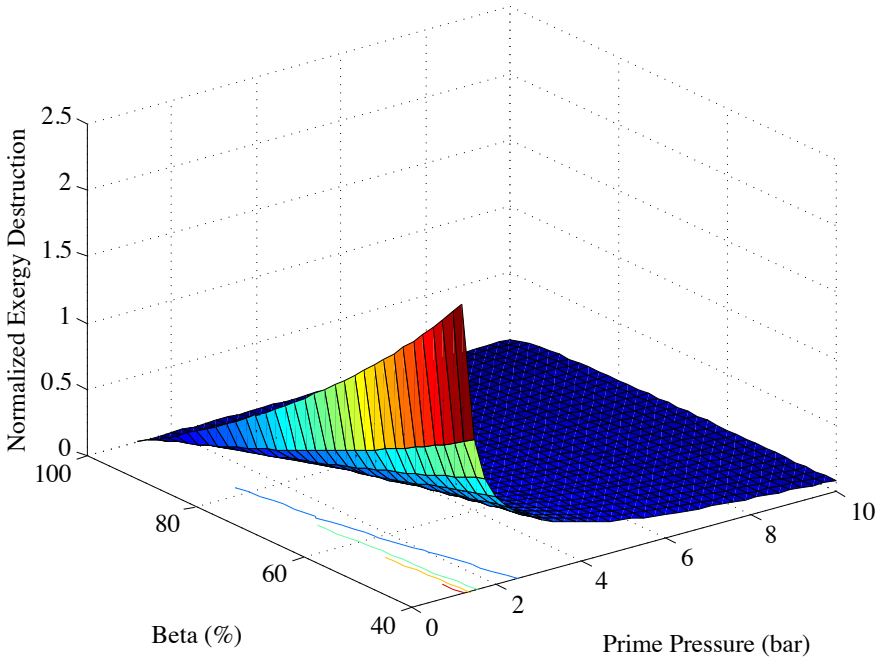


**Figure 7.6: Normalized exergy destruction of the pressure regulative valve as a function of the energy distribution fraction and the prime pressure**

Similarly, the normalized exergy destruction of the cavern is plotted in Figure 6, as a function of the energy distribution fraction and the prime pressure. A similar trend given by the pressure regulating valve is exhibited by the cavern, however for different reasons. The normalized exergy destruction of the cavern decreases with prime pressure, at the lower end of the beta spectrum where more energy is allocated towards compression, since more mass flow rate is provided by the cavern. At lower prime pressures, the cavern undergoes a larger pressure swing

since the maximum pressure is fixed in this study. Therefore, at higher cavern pressure swings, mixing losses within the cavern become more apparent. With increased irreversibilities associated with mixing, the exergy destruction increases as a result.

The sum of both pressure regulating valve and cavern exergy destructions, given by Figures 5 and 6, is given in Figure 7. As will be shown, the exergy destruction associated with throttling and cavern mixing irreversibilities results in the highest avoidable sources of exergy losses within the system. The trend exhibited by their sum is similar to their individual trends, shown in both Figures 5 and 6.

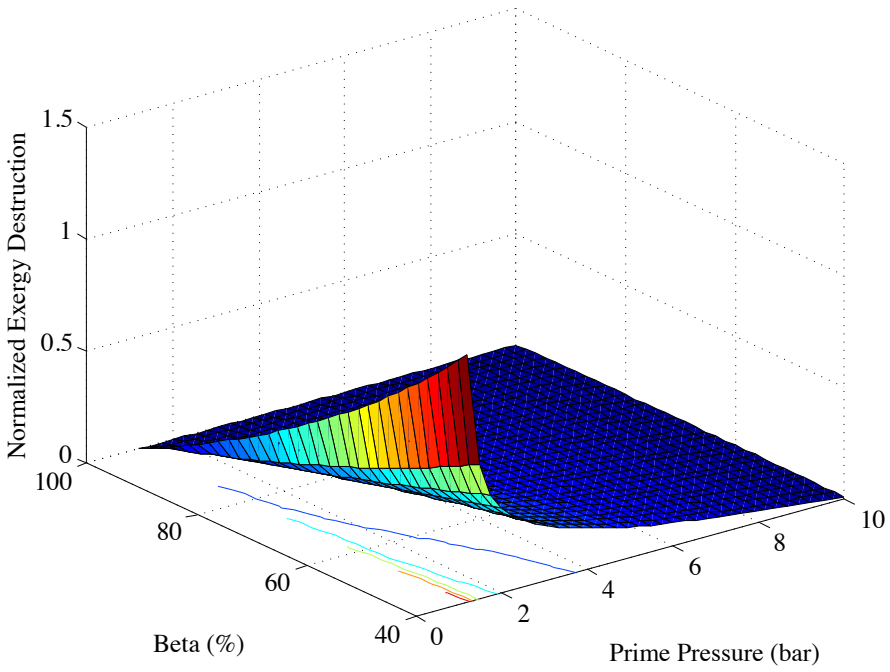


**Figure 7.7: Normalized exergy destruction of the cavern as a function of the energy distribution fraction and the prime pressure**

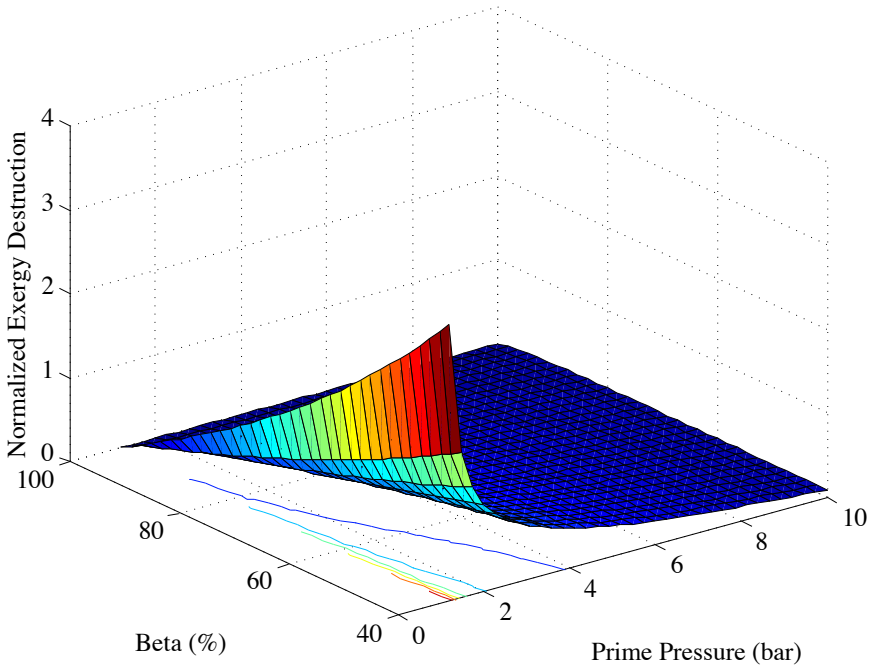


**Figure 7.8: Normalized exergy destruction of the cavern plus pressure regulative valve as a function of the energy distribution fraction and the prime pressure**

The normalized exergy destruction of the compressor as a function of the energy distribution fraction and the prime pressure is given in Figure 8. . The normalized exergy destruction of the compressor decreases with prime pressure, at the lower end of the beta spectrum where more energy is allocated towards compression. The exergy destruction of the compressor is proportional to the mass flow rate provided during compression. As given in Chapter 5, the charge flow rate decreases with prime pressure at the lower end of the beta spectrum, which explains the trends given by Figure 8.

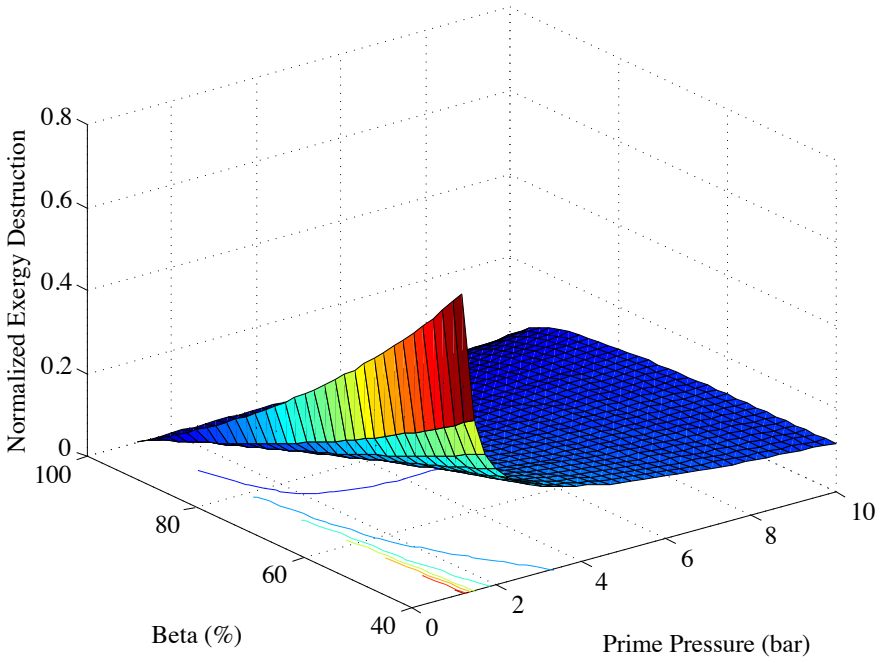


**Figure 7.9: Normalized exergy destruction of the compressor as a function of the energy distribution fraction and the prime pressure**

The normalized exergy destruction of the HTES bypass flow is given in Figure 9. The exergy destruction of the HTES bypass flow rate is also proportional to the total mass flow rate, which is provided in Chapter 5. Therefore, the plot illustrates very large exergy destructions in the regions of high flow rates. In the region where the efficiency is zero and the flow rate is infinite, specifically at Beta=100% and a prime pressure of 11 bar, the exergetic efficiency of the HTES bypass flow becomes increasingly highly, as demonstrated by Figure 9. The increase in irreversibilities, or exergy destruction, is a result of the increase in mixing losses at higher flow rates.

The normalized exergy destruction of the LTES charge heat exchanger is plotted in Figure 10. The exergy destruction exhibits a similar trend observed in the compressor exergy destruction.

The exergy destruction of the LTES discharge heat exchanger is a function the mass flow rates, which decrease with increasing prime pressure, leading to the associated decrease in exergy destruction. The exergy destruction is identically zero at beta=100%, since the airflow rate is identically zero.

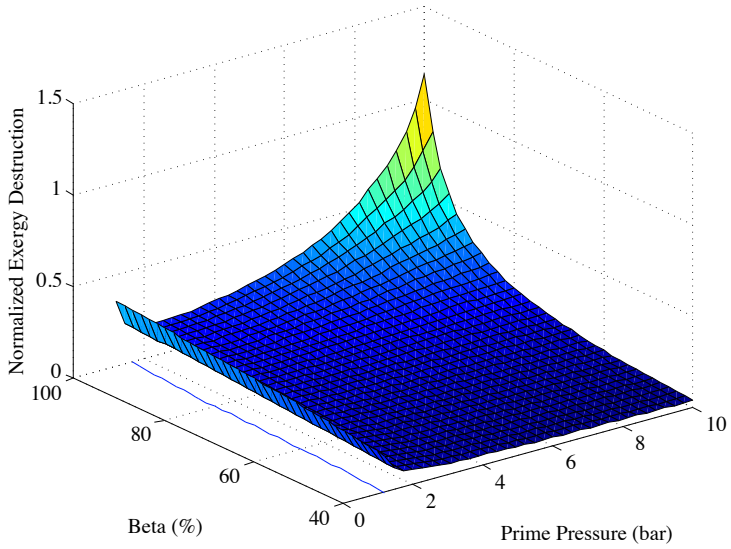


**Figure 7.10: Normalized exergy destruction of the HTES bypass junction as a function of the energy distribution fraction and the prime pressure**

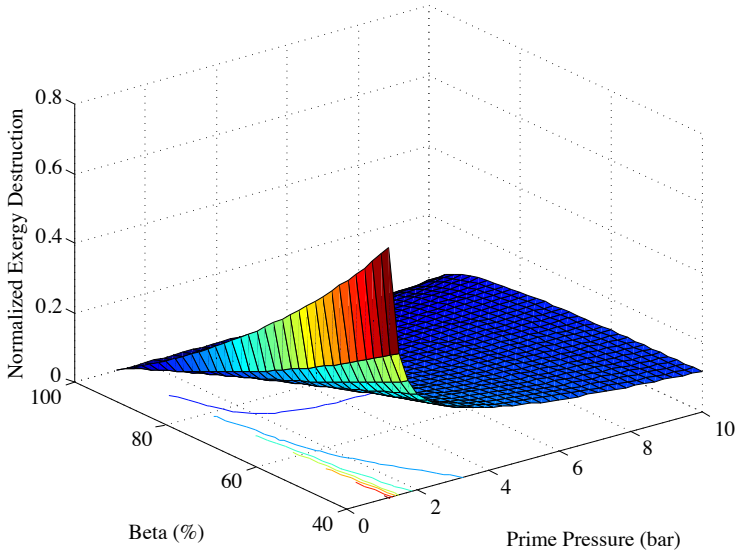


**Figure 7.11: normalized exergy destruction of the LTES charge heat exchanger as a function of the energy distribution fraction and the prime pressure**

The normalized exergy destruction of the regenerator, LTES discharge heat exchanger, and the turbocharger junction is illustrated in Figure 11. The irreversibility has little dependents on the energy distribution fraction, however a strong dependence on the prime pressure. The irreversibilities, which result in exergy destruction, decrease with increasing prime pressure.

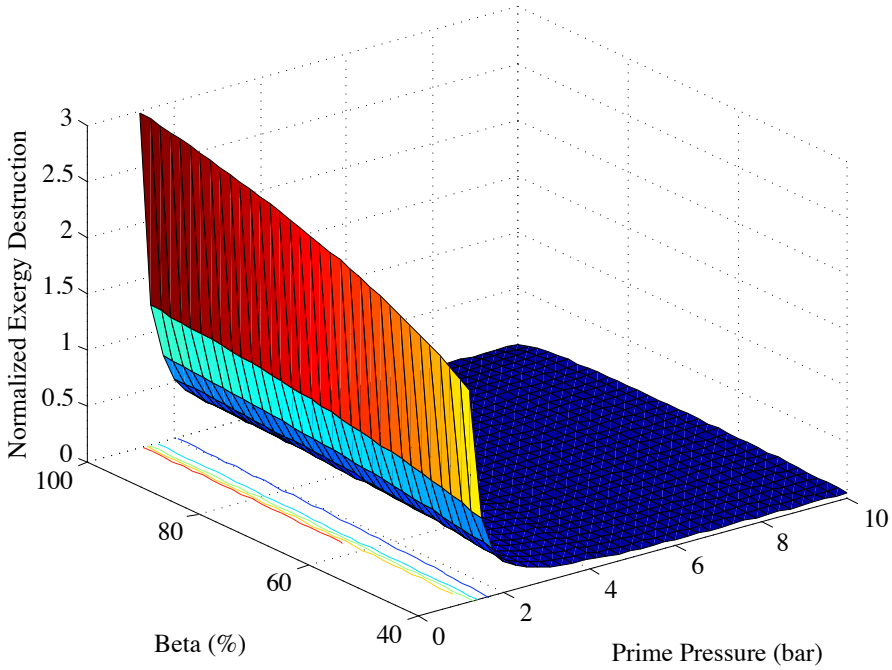


**Figure 7.12: Normalized exergy destruction of the Regenerator, LTES, and turbocharger junction as a function of the energy distribution fraction and the prime pressure**

Figures 12a and 12b show the normalized exergy destructions associated with the turbines and turbocharger compressor respectively. Similarly, the exergy destruction is proportional to the flow rates; leading to relatively high irreversibilities are higher flow rates.

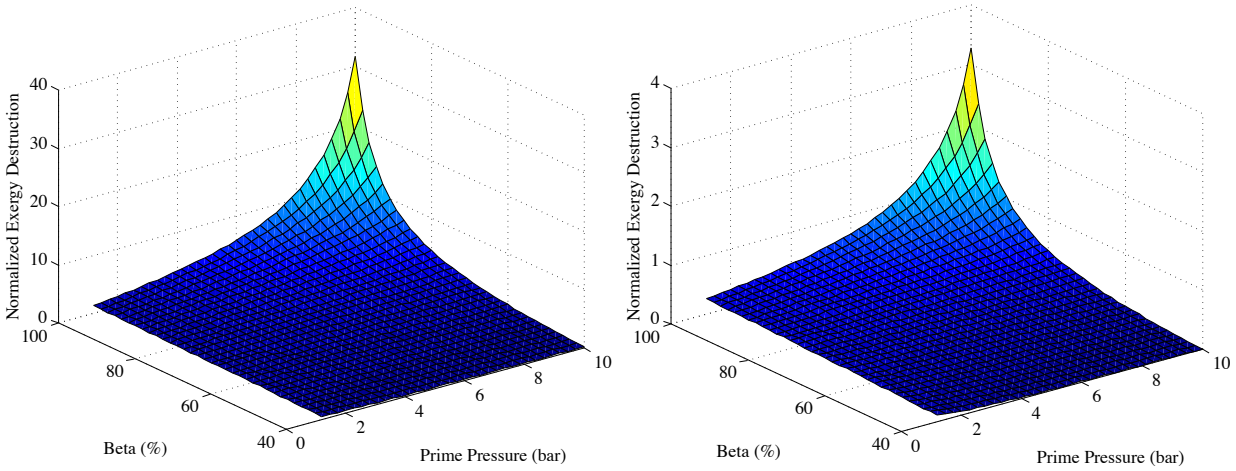


**Figure 7.13: Normalized exergy destruction of the a) turbine and b) turbocharger compressor, as a function of the energy distribution fraction and the prime pressure**

### 7.3.2 Exergetic Component Efficiencies

The exergy efficiency of the pressure regulative valve is illustrated in Figure 13. As the prime pressure increasing, the cavern pressure is throttled to relatively higher pressures resulting in lower irreversibilities and higher exergy efficiencies. The exergy efficiency approaches unity as the prime pressure approaches the maximum cavern pressure, in the case where throttling becomes negligible.

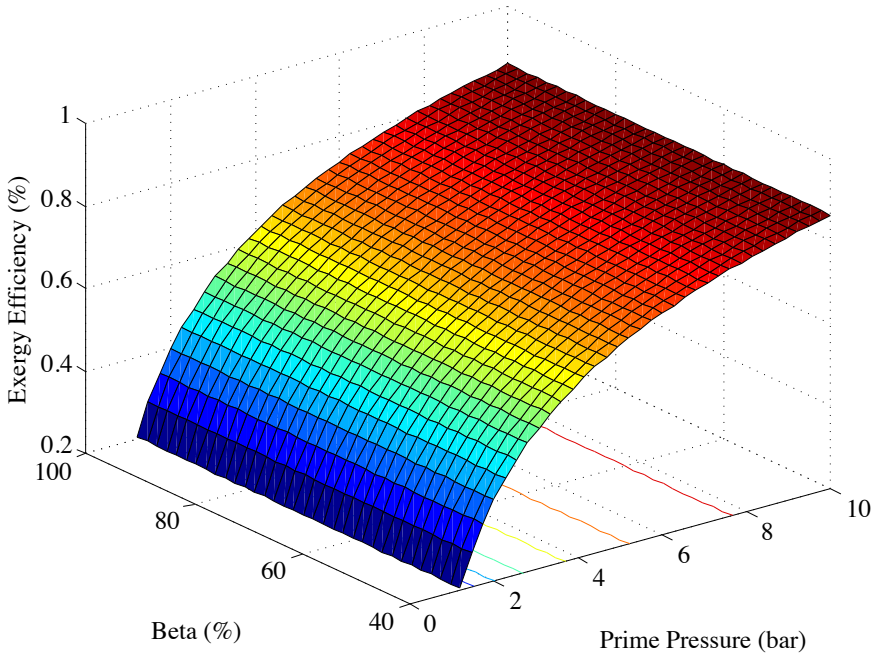


**Figure 7.14: Exergy Efficiency of the pressure-regulating valve as a function of the energy distribution fraction and the prime pressure**

Similarly, the exergy efficiency of the cavern is plotted in Figure 14, as a function of the energy distribution fraction and the prime pressure. A similar trend given by the pressure regulating valve is exhibited by the cavern, however for different reasons. The exergy efficiency of the cavern increases with prime pressure. At lower prime pressures, the cavern undergoes a larger pressure swing since the maximum pressure is fixed in this study. Therefore, at higher cavern pressure swings, mixing losses within the cavern become more apparent. With increased irreversibilities associated with mixing, the exergy efficiency decreases as a result.

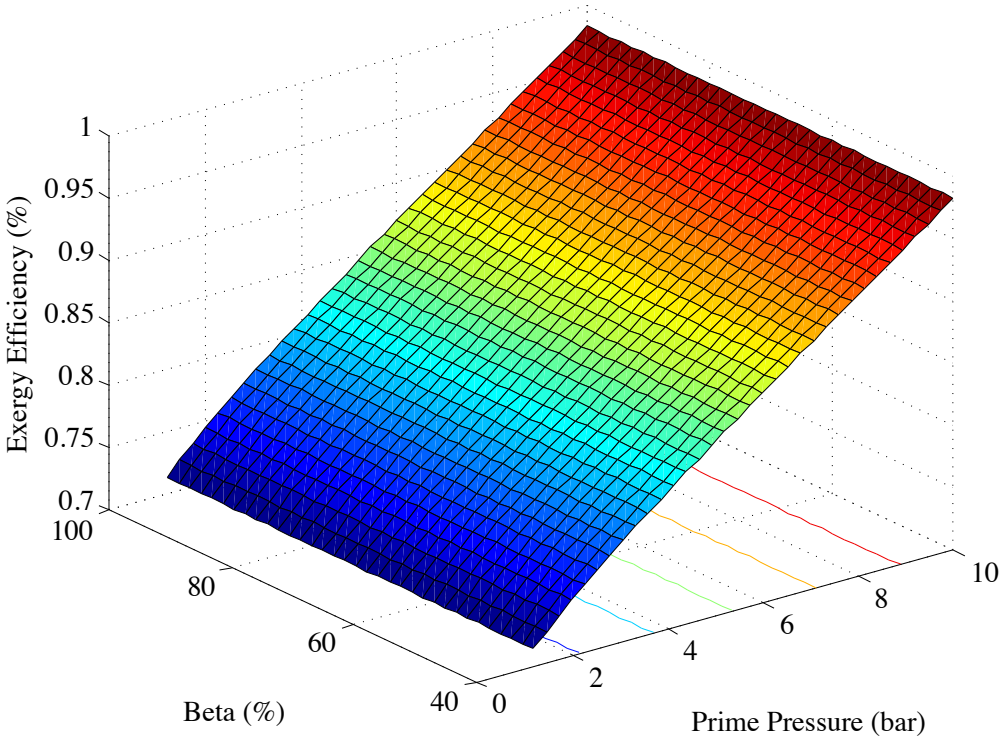


**Figure 7.15: Exergy efficiency of the cavern as a function of the energy distribution fraction and the prime pressure**

The exergy efficiency of the both the pressure regulating valve and the cavern, as one system, results in the plot given by Figure 15. With increased prime pressure, both throttling losses are decreases and mixing losses within the air storage are decreased, therefore resulting in higher exergetic efficiency as the irreversibilities are reduced. However, it is important to note the higher exergetic efficiency at high prime pressures result in larger storage volumes, therefore driving up the total cost of the system.

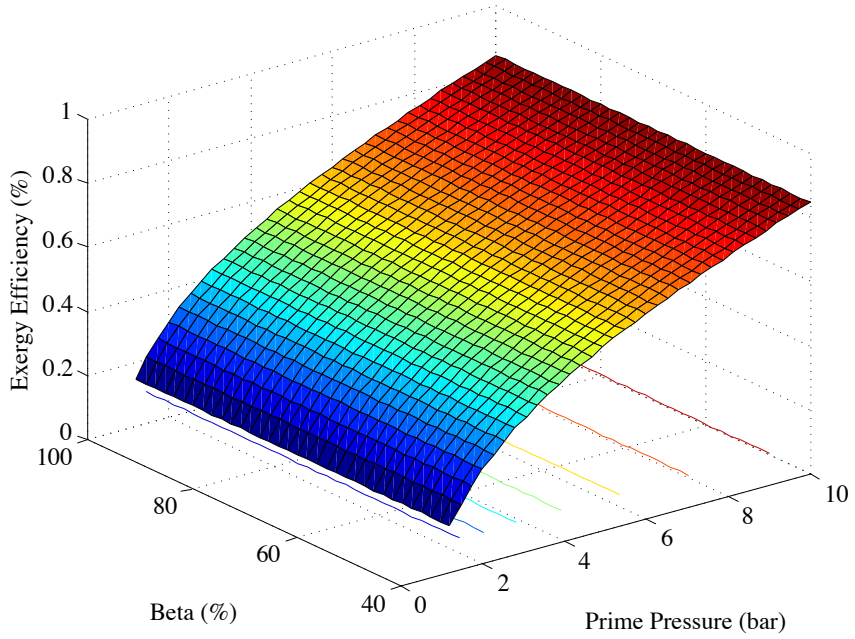


**Figure 7.16: Exergy efficiency of the cavern plus pressure-regulating valve as a function of the energy distribution fraction and the prime pressure**

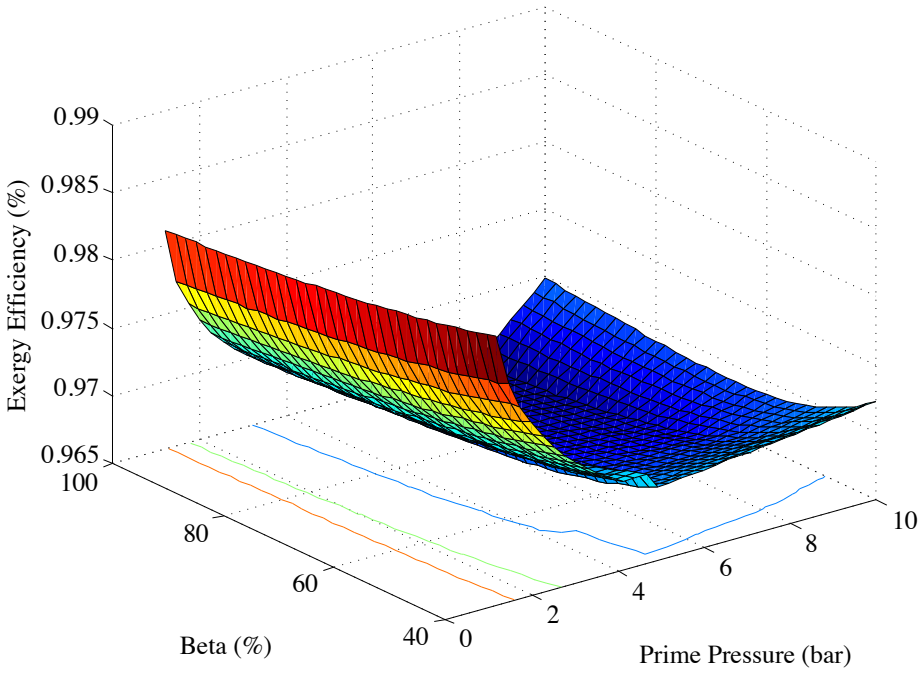


**Figure 7.17: Exergy efficiency of the HTES bypass junction as a function of the energy distribution fraction and the prime pressure**

The roundtrip exergy efficiency of the HTES is given in Figure 17, as functions of the temperature ratios $T_o/T_{min}$ and $(T_{max}-T_{min})/T_o$. The exergy efficiency map of the HTES, in Figure 17, is presented assuming an energy efficiency of 80%. The exergetic efficiency of the HTES is largest at high minimum HTES temperature values. In addition, the HTES exergetic efficiency increases sharply at lower temperature swings due to the decrease in the irreversibilities associated with mixing losses. It is important to note that the exergy efficiency of the HTES is always lower than it corresponding energy efficiency, in contrast to the roundtrip energy and exergy efficiency of the entire hybrid storage system.

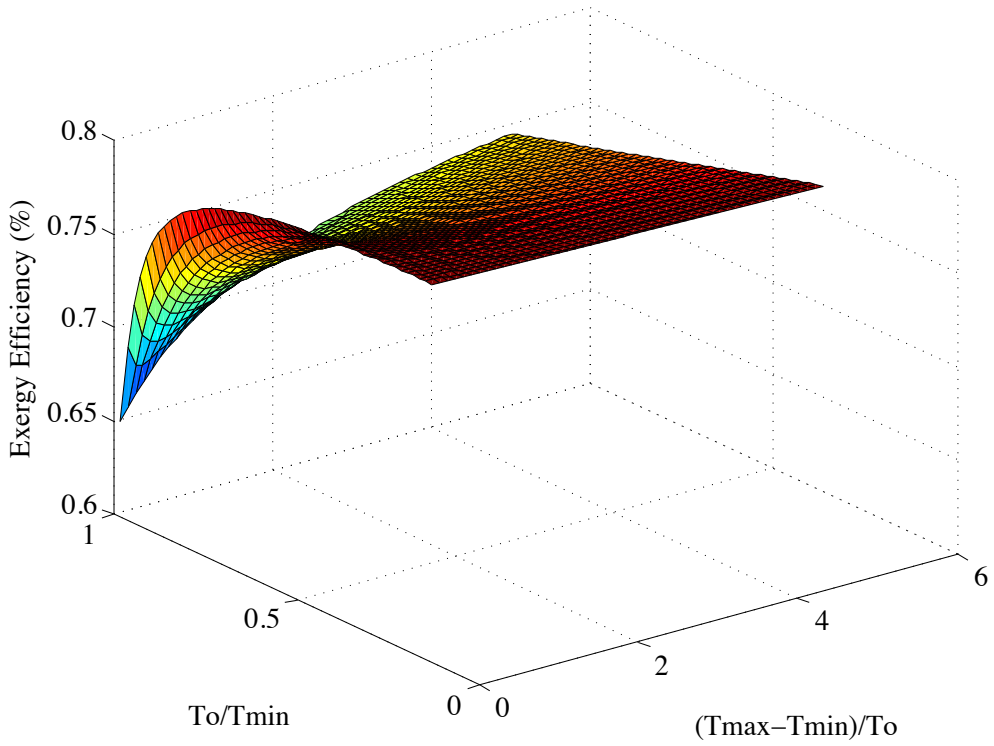


**Figure 7.18: Roundtrip exergy efficiency of HTES, assuming an energy efficiency of 80%, as a function of the energy distribution fraction and the prime pressure**

The exergy efficiency of the regenerator, LTES discharge heat exchanger and the turbocharger junction is illustrated in Figure 18. The exergy efficiency increases with prime pressure, as

higher flow exergies are attained. The discontinuities in the plot are a result of the discontinuity associated with the configuration, as illustrated in Figure 4.

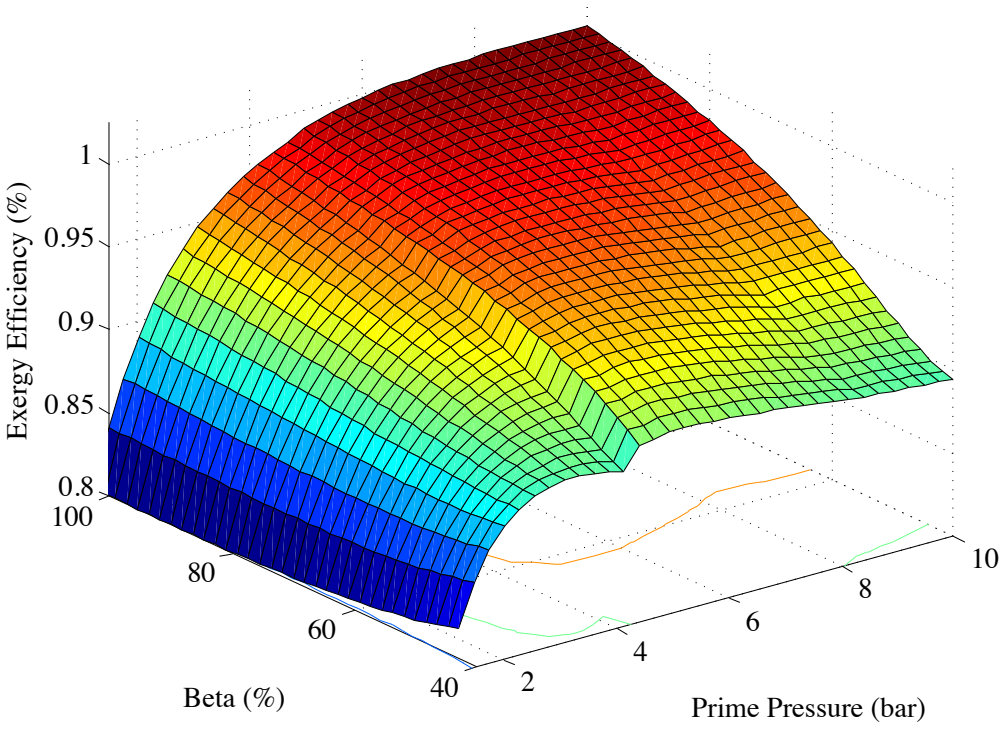


**Figure 7.19: Exergy efficiency of the LTES, Regenerator and turbocharger junction as a function of the energy distribution fraction and the prime pressure**

The turbine and turbocharger compressor exergy efficiencies are illustrated in Figures 19 and 20 respectively. The turbine exergy efficiency is highly on the energy distribution fraction, as the total power output is assumed constant in the study, however, the flow rate is highly dependent on the energy allocation fraction, Beta. In contrast, the compressor exergetic efficiency is independent of the energy allocation fraction, Beta. The energy allocation fraction only determines the necessary turbocharger flow rate, which is not a variable of the exergetic compressor efficiency. The output compressor power is not a constant and increases with the prime pressure, therefore decreases the exergetic efficiency of the compressor.

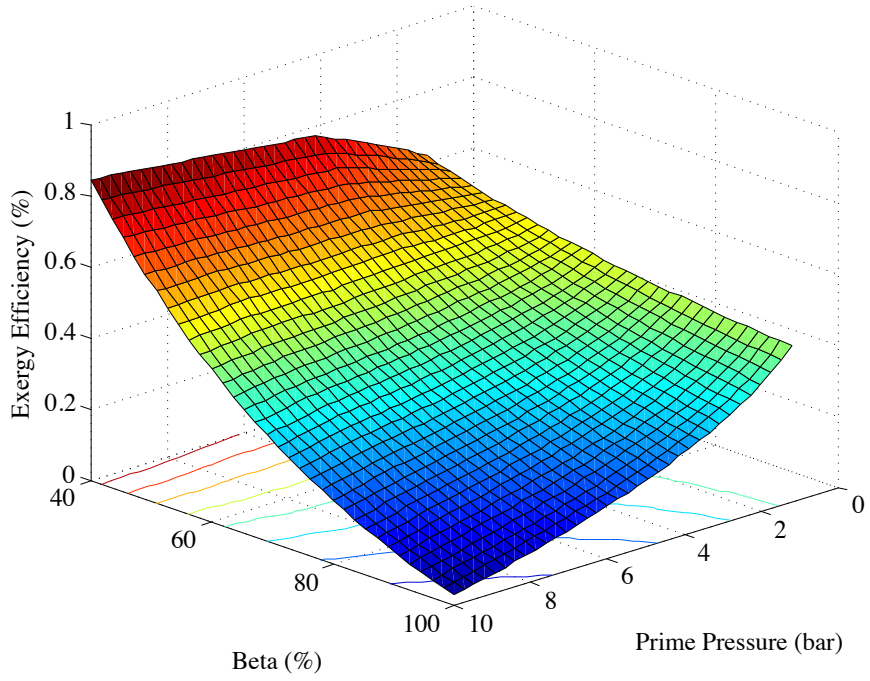


**Figure 7.20: Exergy efficiency of the turbine as a function of the energy distribution fraction and the prime pressure**

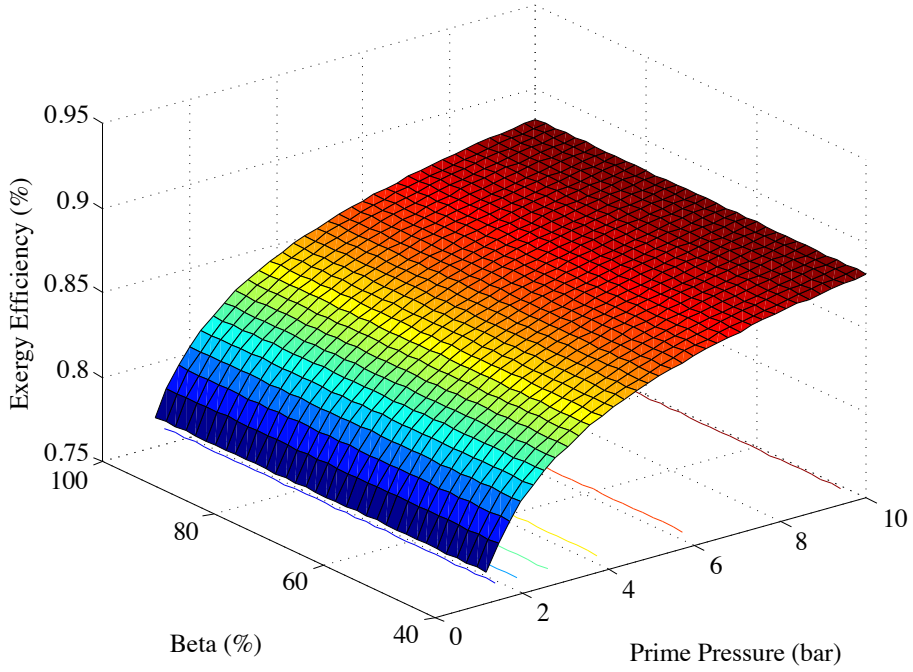


**Figure 7.21: Exergy efficiency of the turbocharger compressor as a function of the energy distribution fraction and the prime pressure**

Finally, the exergy efficiency of the LTES charge heat exchanger is a constant and equal to 76.35%, and the compressor exergy efficiency is also a constant and equal to 90.5%. The exergetic efficiency of the compressor is constant become the maximum pressure in the study remains constant, which results in a constant exhaust temperature, independent of the energy allocation fraction or the prime pressure. The exergy efficiency of the LTES charge heat exchanger is a constant for similar reasons, as the hot inlet temperature remains a constant and the cold to hot stream flow rate ratio in the exergy efficiency definition is a constant and equal to the ratio of their specific heats, assuming a balanced heat exchanger.

## 7.4 Discussion

The component exergy destruction magnitudes and their exergetic efficiencies present a means of locating the sources of largest deviation from ideal component operations. However it is important to note that some sources of irreversibilities are unavoidable. For example, one major advantage of the hybrid thermal and compressed air energy is its utilization of off-the-shelf and available machinery, such as compressors and turbines. Therefore, although the calculated exergy destruction and efficiency is an important means of determining the deviations from ideal operation, these irreversibilities are unavoidable as their use is necessary for proper operation of the plant. In addition, the minimization of internal irreversibilies does not necessarily correlate with maximum roundtrip energy and exergy efficiencies of the plant, as was demonstrated in chapter 6. Therefore as an example, although one can minimize the compressor irreversibilities through an increase in its operating pressure, the design point does not coincide with the local

optimum operating pressure leading to maximum energy and exergy efficiency of the hybrid storage system, as was demonstrated in chapter 5. The exergy destruction and exergetic efficiency of the pressure regulative valve presented in the results section demonstrates a substantial loss in otherwise available work. Throughout the investigation, an ideal gas model for air was assumed. An ideal gas assumption is reasonable as the hybrid system operates at low pressures, which leads to low compressibility factors. Moreover, in the case of an ideal gas the internal energy is only a function of temperature. Therefore, from an energy balance perspective the throttling valve energy inlet to exit is conserved, as enthalpy remains constant through the valve. Only in the presented exergy analysis do losses associated with throttling become apparent. Throttling losses can be eliminated through the use of variable pressure turbines. While a positive-displacement machine with proper valve-timing control can adjust to the time-varying pressure in the cavern and maintain optimal performance, a variable expander assumption over-estimates the power output with turbo-expanders. The optimal performance of a turbo-expander, characterized by its isentropic efficiency, is limited to a very narrow range of inlet operating conditions of pressure, temperature and mass flow rate. Slight deviations from the design conditions results in a sharp decrease in isentropic efficiency of the machine. Therefore, such machinery must be developed to withstand a large pressure swing without a substantial compromise in its performance. The cavern itself also presents a substantial source of avoidable irreversibilities due to its associated mixing losses. The air storage cavern is assumed isochoric, however in the case of an isobaric cavern mixing loss within the cavern are eliminated as the cavern acts just as a delay time in the operation of the plant, whereas an adiabatic constant volume cavern changes the quality of energy through the cavern. Isobaric cavern architectures however are geologically more restricting and require higher capital costs.

## 7.5 Conclusion

The exergy destruction of each component in the Hybrid thermal and compressed air energy storage system was calculated and presented. The exergy destruction of each component within the system was presented as functions of the energy allocation fraction, beta, and the prime pressure. These two variables are the center of investigation throughout the chapter as their variance provides the entire operational map of the system. This chapter provided the associated map of the internal component irreversibility magnitudes of the hybrid storage system. The exergy destruction was normalized by the constant output energy of the plant, 600MWh, as was the case in chapter 5. The calculated and normalized exergy destruction maps provided a means of comparing the component exergy destruction magnitudes for assessing and pinpointing the sources of largest irreversibilities. In addition to the exergy destruction, the exergetic component efficiencies were also presented and compared. Both component exergy destruction and their exergetic efficiencies demonstrate that the largest source of avoidable exergy destruction result from the irreversibilities associated with throttling and the irreversibilities associated with mixing losses within the air storage medium. In the case of an isochoric air storage medium, introducing variable pressure turbines can eliminate throttling losses. However, large-scale variable pressure turbines capable of withstanding large pressure swings, without a compromise in their isentropic efficiencies, must be research and developed despite their limited potential market. Moreover, the mixing losses within an isochoric cavern can be eliminated through the use of an isobaric air storage medium, which are typically constructed in underground rock formations with a water-equalizing pit, or through underwater air storage. In addition to eliminating mixing losses, such air storage architecture also eliminates the need for throttling,

therefore the input flow exergy into and out of the medium become identical. Isobaric air storage however is typically more costly and less available as compared with an isochoric type.

# Chapter 8: Summary & Future Work

With increased interest in adoption of renewable energies, energy storage has become a logical solution to the renewable power intermittency. Compressed air energy storage has received much attention, however conventional systems require the combustion of natural gas, necessitate large storage volumes, and operate at high pressures, which possess inherent problems such as strict geological locations, high costs, and the production of global warming emissions. Through this research, a novel and patent hybrid thermal-compressed air energy storage system is presented as a viable solution. In an attempt to investigate the theoretical performance limits of the system, An ideal thermodynamic model was developed of the hybrid storage system. The analysis considered perfect performance indices for the components (isentropic efficiency and effectiveness) and explored the integral built-in boundaries of operation of the storage cycle with respect to the corresponding Brayton and Carnot cycles. The models included cycles with and without regeneration. The results of this research conclude that consistent with the advanced adiabatic compressed air energy storage concept, in the limit of no heat addition to the system the ideal cycle has 100% theoretical roundtrip efficiency. In this limit the compression and expansion occur along the same isentrope. The addition of heat through thermal storage takes the expansion process off the compression isentrope and results in a non-unity round trip efficiency even in the case of perfect components. The efficiency of the storage cycle approaches that of a classical Brayton cycle as the temperature of the thermal storage increases. In general, the energy storage cycle, namely compressed air energy storage, is not bound by the Carnot efficiency, as the Carnot efficiency is limited to heat engines, not energy storage cycles.

A realistic hybrid storage system was investigated, with irreversibilities dictated through specified isentropic component efficiencies. A sliding-pressure cavern is throttled in the discharge process to a constant pressure, i.e. the prime pressure, under both isothermal and adiabatic cavern conditions. The two assumptions were investigated as they demonstrate the two possible extreme cavern conditions. Parametric studies of the prime pressure were investigated for both cavern conditions. Through the parametric study, the existence of an optimum prime pressure leading to maximum roundtrip efficiency was found. For both isothermal and adiabatic cavern conditions, the maximum round trip efficiency is within the same proximity, although the associated optimum prime pressure for an adiabatic cavern is considerably higher. An AA-CAES system was also modeled as a comparison with a throttled, isothermal, sliding pressure cavern employing the same isentropic component efficiencies used for the HT-CAES model. It was found that the roundtrip efficiency of the AA-CAES system is highly dependent on the storage temperature. In the limiting case when the heat rate capacity ratio is unity, $C_r$=1, i.e. when the LTES can reach the highest possible temperatures, the roundtrip efficiency for a practical yet high prime pressure of 50 bar is approximately 47%. The roundtrip efficiency of an HT-CAES system with same output power of 100MW, a flow rate of 150kg/s and a prime pressure of 15bar is about 53%. The implication of this result is that even in the case of maximum LTES temperature, 725K, which is higher than what can be provided by currently available compressors, an HT-CAES system is more efficient by 6.5%.

A modified hybrid thermal and compressed air energy storage configuration is presented which includes a turbocharger on the discharge side. The addition of both thermal energy storage and a turbocharger have the effect of significantly leveraging the cost of the system, as supplementary

mass flow rate is provided along side the stored air, and the cost of thermal storage is considerably cheaper than air storage. The reduced system cost, however, comes at the expense of a reduced efficiency, as the performance of heat engines are bound by the Carnot limit and compressed air energy storage, theoretically, has no such constraint. The modified hybrid system provides the flexibility of adjusting to a myriad of storage volumes based on available geological restrictions. In addition, the hybrid storage system performs best at low storage pressures, which reduces the complexity as it alleviates the need for multistage compression and expansion. The thermodynamic optimization results provide the operational efficiency, cost and storage sizing (thermal and air volume) maps, which can be used as a reference in future development endeavors. In addition all mass flow rate maps are provided, which dictate the necessary machinery sizes. The operational flexibility of HT-CAES is particularly useful as the priorities of various energy applications are not unique, these priorities may include cost, efficiency, and footprint.

An optimization objective based on minimum entropy generation was investigated in the hybrid thermal and compressed air energy storage system. The cases of both internally reversible and irreversible conditions were analyzed. It is shown that a hybrid compressed air energy storage system designed based on this criteria may operate at an output power, energy, and exergy efficiency, which is lower than what is theoretically feasible. Only under certain circumstance does the minimum entropy generation coincide with maximum energy and exergy efficiencies. Moreover it was generally observed that the optimum operating pressure conditions based on maximum energy efficiency, maximum exergy efficiency, and minimum entropy generation can be ordered in the following manner: $r(S_{gen,min}) < r(\eta_{II,max}) < r(\eta_{I,max})$.

An exergy analysis of the system was undertaken. Specifically, the exergy destruction of each component in the Hybrid thermal and compressed air energy storage system was calculated and presented. The exergy destruction of each component within the system was presented as functions of the energy allocation fraction, beta, and the prime pressure. These two variables are the center of investigation throughout this research as their variance provides the entire operational map of the system. The associated maps corresponding to internal component irreversibility magnitudes of the hybrid storage system were provided. The exergy destruction was normalized by the constant output energy of the plant, 600MWh. The calculated and normalized exergy destruction maps provided a means of comparing the component exergy destruction magnitudes for assessing and pinpointing the sources of largest irreversibilities. The exergetic component efficiencies were also presented and compared. Both component exergy destruction and their exergetic efficiencies demonstrate that the largest source of avoidable exergy destruction result from the irreversibilities associated with throttling and the irreversibilities associated with mixing losses within the air storage medium. In the case of an isochoric air storage medium, introducing variable pressure turbines can eliminate throttling losses. Moreover, the mixing losses within an isochoric cavern can be eliminated through the use of an isobaric air storage medium, however such architecture is not as available and typically requires higher capital costs. Future works should include proper account of HTES heat losses during charge and discharge to quantify the roundtrip efficiency of thermal energy storage. In addition, future works should account for pressure losses throughout the cycle

# References


[1] Sun Can, Zhaohong Bie, Zijun Zhang, A new framework for the wind power curtailment and absorption evaluation, International Transactions on Electrical Energy Systems, 2016:2016 vol: 26 iss: 10 pg: 2134 -2147 doi: 10.1002/etep.2194

[2] Li CB, Shi HQ, Cao YJ, et al. Comprehensive review of renewable energy curtailment and avoidance: a specific example in China. Renewable & Sustainable Energy Reviews 2015; 41:1067–1079.

[3] Zou, J (Zou, Jin)[ 1 ] ; Rahman, S (Rahman, Saifur)[ 2 ] ; Lai, X (Lai, Xu)[ 1 ], Mitigation of Wind Output Curtailment by Coordinating with Pumped Storage and Increasing Transmission Capacity, 2015 IEEE POWER & ENERGY SOCIETY GENERAL MEETING

[4] Waite, M (Waite, Michael)[ 1 ] ; Modi, V (Modi, Vijay)[ 1 ], Modeling wind power curtailment with increased capacity in a regional electricity grid supplying a dense urban demand, 2016, APPLIED ENERGY, Volume: 183 Pages: 299-317 DOI: 10.1016/j.apenergy.2016.08.078

[5] Wang, CX (Wang, Caixia)[ 1 ], Study of Unit Commitment Strategies in Combating Wind Curtailment in China, 2015 4TH INTERNATIONAL CONFERENCE ON ENERGY AND ENVIRONMENTAL PROTECTION (ICEEP 2015) Pages: 1137-1140

[6] Fan, XC (Fan, Xiao-chao)[ 1,2 ] ; Wang, WQ (Wang, Wei-qing)[ 1,2 ] ; Shi, RJ (Shi, Rui-jing)[ 1 ] ; Li, FT (Li, Feng-ting)[ 1,2 ], Analysis and countermeasures of wind power curtailment in China, 2015, ENEWABLE & SUSTAINABLE ENERGY REVIEWS, Volume: 52. Pages: 1429-1436, DOI: 10.1016/j.rser.2015.08.025

[7] Gunter, N (Gunter, Niklas)[ 1,2 ] ; Marinopoulos, A (Marinopoulos, Antonios)[ 3 ], Energy storage for grid services and applications: Classification, market review, metrics, and methodology for evaluation of deployment cases, 2016, JOURNAL OF ENERGY STORAGE, Volume: 8, Pages: 226-234, DOI: 10.1016/j.est.2016.08.011

[8] Zakeri, B (Zakeri, Behnam)[ 1 ] ; Syri, S (Syri, Sanna)[ 1 ], Electrical energy storage systems: A comparative life cycle cost analysis, 2015, RENEWABLE & SUSTAINABLE ENERGY REVIEWS, Volume: 42, Pages: 569-596, DOI: 10.1016/j.rser.2014.10.011

[9] Zidar, Matija)[ 1 ] ; Georgilakis, PS (Georgilakis, Pavlos S.)[ 2 ] ; Hatziargyriou, ND (Hatziargyriou, Nikos D.)[ 2 ] ; Capuder, T (Capuder, Tomislav)[ 1 ] ; Skrlec, D (Skrlec, Davor)[ 1 ], Review of energy storage allocation in power distribution networks: applications, methods and future research, 2016, IET GENERATION TRANSMISSION & DISTRIBUTION, Volume: 10, Issue: 3, Pages: 645-652, Special Issue: SI, DOI: 10.1049/iet-gtd.2015.0447

[10] A.G. Olabi, Renewable energy and energy storage systems, In Energy, Volume 136, 2017, Pages 1-6, ISSN 0360-5442, https://doi.org/10.1016/j.energy.2017.07.054.

[11] Anuta, OH (Anuta, Oghenetejiri Harold)[ 1 ] ; Taylor, P (Taylor, Phil)[ 1 ] ; Jones, D (Jones, Darren)[ 2 ] ; McEntee, T (McEntee, Tony)[ 2 ] ; Wade, N(Wade, Neal)[ 1 ], An international review of the implications of regulatory and electricity market structures on the emergence of grid scale electricity storage, 2014, RENEWABLE & SUSTAINABLE ENERGY REVIEWS, Volume: 38, Pages: 489-508, DOI: 10.1016/j.rser.2014.06.006

[12] Hameer, S (Hameer, Sameer)[ 1 ] ; van Niekerk, JL (van Niekerk, Johannes L.)[ 1 ], A review of large-scale electrical energy storage, 2015, INTERNATIONAL JOURNAL OF ENERGY RESEARCH, Volume: 39, Issue: 9, Pages: 1179-1195, DOI: 10.1002/er.3294

[13] Freeman, E (Freeman, Eugene); Occello, D (Occello, Davide)[ 1 ] ; Barnes, F (Barnes, Frank)[ 2 ], Energy storage for electrical systems in the USA, 2016, AIMS ENERGY, Volume: 4, Issue: 6, Pages: 856-875, DOI: 10.3934/energy.2016.6.856

[14] Zakeri, B (Zakeri, Behnam)[ 1 ] ; Syri, S (Syri, Sanna)[ 1 ], Electrical energy storage systems: A comparative life cycle cost analysis, 2015, ENEWABLE & SUSTAINABLE ENERGY REVIEWS, Volume: 42, Pages: 569-596, DOI: 10.1016/j.rser.2014.10.011

[15] Obi, M (Obi, Manasseh)[ 1 ] ; Jensen, SM (Jensen, S. M.)[ 2 ] ; Ferris, JB (Ferris, Jennifer B.)[ 3 ] ; Bass, RB (Bass, Robert B.)[ 1 ], Calculation of levelized costs of electricity for various

electrical energy storage systems, 2017, RENEWABLE & SUSTAINABLE ENERGY REVIEWS, Volume: 67, Pages: 908-920, DOI: 10.1016/j.rser.2016.09.043

[16] Erren Yao, Huanran Wang, Ligang Wang, Guang Xi, François Maréchal, Multi-objective optimization and exergoeconomic analysis of a combined cooling, heating and power based compressed air energy storage system, Energy Conversion and Management, Volume 138, 15 April 2017, Pages 199-209, ISSN 0196-8904, http://dx.doi.org/10.1016/j.enconman.2017.01.071.

[17] Wei Ji, Yuan Zhou, Yu Sun, Wu Zhang, Baolin An, Junjie Wang, Thermodynamic analysis of a novel hybrid wind-solar-compressed air energy storage system, Energy Conversion and Management, Volume 142, 15 June 2017, Pages 176-187, ISSN 0196-8904, http://dx.doi.org/10.1016/j.enconman.2017.02.053.

[18] Adriano Sciacovelli, Yongliang Li, Haisheng Chen, Yuting Wu, Jihong Wang, Seamus Garvey, Yulong Ding, Dynamic simulation of Adiabatic Compressed Air Energy Storage (A-CAES) plant with integrated thermal storage – Link between components performance and plant performance, Applied Energy, Volume 185, Part 1, 1 January 2017, Pages 16-28, ISSN 0306-2619, http://dx.doi.org/10.1016/j.apenergy.2016.10.058.

[19] Daniel Wolf, Marcus Budt, LTA-CAES – A low-temperature approach to Adiabatic Compressed Air Energy Storage, Applied Energy, Volume 125, 15 July 2014, Pages 158-164, ISSN 0306-2619, http://dx.doi.org/10.1016/j.apenergy.2014.03.013.

[20] Hao Peng, Yu Yang, Rui Li, Xiang Ling, Thermodynamic analysis of an improved adiabatic compressed air energy storage system, Applied Energy, Volume 183, 1 December 2016, Pages 1361-1373, ISSN 0306-2619, http://dx.doi.org/10.1016/j.apenergy.2016.09.102.

[21] Adewale Odukomaiya, Ahmad Abu-Heiba, Kyle R. Gluesenkamp, Omar Abdelaziz, Roderick K. Jackson, Claus Daniel, Samuel Graham, Ayyoub M. Momen, Thermal analysis of near-isothermal compressed gas energy storage system, Applied Energy, Volume 179, 1 October 2016, Pages 948-960, ISSN 0306-2619, http://dx.doi.org/10.1016/j.apenergy.2016.07.059.

[22] Gayathri Venkataramani, Prasanna Parankusam, Velraj Ramalingam, Jihong Wang, A review on compressed air energy storage – A pathway for smart grid and polygeneration, Renewable and Sustainable Energy Reviews, Volume 62, September 2016, Pages 895-907, ISSN 1364-0321, http://dx.doi.org/10.1016/j.rser.2016.05.002.

[23] Seamus D. Garvey and Andrew Pimm, Chapter 5 - Compressed Air Energy Storage, In Storing Energy, edited by Trevor M. Letcher, Elsevier, Oxford, 2016, Pages 87-111, ISBN 9780128034408, http://dx.doi.org/10.1016/B978-0-12-803440-8.00005-1.

[24] Odukomaiya, A (Odukomaiya, Adewale)[ 1 ] ; Abu-Heiba, A (Abu-Heiba, Ahmad)[ 2 ] ; Gluesenkamp, KR (Gluesenkamp, Kyle R.)[ 2 ] ; Abdelaziz, O(Abdelaziz, Omar)[ 2 ] ; Jackson, RK (Jackson, Roderick K.)[ 2 ] ; Daniel, C (Daniel, Claus)[ 2 ] ; Graham, S (Graham, Samuel)[ 1,2 ] ; Momen, AM (Momen, Ayyoub M.)[ 2 ], Thermal analysis of near-isothermal compressed gas energy storage system, 2016, APPLIED ENERGY, Volume: 179, Pages: 948-960, DOI: 10.1016/j.apenergy.2016.07.059

[25] Kilic, M (Kilic, M.)[ 1 ] ; Mutlu, M (Mutlu, M.)[ 2 ], A novel design of a compressed air storage system with liquid pistons, 2016, BULGARIAN CHEMICAL COMMUNICATIONS, Volume: 48, Pages: 318-324, Special Issue: E2

[26] Li, PY (Li, Perry Y.)[ 1 ] ; Saadat, M (Saadat, Mohsen)[ 1 ], An approach to reduce the flow requirement for a liquid piston near-isothermal aircompressor/expander in a compressed air energy storage system, 2016, IET RENEWABLE POWER GENERATION, Volume: 10, Issue: 10, Pages: 1506-1514, Special Issue: SI, DOI: 10.1049/iet-rpg.2016.0055

[27] Qin, C (Qin, Chao)[ 1 ] ; Loth, E (Loth, Eric)[ 1 ], Liquid piston compression efficiency with droplet heat transfer, 2014, APPLIED ENERGY, Volume: 114, Pages: 539-550, Special Issue: SI, DOI: 10.1016/j.apenergy.2013.10.005

[28] Daniel Buhagiar, Tonio Sant, Modelling of a novel hydro-pneumatic accumulator for large-scale offshore energy storage applications, In Journal of Energy Storage, 2017, ISSN 2352-152X, https://doi.org/10.1016/j.est.2017.05.005.

[29] Marcus Budt, Daniel Wolf, Roland Span, Jinyue Yan, A review on compressed air energy storage: Basic principles, past milestones and recent developments, In Applied Energy, Volume 170, 2016, Pages 250-268, ISSN 0306-2619, https://doi.org/10.1016/j.apenergy.2016.02.108.

[30] Qin, C (Qin, C.)[ 1 ] ; Loth, E (Loth, E.)[ 1 ], Simulation of spray direct injection for compressed air energy storage, 2016, APPLIED THERMAL ENGINEERING, Volume: 95, Pages: 24-34. DOI: 10.1016/j.applthermaleng.2015.11.008

[31] McBride T, Bell A, Kepshire D. ICAES innovation: foam-based heat exchange. USA: Seabrook; 2013.

[32] Kentschke T. Druckluftmaschinen als Generatorantrieb inWarmluftspeichern. Dissertation. Clausthal; 2004.

[33] Lukasz Szablowski, Piotr Krawczyk, Krzysztof Badyda, Sotirios Karellas, Emmanuel Kakaras, Wojciech Bujalski, Energy and exergy analysis of adiabatic compressed air energy storage system, In Energy, Volume 138, 2017, Pages 12-18, ISSN 0360-5442, https://doi.org/10.1016/j.energy.2017.07.055.

[34] Hao Peng, Yu Yang, Rui Li, Xiang Ling, Thermodynamic analysis of an improved adiabatic compressed air energy storage system, In Applied Energy, Volume 183, 2016, Pages 1361-1373, ISSN 0306-2619, https://doi.org/10.1016/j.apenergy.2016.09.102.

[35] Baghaei Lakeh R., Villanava, I., Houssainy, S., Anderson, K., Kavehpour, H.P., 2016, Design of a Modular Solid-Based Thermal Energy Storage for a Hybrid Compressed Air Energy Storage System, Paper No. PowerEnergy2016-59160, Proc. of 2016 ASME Int. Conference on Energy Sustainability Charlotte, NC

[36] Houssainy, S Baghaei Lakeh R., Kavehpour, H.P., 2016, A Thermodynamic Model of High Temperature Hybrid Compressed Air Energy Storage System for Grid Storage, Paper No. PowerEnergy2016-59431, Proc. of 2016 ASME Int. Conference on Energy Sustainability Charlotte, NC

[37] Ip PP, Houssainy S, Kavehpour. Modeling of a Low Cost Thermal Energy Storage System to Enhance Generation From Small Hydropower Systems. 2017, ASME Power Conference, doi:10.1115/POWER-ICOPE2017-3684

[38] Sammy Houssainy, Mohammad Janbozorgi, Peggy Ip, Pirouz Kavehpour, Thermodynamic Analysis of a High Temperature Hybrid Compressed Air Energy Storage (HTH-CAES) System, Renewable Energy, Available online 12 September 2017, ISSN 0960-1481, https://doi.org/10.1016/j.renene.2017.09.038.

[39] Peng, H (Peng, Hao)[ 1 ] ; Yang, Y (Yang, Yu)[ 1 ] ; Li, R (Li, Rui)[ 1 ] ; Ling, X (Ling, Xiang)[ 1 ], Thermodynamic analysis of an improved adiabatic compressed air energy storage system, 2016, APPLIED ENERGY, Volume: 183, Pages: 1361-1373, DOI: 10.1016/j.apenergy.2016.09.102

[40] Wolf D, Budt M. LTA-CAES – a low-temperature approach to adiabatic compressed air energy storage. Appl Energy 2014;125:158–64.

[41] Luo, X (Luo, Xing)[ 1 ] ; Wang, JH (Wang, Jihong)[ 1,3 ] ; Krupke, C (Krupke, Christopher)[ 1 ] ; Wang, Y (Wang, Yue)[ 1 ] ; Sheng, Y (Sheng, Yong)[ 2 ] ; Li, J (Li, Jian)[ 3 ] ; Xu, YJ (Xu, Yujie)[ 2 ] ; Wang, D (Wang, Dan)[ 3 ] ; Miao, SH (Miao, Shihong)[ 3 ] ; Chen, HS (Chen, Haisheng)[ 2 ],Modelling study, efficiency analysis and optimisation of large-scale Adiabatic Compressed Air Energy Storage systems with low-temperature thermal storage, 2016, APPLIED ENERGY, Volume: 162, Pages: 589-600, DOI: 10.1016/j.apenergy.2015.10.091

[42] B. Cárdenas, A.J. Pimm, B. Kantharaj, M.C. Simpson, J.A. Garvey, S.D. Garvey, Lowering the cost of large-scale energy storage: High temperature adiabatic compressed air energy storage, In Propulsion and Power Research, Volume 6, Issue 2, 2017, Pages 126-133, ISSN 2212-540X, https://doi.org/10.1016/j.jppr.2017.06.001.

[43] V. de Biasi, Fundamental analyses to optimize adiabatic CAES plant effi- ciencies, Gas Turbine World 39 (2009) 26e28.

[44] Doetsch C, Budt M, Wolf D, Kanngießer A. Adiabates Niedertemperatur-Druckluftspeicherkraftwerk zur Unterstützung der Netzintegration von Windenergie. Abschlussbericht zu FKZ 0325211; 2012.

[45] Barbour E, Mignard D, Ding Y, Li Y. Adiabatic compressed air energy storage with packed bed thermal energy storage. Appl Energy 2015;155:804–15.

[46] Dreißigacker V, Zunft S, Müller-Steinhagen H. A thermo-mechanical model of packed-bed storage and experimental validation. Appl Energy 2013;111:1120–5.

[47] Yang Z, Wang Z, Ran P, Li Z, Ni W. Thermodynamic analysis of a hybrid thermal-compressed air energy storage system for the integration of wind power. Applied Thermal Engineering 2014;66:519-527.

[48] Ibrahim Dincer, Marc Rosen, Thermal Energy Storage Systems and Applications (2nd Edition), 2011, John Wily & Sons Ltd, United Kingdom

[49] Chen H, Cong TN, Yang W, Tan C, Li Y, Ding Y. Progress in electrical energy storage system: a critical review. Progr Nat Sci 2009;19(3):291–312.

[50] Mathiesen BV, Lund H, Connolly D, Wenzel H, Østergaard PA, Möller B, et al. Smart Energy Systems for coherent 100% renewable energy and transport solutions. Appl Energy 2015;145:139–54.

[51] Zakeri B, Syri S. Electrical energy storage systems: a comparative life cycle cost analysis. Renew Sustain Energy Rev 2015;42:569–96.

[52] Dell RM, Rand DAJ. Energy storage – a key technology for global energy sustainability. J Power Sources 2001;100:2–17.

[53] Ferreira HL, Garde R, Fulli G, Kling W, Lopes JP. Characterisation of electrical energy storage technologies. Energy 2013;53:288–98.

[54] Beaudin M, Zareipour H, Schellenberglabe A, Rosehart W. Energy storage for mitigating the variability of renewable electricity sources: an updated re- view. Energy Sustain Dev 2010;14(4):302–14.

[55] Ela E, Kirby B. Ercot event on February 26, 2008: Lessons learned. Tech. Rep. NREL/TP-500-

43373. Golden, USA: National Renewable Energy Lab; 2008.

[56] Lund PD, Lindgren J, Mikkola J, Salpakari J. Review of energy system flexibility measures to enable high levels of variable renewable electricity. Renew Sustain Energy Rev 2015;45:785–807.

[57] Paatero JV, Lund PD. Effects of large-scale photovoltaic power integration on electricity distribution networks. Renew Energy 2007;32:216–34.

[58] Agrawal P, Nourai A, Markel L, Fioravanti R, Gordon P, Tong N, Huff G. Characterization and assessment of novel bulk storage technologies Sandia Report SAND2011–3700. Albuquerque, USA: Sandia National Laboratories; 2011.

[59] Gravity Power. Grid Scale Energy Storage. 〈http://www.gravitypower.net/〉 (Last accessed: 20/09/2015).

[60] Pimm AJ, Garvey SD, Drew RJ. Shape and cost analysis of pressurized fabric structures for subsea compressed air energy storage. Proc Inst Mech Eng C: J Mech Eng Sci 2011;225(5):1027–43.

[61] Pimm AJ, Garvey SD, de Jong M. Design and testing of Energy Bags for un- derwater compressed air energy storage. Energy 2014;66:496–508.

[62] Hydrostor. Underwater Compressed Air Energy Storage – Islands & Microgrid White Paper; 2013. 〈http://www.homerenergy.com/microgrid-white-papers. html〉 (Last accessed: 20/09/2015).

[63] Barbour E. An investigation into the potential of energy storage to tackle intermittency in renewable energy generation.Edinburg, UK: University Of Edinburg; 2013.

[64] California Independent System Operator, (2016) https://www.caiso.com/Documents/FlexibleResourcesHelpRenewables_FastFacts.pdf

[65] Haisheng Chen, Thang Cong, Wei Yang, Chunqing Tan, Yongliang Li, Yulong Ding, (2009) "Progress in electrical storage system A critical review", Progress in Natural Science 19 (2009) 291-312

[66] D. T. Bradshaw, B (2000), "Pumped hydroelectric storage (PHS) and compressed air energy storage (CAES)", presented at the IEEE PES Meeting Energy Storage, Seattle, WA

[67] Schoenung, B, (2001) “Characteristics and technologies for long- vs. short-term energy storage”, Sandia Rep. SAND2001-0765

[68] S. Van der Linden, B, (2006) “Bulk energy storage potential in the USA, current developments and future prospects”, Energy, vol. 31, pp. 3446–3457

[69] Young Min Kim, Jang Hee Lee, Seok Joon kim, Daniel Favrat, (2012), “Potential and Evolution of Compressed Air Energy Storage: Energy and Exergy Analysis” Entropy, 14, 1501-1521

[70] National Renewable Energy Laboratory, (2016) “Energy Storage, Possibilities for Expanding Electric Grid Flexibility ”. www.nrel.gov

[71] M. W. Coney, P. Stephenson, A. Malmgren, and C. Linnemann, B, (2002)“Development of a reciprocating compressor using water injection to achieve quasi-isothermal compression” presented at the 16th Int. Compressor Eng. Conf., West Lafayette, IN, Jul. 16–19

[72] G. Bidini, C. N. Grimaldi, and L. Postrioti, B, (1999) “Performance analysis of a hydraulic air compressor, I. Mech. E. Proc. Inst. Mech. Eng., vol. 213, pt. A, pp. 191–203

[73] Power South Energy Cooperative, “Compressed Air Energy Storage” McIntosh Power Plant, McIntosh, Alabama, www.powersouth.com

[74] D. R. Mack, B, (1993)“Something new in power technology”, IEEE Potentials, vol. 12, no. 2, pp. 40–42, Apr.

[75] BBC Brown Boveri “Huntorf Air Storage Gas Turbine Power Plant” Publication No. D GK 90 202 E

[76] Curzon FL, Ahlborn B. Efficiency of a Carnot engine at maximum power output. Am J Phys 1975;43(1):22–4.

[77] Bejan A. Theory of heat-transfer irreversible power-plants. Int J Heat Mass Transf 1988;31(6):1211–9.

[78] Bejan A. Theory of heat transfer-irreversible power plants. II. The optimal allocation of heat exchange equipment. Int J Heat Mass Transf 1995;3 (3):433–44.

[79] Wu C. Power optimization of a finite time Carnot heat engine. Energy 1988;13 (9):681–7.

[80] Gordon JM. Observations on efficiency of heat engines operating at maximum power. Am J Phys

1990;58(4):370–5.

[81] Wu C, Kiang RL. Finite-time thermodynamic analysis of a Carnot engine with internal irreversibility. Energy 1992;1(12):1173–8.

[82] Bejan A, Tsatsaronis G, Moran M. Thermal design and optimization. New York: Wiley; 1996.

[83] Cheng CY, Chen CK. Power optimization of an endoreversible regenerative Brayton cycle. Energy 1996;2(4):241–7.

[84] Cheng CY, Chen CK. Power optimization of an irreversible Brayton heat engine. Energy Sources 1997;1(5):461–74.

[85] Chen LG, Sun FR, Wu C, Kiang RL. Theoretical analysis of the performance of a regenerative closed Brayton cycle with internal irreversibilities. Energy Convers Manage 1997;3(9):871–7.

[86] Bejan A. Thermodynamic optimization alternatives: minimization of physical size subject to fixed power. Int J Energy Res 1999;23:1111–21.

[87] Chen LG, Zheng JL, Sun FR, Wu C. Power density analysis and optimization of a regenerated closed variable-temperature heat reservoir Brayton cycle. J Phys D: Appl Phys 2001;3(11):1727–39.

[88] Herrera Carlos A, Sandoval Jairo A, Rosillo Miguel E. Power and entropy generation of an extended irreversible Brayton cycle: optimal parameters and performance. J Phys D: Appl Phys 2006;39:3414–24.

[89] Ust Y, Sahin B, Yilmaz T. Optimization of a regenerative gas-turbine cogeneration system based on a new exergetic performance criterion: exergetic performance coefficient. Proc IMechE Part A: J Power Energy 2007;221:447–58.

[90] Yang B, Chen L, Sun F. Exergoeconomic performance analyses of an endoreversible intercooled regenerative Brayton cogeneration type model. Int J Sustainable Energy 2011;30:65–81.

[91] H. Ibrahim, A. Ilinca, J. Perron, Energy storage systems Characteristics and comparisons, Renewable and Sustainable Energy Reviews, Volume 12, Issue 5, June 2008, Pages 1221-1250, ISSN 1364-0321

[92] Erren Yao, Huanran Wang, Ligang Wang, Guang Xi, François Maréchal, Multi-objective optimization and exergoeconomic analysis of a combined cooling, heating and power based compressed air energy storage system, Energy Conversion and Management, Volume 138, 15 April 2017, Pages 199-209, ISSN 0196-8904, http://dx.doi.org/10.1016/j.enconman.2017.01.071.

[93] Wei Ji, Yuan Zhou, Yu Sun, Wu Zhang, Baolin An, Junjie Wang, Thermodynamic analysis of a novel hybrid wind-solar-compressed air energy storage system, Energy Conversion and Management, Volume 142, 15 June 2017, Pages 176-187, ISSN 0196-8904, http://dx.doi.org/10.1016/j.enconman.2017.02.053.

[94] Adriano Sciacovelli, Yongliang Li, Haisheng Chen, Yuting Wu, Jihong Wang, Seamus Garvey, Yulong Ding, Dynamic simulation of Adiabatic Compressed Air Energy Storage (A-CAES) plant with integrated thermal storage – Link between components performance and plant performance, Applied Energy, Volume 185, Part 1, 1 January 2017, Pages 16-28, ISSN 0306-2619, http://dx.doi.org/10.1016/j.apenergy.2016.10.058.

[95] Daniel Wolf, Marcus Budt, LTA-CAES – A low-temperature approach to Adiabatic Compressed Air Energy Storage, Applied Energy, Volume 125, 15 July 2014, Pages 158-164, ISSN 0306-2619, http://dx.doi.org/10.1016/j.apenergy.2014.03.013.

[96] Hao Peng, Yu Yang, Rui Li, Xiang Ling, Thermodynamic analysis of an improved adiabatic compressed air energy storage system, Applied Energy, Volume 183, 1 December 2016, Pages 1361-1373, ISSN 0306-2619, http://dx.doi.org/10.1016/j.apenergy.2016.09.102.

[97] Adewale Odukomaiya, Ahmad Abu-Heiba, Kyle R. Gluesenkamp, Omar Abdelaziz, Roderick K. Jackson, Claus Daniel, Samuel Graham, Ayyoub M. Momen, Thermal analysis of near-isothermal compressed gas energy storage system, Applied Energy, Volume 179, 1 October 2016, Pages 948-960, ISSN 0306-2619, *http://dx.doi.org/10.1016/j.apenergy.2016.07.059*.

[98] Gayathri Venkataramani, Prasanna Parankusam, Velraj Ramalingam, Jihong Wang, A review on compressed air energy storage – A pathway for smart grid and polygeneration, Renewable and

Sustainable Energy Reviews, Volume 62, September 2016, Pages 895-907, ISSN 1364-0321, http://dx.doi.org/10.1016/j.rser.2016.05.002.

[99] Seamus D. Garvey and Andrew Pimm, Chapter 5 - Compressed Air Energy Storage, In Storing Energy, edited by Trevor M. Letcher, Elsevier, Oxford, 2016, Pages 87-111, ISBN 9780128034408, *http://dx.doi.org/10.1016/B978-0-12-803440-8.00005-1*.

[100] ADELE Isothermal CAES. http://enipedia.tudelft.nl/wiki/ Adele_Isothermal_CAES. Accessed Sept 6, 16

[101] Apex CAES. *http://www.apexcaes.com/project*. Accessed August 2, 17.

[102] Transient thermofluids analysis of a ground-level integrated diverse energy storage (GLIDES) system 2015 international mechanical engineering congress & exposition, ASME, Houston (TX, US) (2015)

[103] Hydrostor. *https://hydrostor.ca/*. Accessed August 2, 17.

[104] Pickard WF, Hansing N, Shen AQ. Can large-scale advanced-adiabatic com- pressed air energy storage be justified economically in an age of sustainable energy? Journal of Renewable and Sustainable Energy 2009;3:033102.

[105] Sixian Wang, Xuelin Zhang, Luwei Yang, Yuan Zhou, Junjie Wang, Experimental study of compressed air energy storage system with thermal energy storage, Energy, Volume 103, 15 May 2016, Pages 182-191, ISSN 0360-5442, *http://dx.doi.org/10.1016/j.energy.2016.02.125*.

[106] Baghaei Lakeh R., Villanava, I., Houssainy, S., Anderson, K., Kavehpour, H.P., 2016, Design of a Modular Solid-Based Thermal Energy Storage for a Hybrid Compressed Air Energy Storage System, Paper No. PowerEnergy2016-59160, Proc. of 2016 ASME Int. Conference on Energy Sustainability Charlotte, NC

[107] Houssainy, S Baghaei Lakeh R., Kavehpour, H.P., 2016, A Thermodynamic Model of High Temperature Hybrid Compressed Air Energy Storage System for Grid Storage, Paper No. PowerEnergy2016-59431, Proc. of 2016 ASME Int. Conference on Energy Sustainability Charlotte, NC

[108] Yang Z, Wang Z, Ran P, Li Z, Ni W. Thermodynamic analysis of a hybrid thermal-compressed air energy storage system for the integration of wind power. Applied Thermal Engineering 2014;66:519-527.

[109] J, R, Roebuck, (1926) The Joule -Thomson Effect in Air, Physics: J. R. Roebuck, Vol 12, 1926

[110] Flack, Ronald D. (2005), Chapter 8: Axial Flow Turbines, Fundamentals of Jet Propulsion with Applications. Cambridge Aerospace Series. New York, NY: Cambridge University Press. *ISBN 978-0-521-81983-1*.

[111] V. de Biasi, Fundamental analyses to optimize adiabatic CAES plant efficiencies, Gas Turbine World 39 (2009) 26e28.

[112] Sesto E, Casale C. Exploitation of wind as an energy source to meet the world's electricity demand. J Wind Eng Ind Aerodyn 1998;74–76:375–87.

[113] Mahlia TMI, Saktisahdan TJ, Jannifar A, Hasan MH, Matseelar HSC. A review of available methods and development on energy storage; technology update. Renew Sust Energy Rev 2014;33:532–45.

[114] Yao E, Wang H, Liu L, Xi G. A novel constant-pressure pumped hydro combined with compressed air energy storage system. Energies 2015;8:154–71.

[115] Zhao P, Gao L, Wang J, Dai Y. Energy efficiency analysis and off-design analysis of two different discharge modes for compressed air energy storage system using axial turbines. Renew Energy 2016;85:1164–77.

[116] Zafirakis D, Chalvatzis KJ, Baiocchi G, Daskalakis G. Modeling of financial incentives for investments in energy storage systems that promote the largescale integration of wind energy. Appl Energy 2013;105:138–54.

[117] Liu H, He Q, Borgia A, Pan L, Oldenburg CM. Thermodynamic analysis of a compressed carbon dioxide energy storage system using two saline aquifers at different depths as storage reservoirs. Energy Convers Manage 2016;127:149–59.

[118] Zhang Y, Yang K, Li X, Xu J. Thermodynamic analysis of energy conversion and transfer in hybrid system consisting of wind turbine and advanced adiabatic compressed air energy storage. Energy 2014;77:460–77.

[119] Budt M, Wolf D, Span R, Yan J. A review on compressed air energy storage: Basic principles, past milestones and recent developments. Appl Energy 2016;170:250–68.

[120] Wu J, Wang J, Li S. Multi-objective optimal operation strategy study of microCCHP system. Energy 2012;48:472–83.

[121] Kim YM, Favrat D. Energy and exergy analysis of a micro-compressed air energy storage and air cycle heating and cooling system. Energy 2010;35:213–20.

[122] Li Y, Wang X, Li D, Ding Y. A trigeneration system based on compressed air and thermal energy storage. Appl Energy 2012;99:316–23.

[123] Ibrahim Dincer, Marc Rosen, Thermal Energy Storage Systems and Applications (2nd Edition), 2011, John Wily & Sons Ltd, United Kingdom

[124] Hossein Pirouz KAVEHPOUR, Hamarz ARYAFAR, Ariana THACKER, Mohammad JANBOZORGI, Sammy HOUSSAINY, Walid ISMAIL, The Regents of the University of California, Low-Cost Hybrid Energy Storage System, United States Patent, WO2017044658 A1, 2017 March 16.

[125] Agazzani AA, Massardo AF. A Tool for Thermoeconomic Analysis and Optimization of Gas, Steam, and Combined Plants. ASME. Eng. Gas Turbines Power. 1997;119(4):885-892. Doi:10.1115/1.2817069.

[126] Nikhil, Dev, et al. "Economic and performance analysis of thermal system." *Research Journal of Recent Sciences* 1.4 (2012): 57-59.

[127] Zakeri, Behnam & Syri, Sanna. Electrical energy storage systems A comparative life cycle cost analysis Renwable and Sustainable Energy Reviews, 42 (2015) 569-596

[128] Wang L. Thermo-economic evaluation, optimization and synthesis of largescale coal-fired power plants; 2016.

[129] Lazzaretto A, Tsatsaronis G. SPECO: a systematic and general methodology for calculating efficiencies and costs in thermal systems. Energy 2006;31:1257–89.

[130] Fu P, Wang N, Wang L, Morosuk T, Yang Y, Tsatsaronis G. Performance degradation diagnosis of thermal power plants: a method based on advanced exergy analysis. Energy Convers Manage 2016;130:219–29.

[131] Wang L. Thermo-economic evaluation, optimization and synthesis of largescale coal-fired power plants; 2016.

[132] Buffa F, Kemble S, Manfrida G, Milazzo A. Exergy and exergoeconomic model of a ground-based CAES plant for peak-load energy production. Energies 2013;6:1050–67.

[133] Bagdanavicius A, Jenkins N. Exergy and exergoeconomic analysis of a compressed air energy storage combined with a district energy system. Energy Convers Manage 2014;77:432–40.

[134] EBSILON Professional Rel. 11. Simulation tool for all kinds of power processes by STEAG Energy Services GmbH, Wetzbach 35, 64673 Zwingenberg, Germany; 2014.

[135] Wang JL, Wu JY, Zheng CY. Simulation and evaluation of a CCHP system with exhaust gas deep-recovery and thermoelectric generator. Energy Convers Manage 2014;86:992–1000.

[136] Yang Y, Wang L, Dong C, Xu G, Morosuk T, Tsatsaronis G. Comprehensive exergy-based evaluation and parametric study of a coal-fired ultrasupercritical power plant. Appl Energy 2013;112:1087–99.

[137] Boyaghchi FA, Heidarnejad P. Thermoeconomic assessment and multi objective optimization of a solar micro CCHP based on Organic Rankine Cycle for domestic application. Energy Convers Manage 2015;97:224–34.

[138] Wang L, Yang Y, Dong C, Yang Z, Xu G, Wu L. Exergoeconomic evaluation of a modern ultra-supercritical power plant. Energies 2012;5:3381–97.

[139] Zare V, Mahmoudi S, Yari M. An exergoeconomic investigation of waste heat recovery from the Gas Turbine-Modular Helium Reactor (GT-MHR) employing an ammonia–water power/cooling

cycle. Energy 2013;61:397–409. [33] Storn R, Price K. Differential evolution-a simple and efficient adaptive scheme for global optimization over continuous spaces. Berkeley: ICSI; 1995.

[140] Sadeghi M, Chitsaz A, Mahmoudi SMS, Rosen MA. Thermoeconomic optimization using an evolutionary algorithm of a trigeneration system driven by a solid oxide fuel cell. Energy 2015;89:191–204.

[141] Ahmadi P, Rosen MA, Dincer I. Multi-objective exergy-based optimization of a polygeneration energy system using an evolutionary algorithm. Energy 2012;46:21–31. [36] Bianco V, De Rosa M, Scarpa F, Tagliafico LA. Implementation of a cogeneration plant for a food processing facility. A case study. Appl Therm Eng 2016;102:500–12.

[142] Açıkkalp E, Aras H, Hepbasli A. Advanced exergoeconomic analysis of a trigeneration system using a diesel-gas engine. Appl Therm Eng 2014;67:388–95.

[143] François J, Mauviel G, Feidt M, Rogaume C, Rogaume Y, Mirgaux O, et al. Modeling of a biomass gasification CHP plant: influence of various parameters on energetic and exergetic efficiencies. Energy Fuels 2013;27:7398–412.

[144] Bejan A, Tsatsaronis G. Thermal design and optimization. John Wiley & Sons; 1996.

[145] Pierobon L, Nguyen T, Larsen U, Haglind F, Elmegaard B. Multi-objective optimization of organic Rankine cycles for waste heat recovery: application in an offshore platform. Energy 2013;58:538–49.

[146] Li H. Environomic modeling and multi-objective optimisation of integrated energy systems for power and cogeneration; 2006.

[147] Mohammad Mahdi Naserian, Said Farahat, Faramarz Sarhaddi, New exergy analysis of a regenerative closed Brayton cycle, Energy Conversion and Management, Volume 134, 15 February 2017, Pages 116-124, ISSN 0196-8904, https://doi.org/10.1016/j.enconman.2016.12.020.

[148] A. Sciacovelli, V. Verda, E. Sciubba, Entropy generation analysis as a design tool—A review, Renewable and Sustainable Energy Reviews, Volume 43, 2015, Pages 1167-1181, ISSN 1364-0321, http://dx.doi.org/10.1016/j.rser.2014.11.104.

[149] Adrian Bejan, Entropy generation minimization: The new thermodynamics of finite-size devices and finite-time processes, Journal of Applied Physics **79**, 1191 (1996); doi: http://dx.doi.org/10.1063/1.362674

[150] M. Jafari, M.J. Parhizkar, E. Amani, H. Naderan, Inclusion of entropy generation minimization in multi-objective CFD optimization of diesel engines, Energy, Volume 114, 2016, Pages 526-541, ISSN 0360-5442, http://dx.doi.org/10.1016/j.energy.2016.08.026.

[151] Yanlin Ge, Lingen Chen, Fengrui Sun, Finite-time thermodynamic modelling and analysis of an irreversible Otto-cycle, Applied Energy, Volume 85, Issue 7, 2008, Pages 618-624, ISSN 0306-2619, http://dx.doi.org/10.1016/j.apenergy.2007.09.008.

[152] Y. Haseli, Optimization of a regenerative Brayton cycle by maximization of a newly defined second law efficiency, Energy Conversion and Management, Volume 68, 2013, Pages 133-140, ISSN 0196-8904, http://dx.doi.org/10.1016/j.enconman.2012.12.033.

[153] Y. Haseli, Performance of irreversible heat engines at minimum entropy generation, Applied Mathematical Modeling, Volume 37, Issue 23, 2013, Pages 9810-9817, ISSN 0307-904X, http://dx.doi.org/10.1016/j.apm.2013.05.010.

[154] Andrew Pimm and Seamus D. Garvey, Chapter 7 - Underwater Compressed Air Energy Storage, In Storing Energy, edited by Trevor M. Letcher,, Elsevier, Oxford, 2016, Pages 135-154, ISBN 9780128034408, https://doi.org/10.1016/B978-0-12-803440-8.00007-5.

[155] Kotas TJ. The exergy method of thermal plant analysis. London: Butterworths; 1985.

[156] Moran MJ. Availability analysis a guide for efficient energy use (corrected edition). New York: ASME; 1989.

[157] Dincer I, Rosen M. Exergy energy environment and sustainable development. Oxford: Elsevier; 2007.

[158] Wark K. Advanced thermodynamics for engineers. New York: McGraw-Hill; 1995.

[159] Winterbone DE. Advanced thermodynamics for engineers. New York: Wiley; 1997.

[160] Bejan A. Advanced engineering thermodynamics. third ed. New York: Wiley; 2006.

[161] Burghardt MD, Harbach JA. Engineering thermodynamics. fourth ed. New York: HarperCollins; 1993.

[162] Borgnakke C, Sonntag RE. Fundamentals of thermodynamics. seventh ed. New York: Wiley; 2009.

[163] Balmer RT. Modern engineering thermodynamics. Oxford: Elsevier; 2011.

[164] Moran MJ, Shapiro HN, Boettner DD, Bailey MB. Fundamentals of engineering thermodynamics. eighth ed. New York: Wiley; 2014.

[165] Çengel YA, Boles MA. Thermodynamics e an engineering approach. eighth ed. New York: McGraw-Hill; 2015.

[166] Dincer I, Cengel YA. Energy, entropy and exergy concepts and their roles in thermal engineering. Entropy 2001;3:116–49.

[167] Gallavotti G. Entropy, thermostats and chaotic hypothesis. Chaos 2006;16:384–9.

[168] Lucia U. Mathematical consequences and Gyarmati's principle in Rational Thermodynamics. Nuovo Cimento 1995;B110(10):1227–35.

[169] Lucia U. Stationary open systems: a brief review on contemporary theories on irreversibility. Physica A 2013; 392(5) 1051-1062. http://dx.doi.org/10.1016/ j.physa.2012.11.027.

[170] Lucia U. Maximum or minimum entropy generation for open systems? Physica A: Statistical Mechanics and its Applications 2012;392:3392–8.

[171] Lucia U. Irreversibility in biophysics and biochemical engineering. Physica A: Statistical Mechanics and its Applications 2012;391:5997–6007.

[172] Lucia U. Probability, ergodicity, irreversibility and dynamical systems. Proceedings of the Royal Society of London Series A 2008;464:1089–184.

[173] Lucia U. Statistical approach of the irreversible entropy variation. Physica A: Statistical Mechanics and its Applications 2008;387/14:3454–60.

[174] Cengel YA, Boles MA. Thermodynamics: an engineering approach. 4th ed. New York: McGraw-Hill; 2001.

[175] Sciubba E, Wall G. A brief commented history of exergy. From the beginnings to 2004. Journal of Chemical Thermodynamics 2007;10(1):1–26.

[176] Dinçer, İbrahim, et al. *Optimization of Energy Systems*. Wiley, 2018. EBSCO*host*, search.ebscohost.com/login.aspx?direct=true&db=nlebk&AN=1517704&site=ehost-live.